POLITECNICO
MILANO 1863

SCUOLA DI INGEGNERIA INDUSTRIALE
E DELL'INFORMAZIONE

Thermal stability of size- and termination-selected polyynes embedded in polymeric nanocomposite films monitored via *in situ* SERS mapping

Tesi di Laurea Magistrale in
Materials Engineering and Nanotechnology
Ingegneria dei materiali e delle nanotecnologie

Author: **Alice Cartoceti**

Student ID: 953325
Advisor: Prof. Carlo S. Casari
Co-advisors: Pietro Marabotti, Sonia Peggiani
Academic Year: 2021-22

Abstract

Carbyne, the 1D allotrope of carbon, can occur into two forms, namely the polyynic and the cumulenic ones. Polyynes are one-dimensional finite chains made of sp-hybridized carbon atoms, bound through alternated single and triple bonds. In this experimental thesis, it is investigated the thermal stability of size- and termination-selected polyynes embedded into polyvinyl alcohol (PVA) nanocomposite films. In sight of future technological applications, it is of fundamental importance to understand the effect of both length and terminations on their thermal stability. Polyynes were synthesized through Pulsed Laser Ablation in Liquid (PLAL), in isopropyl-alcohol or dichloromethane to produce H-capped and Cl-capped chains, respectively. The synthesized mixture was purified, demonstrating a highly effective stabilization of polyynes over long periods. Then, polyynes were size- and termination-selected by means of High Performance Liquid Chromatography (HPLC). The nanocomposite films composition was optimized by dissolving the polymer directly during silver nanoparticles colloid formation, and developing a strategy to maximise the SERS signals of each specific polyyne independently from its concentration. Then, the SERS measurements parameters that allowed to get the maximum SERS signal in the safest conditions possible were found. Finally, I designed and established an experimental apparatus and a methodology to perform nanocomposite films thermal treatment monitored through an *in situ* SERS mapping procedure. This methodology proved to be effective in both allowing long SERS measurements without the risk for films degradation, and providing a reliable statistical description of the samples behaviour upon thermal treatment, reducing the issue related to film inhomogeneity. In particular, it was observed the high thermal stability, up to 100°C, of the nanocomposites polymeric matrix (PVA), well above its glass transition temperature. Regarding polyynes thermal stability, on one side it was possible to observe a faster degradation for increasing chain lengths and treatment temperatures in both H-capped and Cl-capped polyynes nanocomposites, due to a higher molecular reactivity and mobility. On the other side, a much larger stability of the Cl-capped chains compared to the H-capped ones was demonstrated. This was justified by a stronger interaction of chlorine compared to hydrogen terminations with Ag nanoparticles, also considering the effect of endgroups steric hindrance. Specifically,

considering H-capped polyynes, the effect of the laser alone on their degradation was investigated as well, allowing for the decoupling of thermal and laser effects on the stability of H-capped polyynes embedded into the PVA nanocomposites.

Keywords: CAWs, selected polyynes, nanocomposites, HPLC, *in situ* SERS mapping, thermal stability

Abstract in lingua italiana

La carbina, allotropo 1D del carbonio, può presentarsi in due forme, quella poliinica e quella cumulenica. In particolare, le poliine sono catene finite monodimensionali costituite da atomi di carbonio ibridizzati sp, legati da legami singoli e tripli alternati. Oggetto principale di questa tesi sperimentale è lo studio della stabilità termica di poliine selezionate per lunghezza e terminazione incorporate in film nanocompositi di alcol polivinilico (PVA). In vista di future applicazioni tecnologiche, è di fondamentale importanza comprendere l'effetto della loro lunghezza e delle loro terminazioni sulla loro stabilità termica. Le poliine sono state sintetizzate mediante ablazione laser pulsata (PLAL) in alcool isopropilico o diclorometano per produrre, rispettivamente, poliine del tipo HC_nH e HC_nCl. Una volta sintetizzata, la miscela è stata sottoposta a un processo di purificazione, che si è dimostrato molto efficace nello stabilizzare le poliine per lunghi periodi al suo interno. Successivamente, le poliine sono state selezionate per dimensione e terminazione mediante cromatografia liquida ad alte prestazioni (HPLC). La composizione dei film nanocompositi è stata ottimizzata sciogliendo il polimero direttamente durante la formazione delle nanoparticelle d'argento e sviluppando una strategia per massimizzare i segnali SERS di ciascuna poliina incorporata, indipendentemente dalla sua concentrazione. Quindi, sono stati trovati i parametri di misurazione SERS che permettessero di massimizzare l'intensità dei segnali dei film nanocompositi nelle condizioni più sicure possibili. Infine, ho progettato e sviluppato un apparato sperimentale ed una metodologia atti ad eseguire il trattamento termico dei film nanocompositi monitorato attraverso una procedura di mappatura SERS *in situ*. Questa metodologia si è dimostrata efficace nel consentire lunghe misurazioni SERS senza il rischio di degradazione dei film, ed ha eliminato il rischio di invalidazione dei dati a causa della disomogeneità degli stessi, fornendo una descrizione statistica affidabile del comportamento dei campioni quando soggetti a trattamento termico. In particolare, è stata osservata l'elevata stabilità termica della matrice polimerica di PVA fino a 100°C, ben al di sopra della sua temperatura di transizione vetrosa, di circa 85°C. Per quanto concerne la stabilità termica delle diverse catene, da un lato è stato possibile osservare, indipendentemente dalle terminazioni delle poliine incorporate nel nanocomposito, una più rapida degradazione di quelle aventi lunghezze maggiori e sot-

toposte a temperature maggiori, a causa dell'incremento della reattività e mobilità delle molecole stesse; dall'altro lato, è stata dimostrata una maggiore stabilità delle catene terminate con cloro rispetto a quelle idrogenate. Ciò è stato giustificato ipotizzando una più forte interazione tra le terminazioni di cloro rispetto a quelle di idrogeno con le nanoparticelle di argento, considerando anche l'effetto dell'ingombro sterico dei terminali di catena. Nello specifico, la stabilità delle poliine idrogenate è stata studiata anche tenendo conto del solo contributo dato dall'interazione dei rispettivi film nanocompositi con il laser, consentendo di disaccoppiarne gli effetti degradativi termici e laser-indotti.

Parole chiave: CAWs, poliine selezionate, nanocompositi, HPLC, mappatura SERS *in situ*, stabilità termica

Contents

Introduction

It was in 1931 when Mendeleev wrote: "The molecules of coal, graphite, and diamond are very complicated, and carbon atoms exhibit the capability of binding one to another to form complex molecules. None of the elements possesses an ability of complicating in such an extent as does carbon. There is still no basis to define the polymerization degree of the coal, graphite, or diamond molecules. One should believe, however, that they contain C_n species, where 'n' is a large value". As stated by Mendeleev, carbon can be considered a highly versatile element, thanks to its capability to sustain from one up to four chemical bonds and to generate complex structures combining with itself and other elements. It is well known that elemental carbon can adopt different hybridization states to produce a wide variety of allotropic forms, molecules, and nanostructures. For this reasons, being also widespread in nature, carbon has become of great interest in the field of technological applications. Until 1960s, only two allotropic forms of carbon were known: diamond, corresponding to the sp^3 hybridization of carbon atoms, and graphite, corresponding to the sp^2 hybridization of carbon atoms. From that time on, due to the appealing properties of these two carbon allotropes, a huge effort has been done to discover the missing allotrope of carbon, characterized by an infinite one-dimensional linear chain configuration consisting of sp-hybridized carbon atoms. While much is known about diamond and graphite, as well as about more recently discovered carbon nanostructures like fullerenes, nanotubes, and graphene, still little is known about the sp-hybridized allotrope, commonly called carbyne. Indeed, no physical proof of the existence of carbyne has been reported yet, but it has been demonstrated the presence of naturally formed linear sp-carbon chains in interstellar dust, meteorites, and shock-compressed graphite, and a huge scientific endeavor has permitted to find possible ways to synthesize them artificially through chemical and physical methods. These chains, commonly known as Carbon Atomic Wires (CAWs), can exist either in a cumulenic or polyynic configuration, according to their CC bonding arrangement. Thanks to their characteristic π-electron conjugated character, they show both metallic and semiconductive behaviour: in the cumulenic configuration, carbon atoms are bound through equalized double bonds and result in a metallic system, while the polyynic configuration displays an alternation of

single and triple bonds along the whole chain and results in a semiconductor-like system. In particular, the semiconductive/metallic behaviour of very long sp-carbon chains, structurally comparable to the ideal carbyne, depends primarily on Peierls distortion. On the other side, the electronic behaviour of shorter chains, namely CAWs, is solely dependent on endgroup effect, which can both induce semiconductive or metallic structures and give rise to new material properties. Despite their outstanding structure-tunable mechanical, optical and electronic properties, which make them highly appealing materials in many different technological fields, CAWs are highly reactive species. Indeed, being produced under strong non-equilibrium conditions, their configuration is not energetically favoured, and this makes them easily undergo degradation phenomena especially via chain-chain crosslinking and exposure to oxidizing agents. Regarding crosslinking phenomenon, which determines the reorganization of unsaturated sp chains into more stable sp^2-hybridized systems, with consequent loss of their peculiar properties, it becomes more and more probable at increasing temperatures, due to an improve in molecular mobility. For this reason, a significant part of the current research on CAWs is focused on finding effective ways to stabilize them, making possible their safe usage in real devices. Among the proposed stabilization strategies, it is worth to mention the formation of CAWs-metal nanoparticles aggregates or CAWs embedding into solid matrices.

This experimental work aims to study the thermal stability of polyynes embedded in polymeric nanocomposite films, an aspect of great importance within a technological application-oriented vision. In particular, it has been investigated the effect of both polyynes termination and length on their thermal stability. As polymeric matrix, it has been chosen polyvinyl alcohol (PVA) for its capability to efficiently form homogeneous films, its processing ease, filmability and thermal stability even at temperatures over its glass transition point. Polyynes have been synthesized by means of Pulsed Laser Ablation in Liquid (PLAL) and then selected by size and termination via High Performance Liquid Chromatography (HPLC). The nanocomposite films have been obtained by first mixing a solution of silver nanoparticles dispersed in PVA with the polyynes solution of interest, and then by drop casting the mixed solution. The addition of Ag nanoparticles is required to characterize the samples with Surface Enhanced Raman Spectroscopy (SERS), which indeed has been used to develop an *in situ* mapping methodology to probe polyynes thermal stability.

This thesis work is organized as follows:

Chapter 1 is devoted to give an overview on carbon hybridization, followed by a description of CAWs theoretical model, properties and applications, synthesis and characterization techniques, with a final insight on CAWs instability issue.

Chapter 2 describes CAWs-polymer nanocomposites and the role of both polymeric matrix and metal nanoparticles in polyynes stabilization.

Chapter 3 outlines the materials employed for the synthesis of the nanocomposite films and describes the techniques adopted for both their synthesis and their characterization.

Chapter 4 reports the first part of the experimental results of this work, namely the optimization process of both Ag/PVA/polyynes nanocomposite films' composition and SERS measurements parameters.

Chapter 5 reports the second part of the experimental results of this work. The development of a methodology to test the thermal stability of size- and termination-selected polyynes embedded in PVA nanocomposite films is described, together with the procedure employed to decouple thermal and laser effects on the degradation of H-capped polyynes.

1 | Carbon Atomic Wires (CAWs)

1.1. An overview on carbon hybridization

Carbon has always played a major role in Universe history because of both its abundance and its tendency to form complex species thanks to its peculiar electronic configuration. Indeed, it is the fourth most widespread element by mass in the Solar system after hydrogen, helium and oxygen, and much of the diversity and complexity of carbon-based compounds is due to the ability of carbon atoms to bond with one another in many different conformations, as well as to link easily with other elements [1, 2]. The electronic configuration of carbon is $1s^2 2s^2 2p^2$, with four electrons in the outer shell, and it allows the establishment of up to four chemical bonds. This can be explained by looking at the hybridization theory. According to this theory, in fact, the linear combination of atomic orbitals leads to the generation of new hybrid orbitals which introduce new possible symmetries in the electronic distribution of the atom. In the specific case of carbon, the atomic orbitals involved in the hybridization process are the 2s and 2p, whose little difference in energy can be easily overcome when carbon is affected by a perturbation, given, for example, by its proximity to an other atom. The combination of those two orbitals results in three possible hybridized configurations: sp^3, when the 2s orbital combines with three 2p orbitals, sp^2, when the 2s orbital combines with two 2p orbitals, and sp, when the 2s orbital combines with one 2p orbital. In the two latter configurations, respectively one and two non-hybridized 2p orbitals will remain, resulting in the eventual formation of different bonds when interacting with other atoms, generating molecules with unique geometries. When interacting with other carbon atoms, these 2p atomic orbitals can overlap side-by-side, resulting in the generation of a new type of orbital, called π molecular orbital (LCAO theory), directed perpendicularly to the internuclear axis which connects the two bonding atoms. The great importance of this orbital is that it determines the electron delocalization, which is fundamental in determining many of the electronic properties of all π-electron conjugated molecules [3–5].

Carbon hybridization is not only responsible for the interaction between carbon and other elements, indeed, it also explains the existence of different carbon allotropes. These sys-

tems have always attracted the interest of the scientific community, indeed, they represent a widely explored research field still nowadays. It was 1797 when Tennant experimentally proved that diamond is an allotrope of carbon, and, since then, a huge effort has been put in the discovery of its other allotropes and in the study of their highly appealing properties [5, 6]. Carbon hybridization states (namely sp^3, sp^2, sp) were discovered thanks to the development of the hybridization theory, in the 1930s, but until the 1960s the only two known allotropic forms of carbon were diamond and graphite. Despite being constituted by the same building blocks, i.e. carbon atoms, they display extremely different physical properties because of their different hybridization, sp^3 and sp^2 respectively. Indeed, the tetrahedral spatial disposition of carbon atoms induced by sp^3 orbitals determines the peculiar hardness of diamond. On the other hand, sp^2 hybridization determines the graphite planar structure, with strong in-plane bonds and weak Van der Waals interplanar bonding, making graphite one of the softest materials [5, 7, 8]. Such hybridization-tunable behaviour of carbon can be found also at the nanoscale (Fig. 1.1): carbon nanostructures, indeed, can show different geometries and properties according to their hybridization. The most famous systems in this field are graphene (sp^2), a single graphite layer, characterized by outstanding mechanical and transport properties, nanodiamonds (sp^3), the nanometric counterpart of diamond, and, even more recently discovered, carbon nanotubes (CNTs), fullerenes and carbon fibers, characterized by $sp^2 - sp^3$ intermediate hybridization. Less renewed systems, recently theorized and still under investigation, are characterized by sp-sp^2 and sp-sp^3 intermediate hybridization, namely graphynes, graphdiynes and yne-diamond [6].

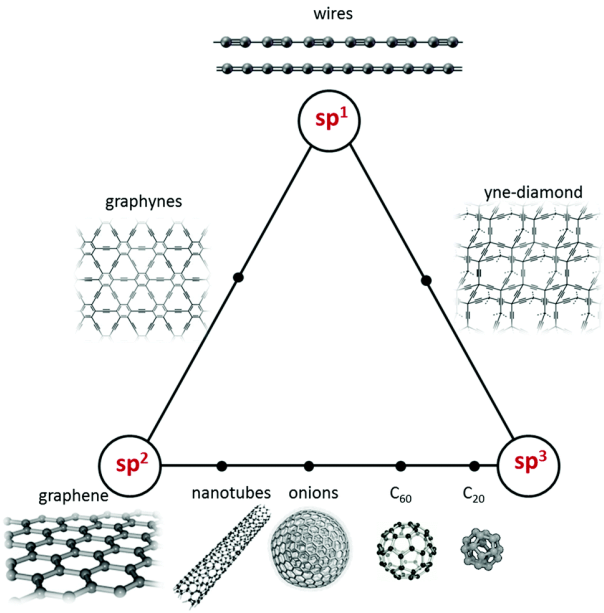

Figure 1.1: Ternary diagram of carbon nanostructures according to their hybridization [6].

1.2. Carbyne and finite carbon atomic wires models

During the 1960s, a great interest grew among scientists towards the demonstration of the existence of "the third carbon allotrope". This elusive allotrope, whose existence has never been physically proved yet, is labeled "carbyne", from the Latin *carboneum* (i.e. carbon) and the suffix "yne" (used in organic chemistry to designate the CC triple bond), and consists of an infinite one-dimensional chain made of sp-hybridized carbon atoms [5]. Despite the theoretical existence of a carbyne crystal is still matter of debate, its realization seems to be utopian, due to instability phenomena (namely, crosslinking) which would determine the sp-to-sp^2 transition. The first serious attempt to synthesize carbyne was made in 1885 by Baeyer who, by means of the oxidative coupling approach proposed by Glaser in 1870 [9], was convinced to be able to address a one-dimensional carbon polymer through a series of transformations starting from acetylene carboxylic acid. Unfortunately, this attempt did not succeed due to the instability of the intermediate structures produced during the reactions, and Baeyer postulated the impossibility of preparing such allotrope referring to it as "explosive diamond" [10]. Despite the damping effect that this failure had on carbyne research, the discovery of carbyne-like compounds in interstellar dust, comets, plants and fungi [2, 5, 11–16] renewed an important stimulus towards these molecules, and finally in 1964 Kudryavtsev *et al.* managed to chemically synthesize carbon atomic wires [17]. The difference between the carbyne elusive carbon allotrope and real carbon

atomic wires consists in the finiteness of the chain length and in the effect that the chain terminations have on material properties. Anyway, as first approximation, structure and properties of CAWs can be investigated starting from the study of the ideal infinite one-dimensional chain model, which can be carried out following a hybridization theory approach or a solid-state physics approach [18–22].

Considering the hybridization-based approach, carbyne is characterized by sp-hybridized carbon atoms. This configuration is obtained by the linear combination of one 2s atomic orbital and one 2p atomic orbital. Due to the fact that two 2p atomic orbitals are not involved in the hybridization process, they will be available to form a triple bond or two double bonds. As a consequence, the ideal carbyne can occur in two isomeric forms, namely the cumulenic and the polyynic forms (Fig. 1.2). In cumulenes, carbon atoms are bound through a sequence of equalized double bonds, while in polyynes carbon atoms are connected through an alternation of single and triple bonds.

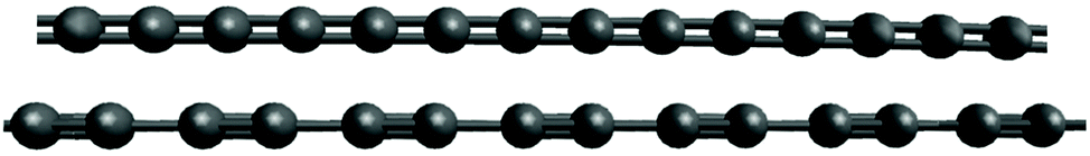

Figure 1.2: The two possible configurations of carbyne: equalized double bonds (cumulene, top) and alternated single-triple bonds (polyyne, bottom) [6].

The electronic configuration, hence the transport properties of the chain, are highly affected by its bond structure. According to the LCAO theory introduced in the previous section, the interaction between the "free" 2p orbitals of carbon results in the formation of delocalized π molecular orbitals, which are responsible of CAWs conjugation. The conjugation is maximized in cumulenic structures, where the sequence of double bonds determines a perfect electrons delocalization along the whole chain, while is limited in the case of polyynic structures, due to the presence of the single bonds. This different electron delocalization along carbyne chains translates into a different behaviour of cumulenes and polyynes: cumulenes display a metallic character, while polyynes feature a semiconducting character. Such diversity in cumulenes and polyynes transport properties can be easily verified also by following a solid-state physics approach. Cumulenes can be described as an infinite 1D crystals with a monoatomic unit cell where each atom contributes with one electron per 2p atomic orbital resulting in a half-filled conduction band, thus promoting the cumulenic metallic behaviour. On the other hand, polyynes can be described as infinite 1D crystals with a biatomic unit cell, which translates into a completely filled valence band and an empty conduction band, separated by a bandgap opened at the edges of the

Brillouin zone which determines their semiconducting behaviour (Fig. 1.3) [6, 23].

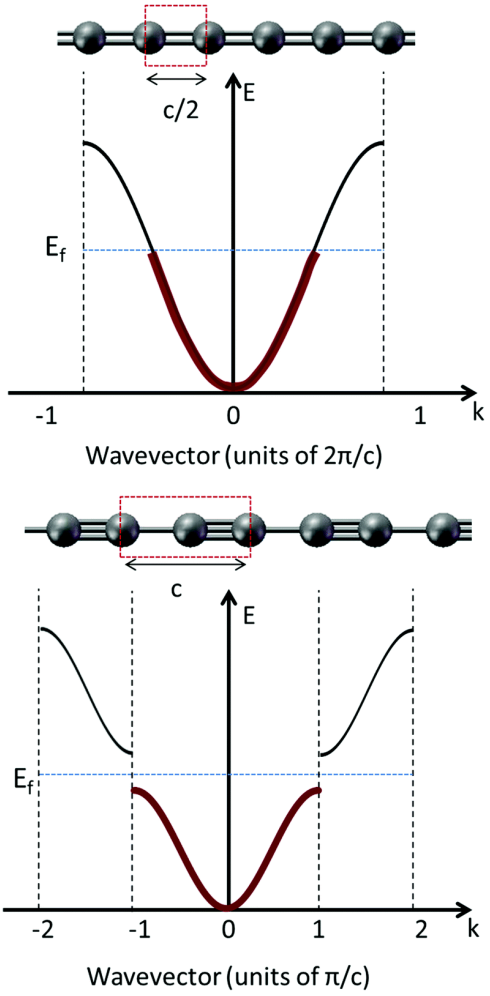

Figure 1.3: A simplified sketch of cumulenic (top) and polyynic (bottom) band structure explains their electronic behaviour by means of a solid-state physics approach. The band filling results in the metallic and semiconductive character of cumulenic and polyynic configurations, respectively [6].

Actually, cumulenes do not differ from polyynes just in terms of transport properties, but also in terms of their vibrational properties. Indeed, looking at their phonon dispersion relation, it is possible to notice that cumulenes show only acoustic branches (one longitudinal and two transverse), while in polyynes also three optical branches appear. Also in this case, this is the result of their different unit cell configurations. The main consequence of the differences in theoretically predicted vibrational properties of cumulenes and polyynes is the absence of cumulenes optically activity, which would result in the impossibility to detect them by vibrational spectroscopy techniques.

A fundamental structural parameter used to characterize carbyne is the so called Bond Length Alternation (BLA), which represents the difference in bond length for adjacent CC bonds. This parameter is affected by the conjugation of the molecule, i.e. it decreases for increasing degree of conjugation, and permits to distinguish cumulenic from polyynic structures, thus representing a very important tool to understand the structural, electronic and vibrational properties of carbyne. In particular, the BLA is non-zero in polyynes, while it is null for cumulenes, which indeed are ideally characterized by an infinite sequence of equivalent double bonds having the same length. Moreover, being influenced by the conjugation of the molecule, the larger is the conjugation, the smaller is the BLA, as well as the extension of the energy gap at the edges of the Brillouin zone (Fig. 1.4) [6].

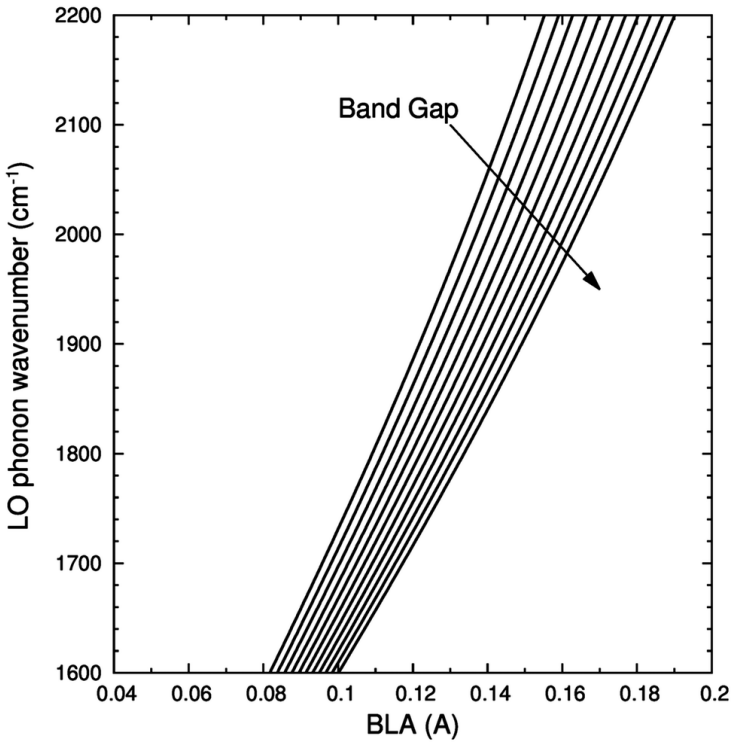

Figure 1.4: Correlation between BLA, longitudinal optical (LO) phonon wavenumber, and band gap in carbyne [6].

Cumulenes and polyynes are not equally probable in terms of stability. This difference can be ascribed to the so called Peierls distorsions. This phenomenon, common to all poly-conjugated materials, consists in the energetically-favoured transition from the cumulenic configuration, characterized by a zero BLA, into one of the two equivalent polyynic structures (triple-single or single-triple alternated bonds), characterized by a non null BLA (Fig. 1.5). This has been theoretically confirmed by pseudopotential DFT calculations, where an equilibrium alternated structure with non-zero band gap has been obtained as

the optimized carbyne configuration [6, 24].

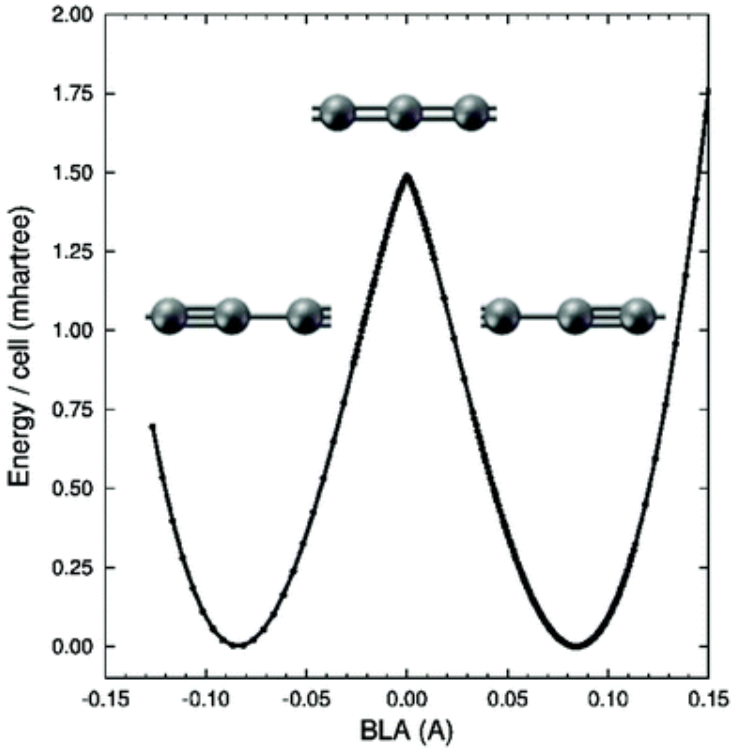

Figure 1.5: Carbyne potential energy as a function of BLA parameter. Peierls distorsion results in the instability of the cumulenic configuration and the stabilization of the two equivalent polyynic structures (triple-single or single-triple alternated bonds) [6].

To conclude the description of carbyne ideal model, its theoretically predicted outstanding properties justify its great appeal as research topic. Together with its appealing electronic and vibrational properties, carbynes ideally show a large effective surface, estimated to be four times the theoretical one of graphene, an impressive strength, with a Young modulus up to 32 TPa and a specific stiffness larger than all other known materials (including diamond), and a thermal conductivity, much higher than the one of graphene and nanotubes [18, 25].

So far, the structure and properties of CAWs have been described by approximating them as an ideal infinite one-dimensional chain. Actually, by means of this model, it is not possible to comprehensively explain the behaviour of real finite CAWs, especially in terms of their structural, electronic and vibrational properties. Indeed, these features can be properly described only by considering the effect of their finite length and the presence of endgroups. Considering the finite CAWs length, Peierls distorsions are expected to play a significant role in the stabilization of the polyynic configuration upon the cumulenic one

just for very long chains, i.e. when their behaviour is well approximated by the ideal infinite carbyne model. According to Yang *et al.* predictions, experimentally demonstrated by Gao *et al.*, this occurs when the number of carbon atoms is, respectively, 52 and 68 [20, 26], while for shorter chains Peierls distorsions are not responsible for the existence of polyynic systems. Indeed, the bonds configuration, and so the transport properties, of short carbon atomic wires is primarily determined by the presence of the endgroups, which result to highly affect the BLA parameter [18, 19, 23]. In order to clarify this concept, two examples are reported: in hydrogen terminated chains, the single CH bond established at the end of the chain determines the formation of a triple bond between the adjacent couple of carbon atoms, which in turn forces another single bond between the subsequent couple of carbon atoms. This is repeated along the whole chain, leading to an alternate polyynic structure with a BLA different from zero (semiconducting behaviour). On the other hand, a CH_2 termination determines the establishment of subsequent double bonds along the whole chain, leading to a cumulenic structure with BLA approaching zero (metallic behaviour) [6].

Considering now the electronic properties of CAWs, a fundamental distinction with respect to their ideal counterpart is related to the fact that, being them confined molecules, they show discrete energy levels, and so the bands theory cannot be applied for their description. As a consequence, the concept of bandgap, previously described in relation to both the BLA parameter and the electronic/vibrational properties of carbyne, is substituted by the difference in energy between the HOMO and LUMO levels, respectively the electrons' Highest Occupied Molecular Orbital and the Lowest Unoccupied Molecular Orbital. An increase in the chain length means an increase in the π-electron conjugation, and so a decrease in the difference between the HOMO and the LUMO levels, making possible the tuning of the semiconducting behaviour of the material by just selecting the proper chain length. Theoretically, by pushing this strategy to the limit, one could expect that the ultimate consequence of the continuous reduction of the HOMO-LUMO gap is the transition from a semiconducting to a metallic behaviour, and so from a polyynic to a cumulenic long chain, but actually, this is not the case. Indeed, when the number of carbon atom constituting the carbon atomic wire exceeds a certain value (namely between 48 and 52 according to Yang predictions [20]) the behaviour of the CAW itself can be well approximated by the one of the ideal carbyne, and so the Peierls distortion takes place resulting in the stabilization of the polyynic configuration in spite of the cumulenic one [18, 21, 22, 27, 28]. Always considering the electronic properties tunability of CAWs, it is worth to mention an interesting work proposed by La Torre et al., who demonstrated the transition from semiconducting to metallic chains by just putting them under strain,

i.e., by varying their BLA into a more equalized geometry [29]. To consider also the effect of terminations on the electronic properties of CAWs, sp-carbon chains terminated with sp^2 π-electron conjugated end-groups (such as phenyl-, bis(biphenyl)-, and naphthalene-capped chains) have been investigated [19, 25]. Considering the case of bis(biphenyl)-capped chains studied by Milani *et al.*, the authors found that the HOMO-LUMO gap is significantly affected when passing from H-capped chains to diphenyl-capped chains, which in fact are characterized respectively by a polyynic and a cumulenic-like configuration [30]. On the contrary, the dimension of the sp^2 π-conjugated end-groups does not seem to affect in a considerable way the BLA or the HOMO-LUMO gap [18].

Considering CAWs vibrational properties, the main difference with respect to carbyne lies in the fact that in real CAWs it has been proved the existence of Raman signatures of cumulene-like structures. This controversial evidence can be justified by "relaxing the carbyne perspective", specifically by considering the effect of the endgroups which make possible the presence of Raman-active vibrations not only relative to phonons located at the centre of the Brillouin zone, but also in different points of it [6]. Following this approach, Raman spectra of cumulenic wires have been predicted by DFT calculations, showing many Raman-active vibrational modes, demonstrating the possibility of detecting not only polyynes but also finite cumulenes by means of vibrational spectroscopy [31, 32].

Considering all the described aspects, and specifically their appeal in terms of properties tunability, it can be easily understood the potential of carbon atomic wires in sight of future technological applications. Indeed, properties such as ballistic and oscillatory conductance, strain-induced metal-to-insulator transition, outstanding stiffness and massive surface area make these systems suitable for many possible applications in nanoelectronic or spintronic devices, nonlinear optical materials, molecular wires, hydrogen storage devices and supermultiplexing imaging [29, 33–37]. Other interesting possibilities involve the integration of sp-carbon chains with other low-dimensional carbon nanostructures, characterized by sp^2 hybridization, for novel functional materials, optoelectronic and photovoltaic applications [36, 38]. Finally, among the still rare examples reported in literature on real CAWs-based devices, field-effect transistors based on cumulenic carbon atomic wires [39, 40] represents a pioneering example for organic electronics.

1.3. Carbon Atomic Wires synthesis

The first successful synthesis of carbon atomic wires can be dated back to the 1964 and is ascribed to the chemists Kundryavtsev and Yu [41]. That period, characterized by a fervent study on CAWs chemical synthesis, ended up with the development of two main

methods, the "polymerization-based" technique, and the Glaser reaction-based technique. The first method, based on polycondensation reactions, permits an efficient single-step production of sp-carbon chains, but the products themselves are characterized by a large polydispersity. The Glazer reaction, instead, based on the dimerization of ethynyl groups, results in the production of molecules with a defined length and allows for a precise control of the products structure, as reported in several works [6, 42–44]. The main advantages of CAWs chemical synthesis methods, in general, are related to the high control over both the chains length and terminations. In particular, being possible the selection of specific bulky endgroups for the sp-carbon chains, chemical methods permit to obtain systems which are quite stable as powders in environmental conditions, allowing for a deeper characterization of CAWs and representing a key step towards CAWs applications. Moreover, chemical synthesis processes allow to produce up to grams of CAWs powders. On the other hand, the main drawbacks of chemical methods are the difficulty to be scaled up at the industrial level, the need of highly-specialized personnel and several purification steps at their end. In particular, the scaling-up difficulty is due to their long processing times, their high costs, their small reproducibility, and their need for the frequent usage of toxic solvents; while the need for purification processes, again time and money consuming, is due to the fact that these processes involve many compounds and complex reaction steps.

More recently, also bottom-up physical synthesis techniques have been developed. Among them, the Submerged Arc Discharge in Liquids (SADL), first applied to CAWs synthesis by Cataldo [45], the Pulsed Microplasma Cluster Source (PMCS) method, developed by Milani et al. [46], the Pulsed Laser Ablation in Liquid (PLAL), employed by Tsuji *et al.* for the first time to produce CAWs [47], and the Pulsed Laser Deposition (PLD), used by Casari *et al.* to fabricate sp-sp^2 carbon nanostructures [48] (Fig. 1.6).

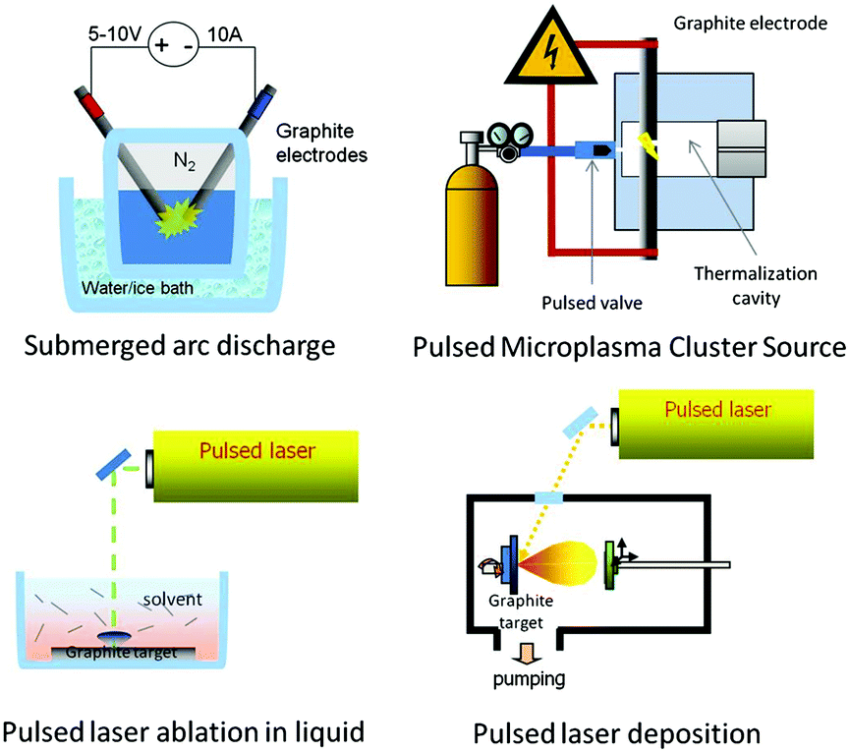

Figure 1.6: Main physical methods for sp-carbon chains synthesis [6].

All these techniques are based on the production of a carbon plasma that is confined by a gas or a liquid to reach the out-of-equilibrium conditions (high temperature and pressure gradients) needed for the formation of sp carbon chains. Specifically referring to the methods performed in liquid, they are very efficient in producing mainly polyynic structures, while the cumulenic counterpart has not been observed yet [6, 49].

The main advantage of physical methods consists in their scalability, in opposition to chemical methods: indeed, they are characterized by much simpler setups, faster processing time, and the possibility to use safer and eco-friendlier materials. Among the physical synthesis methods, the most used ones are SADL and PLAL, both exploiting the presence of a liquid phase as quenching medium for the carbon plasma. When performed in organic solvents, these techniques take advantage of the liquid phase itself as secondary source of carbon, increasing the final polyynes concentration, and as a source of specific chains terminations [6, 49]. In SADL, sp-carbon chains are produced by means of the application of a high voltage between two graphite electrodes immersed into a dielectric solvent (water or organic solvent). An arc discharge is produced between the electrodes, which are kept almost in contact, generating a plasma region which contributes to the etching of carbon atoms from graphite and from the solvent molecules, ending up with the formation of sp-carbon chains.

Pulsed Laser Ablation in Liquids is a physical synthesis process which permits to easily produce nanostructured systems such as polyynes or metal nanoparticles. For this reason, and due to its high versatility and parameters tunability, it has been used as polyynes synthesis method in the present experimental work. Thus, an overview on the technique advantages and the physical processes involved, together with an insight in polyynes production, is given.

The most interesting advantages of PLAL with respect to chemical methods are for sure its scalability, compatibility with the principles of green chemistry, setup simplicity, competitive cost, easy parameters tunability, capability to easily synthesize nanostructures like polyynes and nanoparticles and possibility to produce nanocomposites in a single step process [49–52]. On the other side, PLAL also shows some disadvantages with respect to chemical processes, such as a much lower concentration of the synthesized products, a poor control over their size distribution and over product chemistry [52].

1.3.1. Physics of PLAL process

PLAL-synthesized nanomaterials can be obtained by focusing a high-power pulsed laser onto a target immersed in a solvent. This bottom-up method exploits the generation of a plasma which, upon condensation, forms nanoparticulates. Several reviews exhaustively describe the main steps involved in PLAL as a temporal sequence of events after a single laser pulse interaction with the target (Fig. 1.7) [49, 52, 53]:

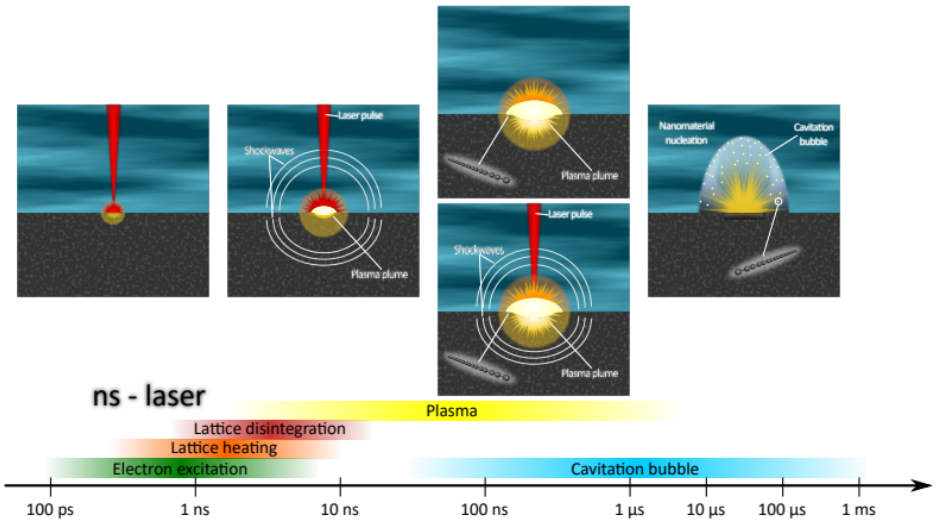

Figure 1.7: Time evolution of fundamental ns-PLAL steps [49].

The first step of the process consists in the laser beam crossing the solvent before reaching

the target. In general, the adopted solvent should be transparent at the laser wavelength to maximize the energy fraction effectively transmitted to the target. When the laser hits the target, different linear and non-linear optical absorption mechanisms can occur, depending on its duration and deposited power. In particular, exploiting shorter pulses (below 1 ps) translates into more intense non-linear phenomena that lead to localized photoionization. Considering a ns-pulsed laser, which is the one adopted for polyynes synthesis in the present work, the pulse duration is longer than the electron-lattice thermalization time, so, in addition to photoionization, the target material can be subjected to thermally-induced ablation processes, such as vaporization, boiling, melting or thermoionic emission. The large amount of energy absorbed by the target from the laser pulse, given by the kinetic energy transferred from the excited electrons towards the lattice, induces the detachment of materials fragments from the target. Depending on the laser pulse duration, it is possible to distinguish between three main types of material detachment mechanisms, namely vaporization, normal boiling and explosive boiling. Considering ns-pulsed lasers, explosive boiling occurs when the target is superheated to the thermodynamic critical temperature, and is typically accompanied also by the so called Coulombic explosion, which contributes to the fragmentation of the already detached particles as a consequence of electrical repulsion effects. The elastic recoil of the detached material, occurring simultaneously to the ablation process, generates two shockwaves that, by propagating at supersonic speed towards the target and into the liquid, heats them and promotes further material detachment. Due to these hazardous environmental conditions inside the liquid (temperature, pressure, and density of approximately 10^3 K, 10^{10} Pa, and $10^{22\div23}$ cm^{-3}), the ablated material arranges in a strong out-of-equilibrium plasma plume which undergoes an expansion process followed by a rapid quenching due to the surrounding solvent. On one side, the presence of a liquid solution determines a huge confinement of the plasma plume, and this in turns leads to the transfer of a large thermal energy fraction to the underneath target, thus favouring detachment of further material from it. On the other side, two possible mechanisms can lower the fraction of thermal energy delivered to the target: the heat transfer by the plasma plume to the surrounding liquid, leading to degradation, ionization, and pyrolisis of the solvent molecules, and/or the so called "plasma shielding", which occurs when the laser pulse duration is comparable to the plasma lifetime and consists in the laser pulse absorption by the plasma plume, resulting in the prolongation of the plume lifetime. This phenomenon is negligible for short pulses ($<$ 1 ns), but becomes more important for longer pulses ($>$ 1 ns), as in the case of the laser employed in this work.

Once the plasma quenching is over, the thermal energy transferred to the liquid generates

a cavitation bubble which, while travelling at supersonic speed, expands and collapses, generating shockwaves that propagate into the liquid and disperse the ablation products. After the shockwaves emission, in a time frame after 10^{-4} s from pulse absorption, the system finally reaches the steady state equilibrium before the next laser pulse is emitted [49, 52].

1.3.2. Polyynes synthesis by ns-PLAL

According to the studies carried on by Tsuji et al. on PLAL-synthesized H-capped polyynes, two competitive mechanisms are thought to be at the basis of sp-carbon chains formation: polymerization and termination by hydrogenation [47]. Polymerization consists in a chain-growth polyreaction where polyynes are produced by radical addition of C atoms or C_2 radicals to a chain previously formed by the ablation process itself. In particular, the source of carbon atoms, and so of carbon radicals involved in the reaction, can be both the target and the ablation solvent. Typically, for polyynes production, a graphite target is employed, while many possible solvents, from water to organic solvents, can be adopted. Hydrogenation, on the other side, consists in the quenching of the growing radical chain by means of the interaction with hydrogen atoms, which, by bonding to the chain head and tail, terminates its growth producing an H-capped polyyne (Fig. 1.8).

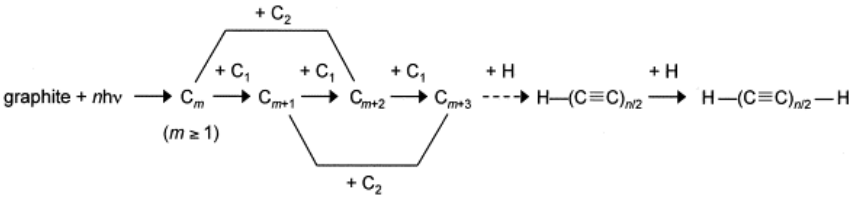

Figure 1.8: Polyynes growth mechanism via radical polyaddition and termination by hydrogenation reaction [47].

The majority of present literature about polyynes produced by PLAL is focused on H-terminated polyynes, since hydrogen is present in most of liquid solvents used for PLAL, and so H-polyynes are the simplest and most probable achievable outcomes of this synthesis method [47, 51, 54]. However, in principle, radical polyaddition reaction can undergo termination by means of other elements, or bulkier groups, with respect to hydrogen, and this possibility can be explored by adopting different solvents. Indeed, it is possible to obtain methyl-terminated and CN-terminated polyynes by operating ablations respectively in water, alcohols, toluene, and acetonitrile [51, 54, 55]. Other studies with PLAL have been carried on trying to achieve different polyynes terminations, like phenyl terminations, by using aromatic compounds as liquid solvents [47], but without any re-

sults. This is probably due to the conditions of polyynes formation in the plasma plume: the high temperatures and pressures are thought to determine the atomization of the solvent molecules, whose constituents subsequently undergo spontaneous aggregation in more stable structures rather than terminate the chains [47, 49].

The yield of polyynes synthesis by PLAL process depends on a large number of parameters, whose selection is crucial in determining polyynes terminations and length: the target material, which may (e.g. graphite) or may not (e.g. gold) act as the primary source of carbon, the adopted solvent, which determines the possible chains terminations and stability together with the degree of plasma confinement, the laser parameters, namely pulse duration, wavelength, pulse energy and repetition rate, and finally the ablation time [47, 51, 56–58]. Despite the huge effort to find the best combination of the abovementioned parameters, still contradictory affirmations are found in literature [47, 56, 57], meaning that a complete comprehension of this process is yet to be achieved.

1.4. Carbon Atomic Wires characterization

Many different techniques have been exploited for the characterization of sp-carbon chains. An overview on the most relevant ones also used in the present thesis work, namely UV-Vis absorption and Raman spectroscopy, Surface Enhanced Raman Scattering (SERS) and High Performance Liquid Chromatography (HPLC), is given below.

1.4.1. UV-Vis absorption spectroscopy

UV-Vis absorption spectroscopy exploits light-matter interaction to obtain information about the optoelectronic properties of the material under investigation. When a molecule is irradiated by an electromagnetic wave whose frequency, and so energy ($E_{ph} = h\nu = \frac{hc}{\lambda}$), corresponds at least to the energy difference between its HOMO and LUMO levels, a photon is absorbed and an electron is promoted from the ground state to the excited state corresponding to that specific energy difference. By irradiating the analysed material with photons having frequencies ranging from the ultraviolet to the near infrared region, it is possible to obtain the absorption spectrum of the material itself, reporting the absorbance as a function of the incident wavelength. Each peak found in the absorption spectrum at a certain wavelengths is related to a specific electronic transition of the sample. Therefore, by knowing the absorption spectrum of a certain material, we can get information about its electronic structure. A second fundamental information that can be extracted by a UV-Vis spectrum is the concentration of the analysed species in a diluted solution, which in fact is related to the measured absorbance. Indeed, the Lambert Beer law establishes a

linear proportionality between light absorbance (A) and the concentration of the absorbing analyte (C) through the molar extinction coefficient ϵ and the optical path L, $A = \epsilon * C * L$.

Focusing now on polyynes, it is possible to observe peculiar absorption progressions, constituted by a series of distinct peaks, in the UV region, together with other secondary peaks at longer wavelengths [51, 59]. In case of polyynes, as in all other conjugated systems, the wavelengths associated to these absorption peaks allow to monitor qualitatively the structure of the chains under investigation. Indeed, due to their π-electron conjugated character, polyynes' electronic properties are strictly related to their BLA, which in turn is largely affected by the chains length and termination, as described in Section 1.1. For this reason, passing from shorter to longer polyynes determines an increase in the π-electron conjugation, and so a reduction in the BLA value, that in turns translates in the reduction of the HOMO- LUMO gap of the chain, and consequently a red-shift in the absorption peaks (Fig. 1.9) [51, 59].

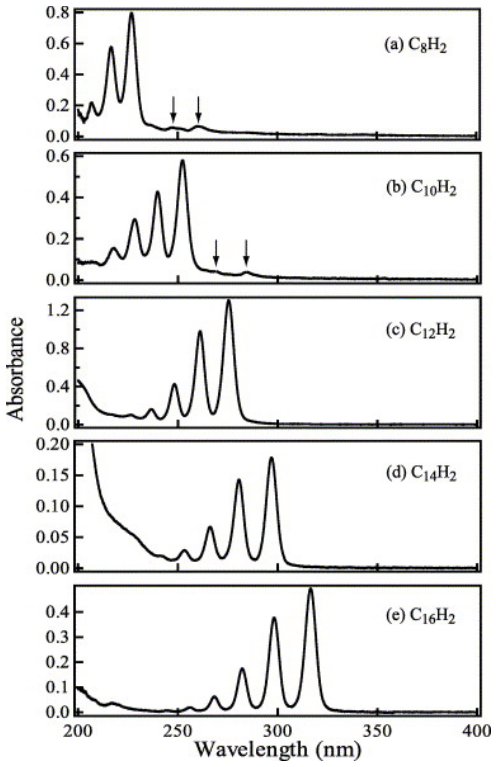

Figure 1.9: UV-Vis absorption spectra of size-selected H-capped polyynes.The small arrows indicate the presence of impurities [59].

1.4.2. Raman and SERS spectroscopy

Raman spectroscopy and Surface-Enhanced Raman Spectroscopy (SERS) are powerful, non-invasive characterization techniques which can provide accurate information on the

molecular properties of materials. Raman spectroscopy is based on inelastic scattering of a monochromatic electromagnetic radiation to detect normal modes of a sample. In particular, as a consequence of the irradiation of the sample by a laser beam, an electron from the electronic ground state is excited to a excited or virtual state, depending if the laser beam is resonant or not with an electronic transition. Then, if the electron undergoes a radiative de-excitation process, finishing its transition in a vibrational level of the electronic ground state different from the original one, the emitted photon, which has a different energy with respect to the one originally absorbed, is called Raman photon. If, by means of the radiative de-excitation process, the electron reaches a vibrational level characterized by a higher energy with respect to the original one, the emitted photon is called Stokes photon. In the opposite case, the emitted photon is called Anti-Stokes photon. It follows that, according to Bose-Einstein distribution, the emission of Stokes photons is much more probable with respect to the Anti-stokes counterpart. Being the energy difference between incident and Raman photon related to the material's vibrational transitions, which are peculiar for each molecule, Raman spectra can be appropriately considered as materials fingerprint.

This technique is highly efficient to analyse and distinguish carbon-based materials, due to its high sensitivity to carbon hybridization states and local order [18, 59–61]. Indeed, different carbon allotropes and nanomaterials show peculiar and well-defined Raman features, as reported in Fig. 1.10 [18].

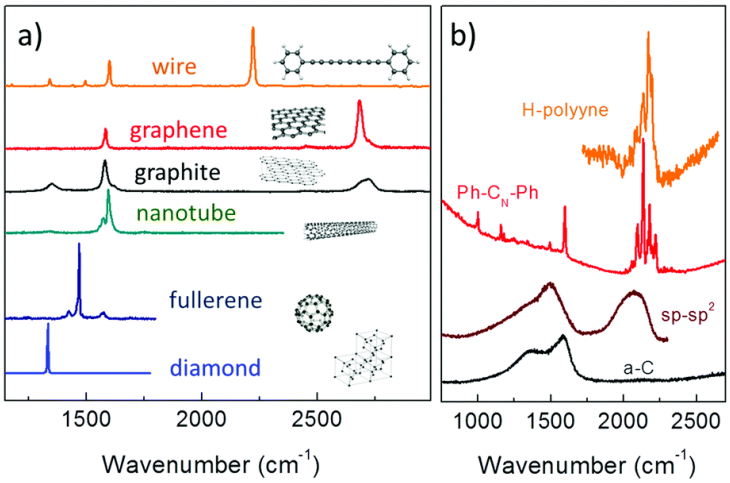

Figure 1.10: a) Experimental Raman spectra of all-carbon systems and (b) sp-carbon based moieties and wires [18].

Specifically considering sp-carbon chains, their main Raman feature is a very intense band, called "α line" or "ECC mode" (from the Effective Conjugation Coordinate model) lying in

the frequency region 1800-2300 cm^{-1} and consisting in BLA oscillation modes [18, 51, 59–61]. In particular, the ECC mode represents the collective stretching of all CC triple bonds and simultaneous shrinking of all CC single bonds. A secondary and less intense band, called β mode, can be observed at smaller wavenumbers, and is described by a different normal mode, corresponding to CC triple bonds out-of-phase stretching [18, 51, 59–61]. α line, in particular, can be interpreted on the basis of the longitudinal optical branches of the phonon dispersion relation of the infinite 1D crystal model described in Section 1.2, while β mode results from the relaxation of the ideal carbyne model, i.e. it exists only when considering the length and the termination of real finite CAWs. Similarly to the electronic properties, also the LO phonon branch is strongly modulated by the BLA parameter, i.e. to the degree of π-electron conjugation of the system. In accordance with DFT calculations computed by Lucotti *et al.*, Tabata *et al.* have shown experimentally that for finite polyynes an increase in chain length determines a prompt increase in the ECC mode intensity, due to the strong electron-phonon coupling, together with a red-shift of its frequency, consistent with an increase of π-electron conjugation [59, 61]. Contrarily, β mode shows a more irregular modulation upon changes in chains length and progressively vanishes approaching the limit of the infinite chain (Fig. 1.11). Indeed, the infinite chain model is characterized by only one collective vibration, i.e. the ECC or α mode.

When dealing specifically with polyynes produced by PLAL, as in the present thesis work, a limitation on the achievable concentration of the synthesized molecules must be taken into account, as mentioned in section 1.2.1. Hence, conventional Raman spectroscopy, given the low efficiency of the Raman process ($\approx 10^{-6}$), cannot provide the vibrational spectra of these poorly concentrated species. Surface Enhanced Raman Scattering, instead, combines Raman sensitivity to carbon hybridization with the electromagnetic and chemical interaction between the analyte and suitable metallic surfaces, typically noble metal nanoparticles, resulting in a great enhancement of the Raman signals. In the case of H-capped polyynes, it has been experimentally proved an enhancement factor of 10^6 with respect to normal Raman (Fig. 1.12) [6, 61, 62].

The electromagnetic SERS effect consists in the near-field enhancement of the Raman laser probe due to resonance with surface plasmons excited in metal nanoparticles. The chemical SERS effect, instead, consists in the charge transfer-induced formation of, in our case, polyynes-metal nanoparticles complexes, which further enhances the polyynic signal [63–69]. Polyynes interaction with silver nanoparticles is reported in many literature works [63–69]. As reported by Lucotti *et al.*, by comparing the "as prepared" SERS silver colloids, which show a plasmon resonance centered near 450 nm, with the plasmon band after mixing the colloid with polyynes, a red-shift and a broadening of the plasmon resonance

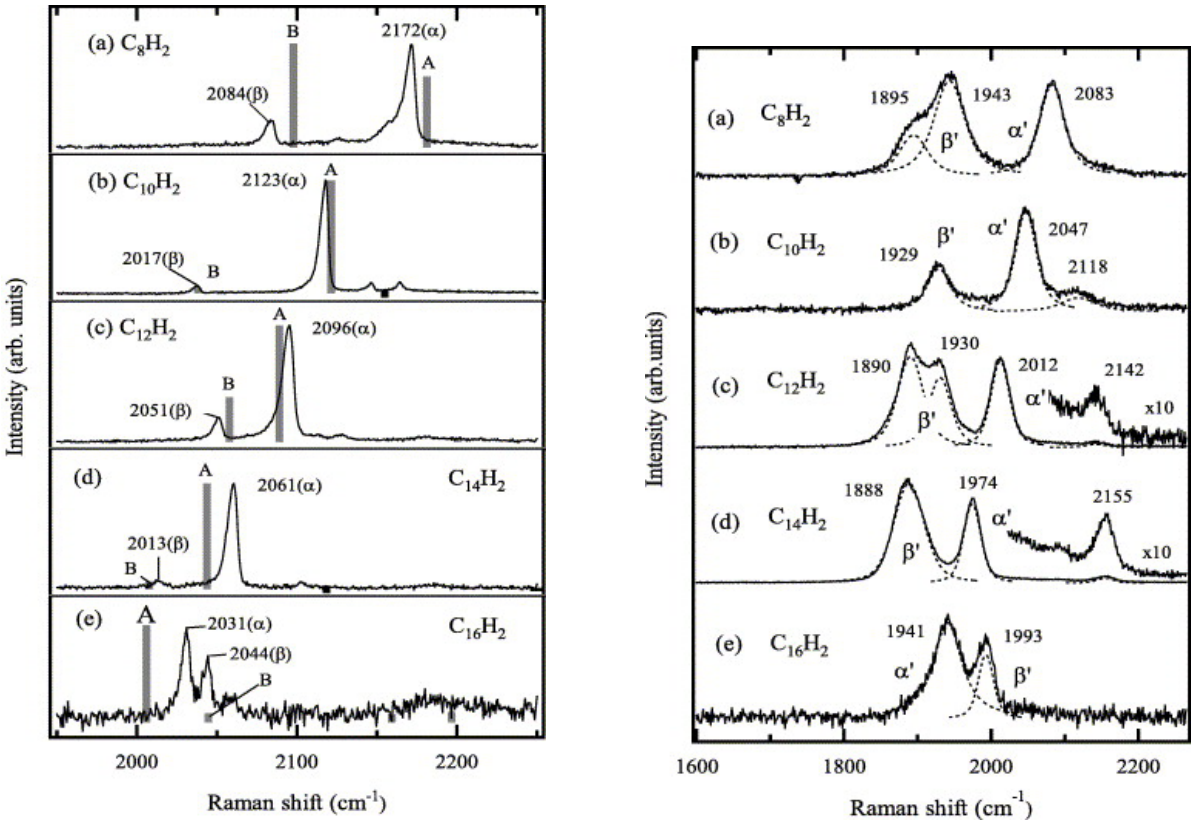

Figure 1.11: Raman spectra of size-selected H-capped polyynes and corresponding DFT calculated Raman active modes (A and B lines in left panel); SERS spectra of the same polyynes (right panel) [59].

peak occur [67]. Indeed, polyynes induce the aggregation of Ag nanoparticles affecting plasmon resonance, since a dipole coupling takes place when nanoparticles are brought at a close distance [67]. A broadening of the absorption spectrum is typically desired since it allows SERS measurements by excitation lines far from the plasmon resonance of pristine silver nanoparticles solutions [60, 67]. Moreover, the efficient interaction between polyynes and silver nanoparticles also justifies the experimentally observed increased stability of sp-carbon chains after their mixing [60].

The comparison between SERS and Raman spectra of hydrogen- and phenyl-capped polyynes, investigated both theoretically, by Milani *et al.*, and experimentally, by Casari *et al.*, highlights the appearance of new bands at frequencies lower than 2000 cm^{-1} and a broadening and red-shift of the ECC mode [6, 60] (Fig. 1.13).

A possible explanation for the appearance of these new bands, proposed by Lucotti *et al.*, is a very strong chemical interaction between polyynes and Ag nanoparticles [61,

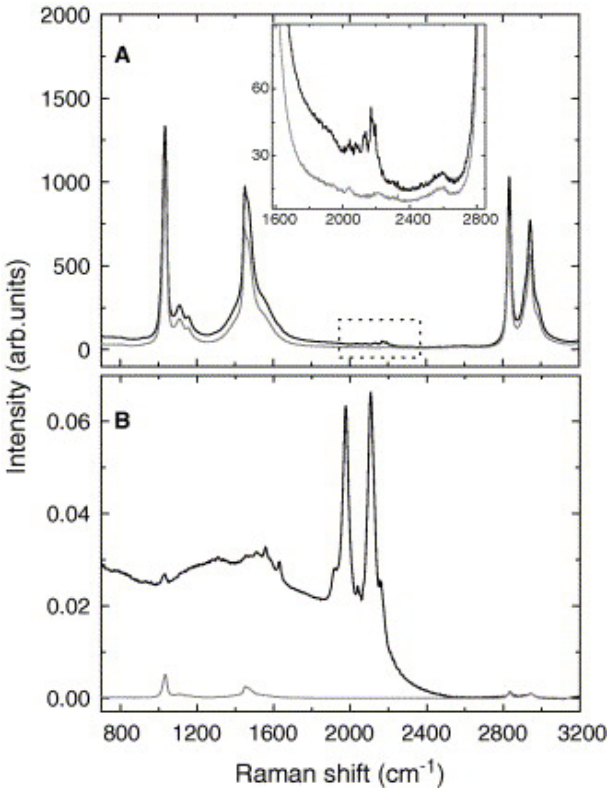

Figure 1.12: (A) Experimental Raman spectra of polyyne solution (black line) with a magnification of the 1800-2200 cm^{-1} region in the inset. (B) Experimental SERS spectra of polyyne solution (black line) [61].

67]. This has been also theoretically demonstrated by the thesis work of Zalla, who, indeed, by studying the interactions between Ag nanoparticles and polyynes, showed the effective appearance of low-frequency modes upon the Ag nanoparticle interaction with polyynes terminals [70]. According to another hypothesis, these bands result from the substitution of the hydrogen termination with silver, as a consequence of their strong chemical interaction [61, 67].

Compagnini et al., while studying polyynes-Ag nanoparticles interaction in polyynes mixtures, noticed the appearance of two bands at, respectively, 2130 and 1980 cm^{-1}, supposed to be due to nanowires adsorption onto silver nanoparticles, as also assumed by Tabata et al [59, 62]. In particular, the peak at 2130 cm^{-1} is thought to correspond to Ag/polyynes complexes, while the assignation of the peak at 1980 cm^{-1} is still under debate [59, 62]. Indeed, Lucotti et al. pointed out by DFT calculations that the existance of these complexes cannot be reproduced by theory [61]. Hence, different explanations for the 1980 cm^{-1} feature have been proposed: the presence of cumulenic sp-carbon chains in the mixture, and/or the formation of longer polyynes starting from shorter ones assisted by

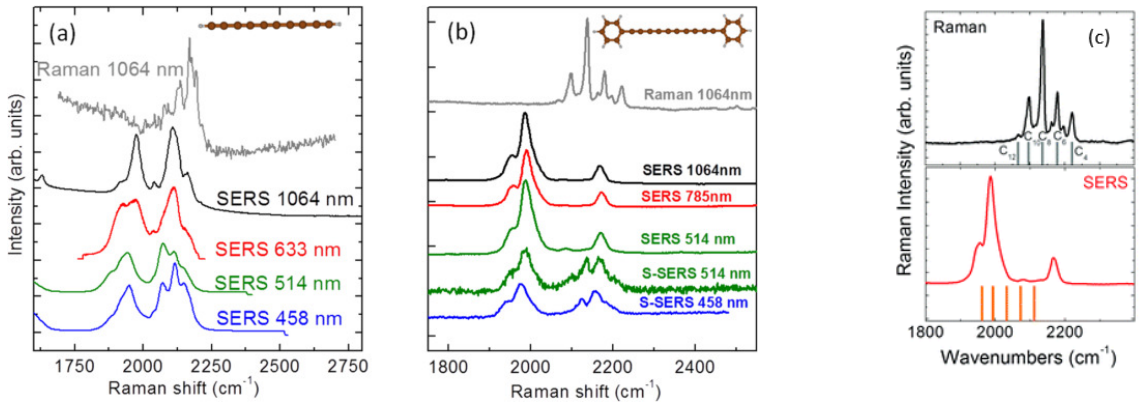

Figure 1.13: Raman and SERS spectra of H- (a) and phenyl-capped (b) polyynes solutions at different laser wavelengths. SERS on solid surfaces (S-SERS) of phenyl-capped polyynes are also reported [60]. Experimental Raman and SERS spectra (1064 nm) of phenyl-terminated polyynes. The DFT-calculated position of Raman peaks as a function of wire length is shown by the straight lines (c) [6].

the absorption on silver nanoparticles [62]. This last hypothesis is in accordance with Cataldo's experimental works on carbynoid structures synthesis [71].

1.4.3. High Performance Liquid Chromatography

High-performance liquid chromatography (HPLC) is a powerful analytical technique that not only permits an accurate detection of the species present into an analysed solution in terms of both their chemical nature and concentration, but also determines the possibility to separate and collect them for further characterization. Specifically in case of polyynes produced by PLAL, HPLC allows to distinguish them, in terms of lengths and terminations, and permits their separation from the original mixture. HPLC is performed through a sophisticated apparatus whose most important components are the packed columns, the high-performance pumps and the detection system (Fig. 1.14).

After the injection of the investigated solution in the system, a continuous flow of solvent is delivered by the pump through the column, from which the different analytes in the solution are gradually separated and eluted depending on their degree of interaction with both the stationary and the mobile phase, which are namely the column packing material and the pump-delivered solvent. Finally, a detection system, constituted in our case by a photodiode array (DAD) UV-vis spectrometer, allows to individuate the differently eluted species present in the sample depending on their distinctive absorption spectrum

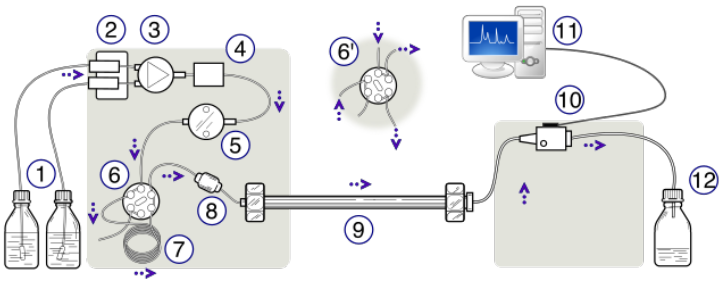

Figure 1.14: Schematic representation of an HPLC unit. The most important features follow: solvent reservoirs(1) and degasser(2), gradient valve(3), mixing vessel for mobile phase delivery(4), high-pressure pump(5), injection valve (6), sample injection loop(7), Pre-column(8), Analytical column(9), detector(10), data acquisition(11), waste collector (12), fraction collector (not shown here) [72].

[51] (Fig. 1.15). Other techniques used to detect and distinguish the different analytes are mass spectroscopy, fluorescence spectroscopy and differential refraction.

A fundamental parameter that enables species differentiation during elution is the so-called "retention time", which is the time needed for a specific analyte to be eluted. This parameter depends on both chemical and physical interactions between the analyte and the stationary and mobile phases: in particular, chemical interaction is here intended as the affinity, in terms of polarity, between the analyte and the two phases, while physical interaction consists in the interplay between the dimension of the pores and that of the analyte. Considering the stationary phase, HPLC columns are packed with porous silica particles, but capping molecules can be adopted for their functionalization in order to tune their interaction with the analysed sample. On the other hand, the mobile phase is typically constituted by a mixture of solvents, and its composition can be either maintained constant during the whole run ("isocratic mode") or it can be changed during the analysis through a controlled variation of the percentage of each solvent present into it ("gradient mode").

Polyynes characterization via HPLC is typically performed in a "reverse-phase" configuration, characterized by an apolar stationary phase and a polar mobile phase [51, 73–75]. The apolarity of the stationary phase is achieved by functionalization with hydrophobic alkyl chains such as, typically, C_8 or C_{18} [51, 73, 75, 76], while the polar mobile phase is typically an aqueous mixture with some water-miscible organic solvent [51, 73, 75, 76]. This configuration exploits the principle "like dissolves like", indeed it promotes an efficient interaction between the stationary phase and polyynes, being both apolar, increasing the resolution power of HPLC thanks to their small tendency to be rapidly eluted by the

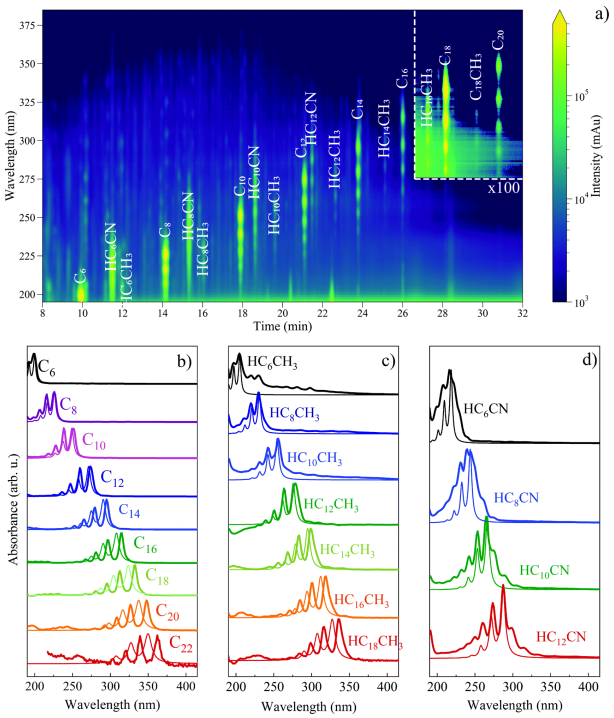

Figure 1.15: (a) Polyynes separation by means of reverse-phase-HPLC and corresponding retention times extracted from DAD coupled with the HPLC system. Experimental (thick lines) and predicted (thin lines) UV-vis spectra of (b) H-polyynes, (c) CH_3-polyynes and (d) CN-polyynes produced by PLAL [51].

interaction with the polar mobile phase. As previously introduced, not only the chemical interactions are responsible for polyynes separation, but also their molecular size: longer chains or chains with bulkier endgroups, and so higher molecular weights, are eluted later [51]. Finally, another advantage of using HPLC for polyynes characterization is the possibility to concentrate them by the proper method optimization, as reported in Peggiani et al. recent work on polyynes in aqueous solution [77].

1.5. CAWs instability and stabilization strategies

Despite the huge effort put in last decades to artificially synthesize the carbyne crystal, this result has not been achieved yet. The main obstacle on the way from polyynes to carbyne lies in their high instability, which becomes larger and larger for increasing chains length [18, 60]. The two main sources of CAWs degradation are crosslinking and oxidation reactions [18, 78]. Moreover, polyynes stability is lost upon exposure to light or thermal treatments [69]. In particular, crosslinking occurs between CC triple bonds of adjacent chains and determines the transition from the polyynic configuration to a more

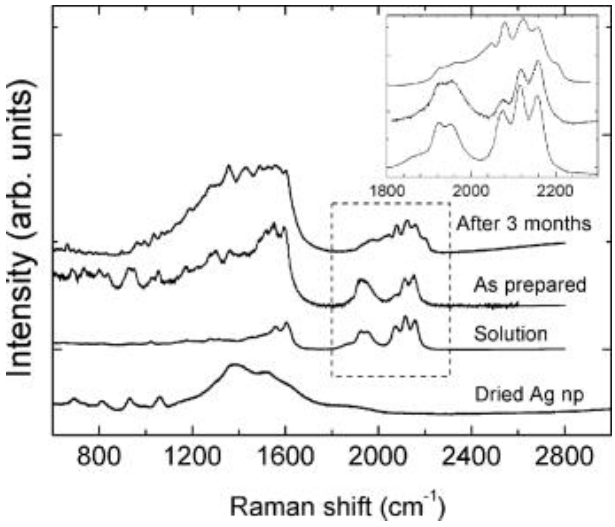

Figure 1.16: SERS spectra of sp-carbon chains in solution and in solid Ag nanoparticle agglomerate, as prepared and after 3 months. The inset of the dashed spectral region is also shown [69].

stable carbon form, namely sp^2 or amorphous carbon. Actually, improved stability of isolated CAWs in liquid environments has been demonstrated, indeed liquids reduce the interactions among chains and oxidative agents [18, 51]. Improving their stability also in dried conditions, however, is fundamental in view of technological applications.

Many strategies have been proposed to reach this goal. The use of bulky endgroups [51, 73, 75, 79, 80] reduces the probability of chains interaction by means of their steric hindrance, and this strategy allowed Tykwinski and co-workers to successfully synthesize the longest isolated polyyne with 48 carbon atoms [81]. The addition of silver nanoparticles to the polyynic solution seems to efficiently embed them in nanoparticle aggregates and stabilize them for long time periods (Fig. 1.16) [60, 69]. Chains protection by means of carbon nanotubes permitted the achievement and stabilization of very long wires. By exploiting this strategy, indeed, Shi and co-workers managed to obtain the longest CAWs ever synthesized, reaching a length of 6000 carbon atoms [82]. Rotaxination, where an isolated polyyne is encapsulated as part of a rotaxane, grant the protection of CAWs by a surrounding macrocyclic ring [83]. Finally, the incorporation of polyynes in solid matrices seems to be a valid method to increase their stability over time. In particular, several studies have been conducted on polyynes embedding through polymeric matrices [50, 63], gel-like structures [84] or even anodized alumina membranes [85], showing the capability of these methods to increase polyynes stability up to several weeks or even months.

Together with the huge effort put in finding ways to improve polyynes stability in dried conditions at room temperature, in view of technological applications, it is fundamental

to study and optimize polyynes thermal stability. Only very few papers can be found in literature about the investigation on polyynes thermal behaviour [64, 86], and still no studies have been conducted to observe the effect of polyynes length and terminations on their thermal stability. Hence, this will be the main goal of this experimental thesis.

2 | CAWs-polymer nanocomposites

The first report about polymeric nanocomposites can be dated back to the 1980s and, from that time on, the interest in their development and properties improvement grew up constantly [87]. With the name "polymeric nanocomposite" it is intended a multi-component system where a polymeric matrix embeds a nanometric filler, i.e. having at least one dimension below 100 nm. The need for the development of such systems can be found in the outstanding properties enhancement that results from the combination of polymers' flexibility, low density and processability with the quantum confinement effect provided by the nanometric fillers [87]. Indeed, despite their interesting properties, polymers lack in mechanical strength, thus resulting unusable in most advanced engineering applications. Thanks to their peculiar dimensions, even a small amount of nanometric filler permits to obtain a remarkable enhancement of polymers toughness without sacrificing their stiffness, due to the large improvement in the load transfer between matrix and filler given by their huge interfacial area [88]. The advantages of these systems are not limited to their mechanical properties, indeed, also polymer transport properties and stability over oxidative phenomena are positively affected [89]. Specifically considering electrical transport properties, a special mention is deserved by carbon-based nanofillers, with conductivity values more than 100 times higher with respect to traditional fillers [87].

While many works can be found in literature about the use of carbon nanotubes as nanometric filler in polymer nanocomposites [89], still only very few reports have been published about the embedding of carbon atomic wires in solid polymeric matrices. While all the previously synthesized carbon-polymer systems had the main goal to enhance matrix performances through the intercalation of a carbonaceous filler inside it, CAWs-polymer nanocomposites have been synthesized with the main purpose of stabilizing sp-carbon chains [50, 63]. Indeed, the presence of a matrix material prevents the chains crosslinking that would instead determine the already described sp-sp^2 transition. Hence, in CAWs-polymer nanocomposite systems a mutual benefit is established between the matrix, which profits from the properties enhancement provided by the nanometric filler, and the filler itself, in this case constituted by the sp-carbon chains, whose stability is

highly improved by the presence of the polymeric material.

2.1. Polymeric nanocomposites as a route to polyynes stabilization

All the case studies reported in literature about polyynes-polymer nanocomposites demonstrate the efficiency of these systems in enhancing polyynes stability in time, even up to several months [50], and this section is devoted to clarify this aspect.

The first successful attempt to stabilize polyynes through their inclusion into a polymeric matrix can be ascribed to Okada *et al.*, who realized Poly(vinyl alcohol) nanocomposite films embedding Ag-polyynes complexes [63]. In particular, this was achieved by firstly mixing, in a volume ratio of 1:4, a polyynes solution with an Ag colloidal solution, both obtained via laser ablation in liquid, and then by dissolving the PVA inside the mixture itself by heating. Finally, the composite solution was cooled down and casted on a glass substrate. Once deposited and let dry, the synthesized nanocomposite films have been characterized via UV-Vis and SERS spectroscopy in order to proof the effective encapsulation of polyynes, and both tests confirmed the desired result [63]. In particular, by comparing the SERS spectrum of an as prepared film containing only PVA and Ag with the corresponding film containing also the polyynes it can be clearly seen the appearance of two bands in the region 1800-2200 cm^{-1}, corresponding to the already mentioned CC stretching vibrational modes of sp-carbon chains [63] (Fig. 2.1). In the same plot it can

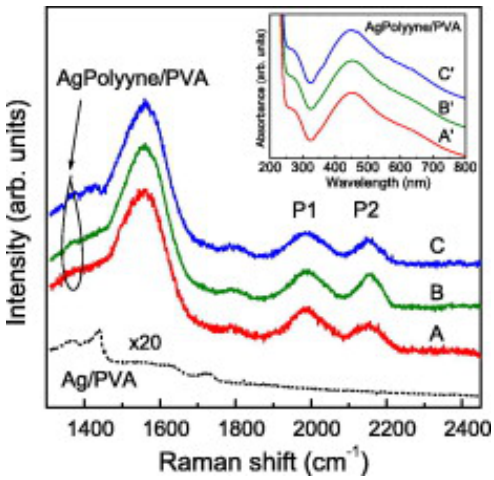

Figure 2.1: Raman spectrum of an as-prepared Ag nanoparticles/PVA film (dashed line) and SERS spectrum of an Ag/polyynes/PVA film monitored in time (lines from A to B to C correspond to the as-prepared film, the film after one week and after 1 month) [63].

be also seen the efficient polyynes stabilization in the polymeric matrix up to one month. Indeed, by monitoring the SERS spectrum of the synthesized film in time and comparing it to the one of a film containing only Ag nanoparticles and PVA [63], it is possible to see that the intensity of the peaks attributed to sp-carbon chains remains almost unchanged from the first spectral acquisition, carried out just after the film obtainment, till the last one, performed after one month (Fig. 2.1).

More recently, An *et al.* realized PVA nanocomposite films embedding size-selected H-polyynes adsorbed on Au nanoparticles [64]. Contrarily to the procedure adopted by Okada group, the authors used a chemical reduction method for the synthesis of Au colloids. Also in this case, after mixing the two solutions and dissolving PVA granules inside it by heating, nanocomposite films were obtained via casting of the prepared solution upon a glass substrate. In agreement with Okada experiments [63], also in this case the inclusion of polyynes in the composite solution determines the appearance of the typical broad bands, here called α and β features, in the region 1800-2200 cm^{-1}, meaning that the successful intercalation of sp-carbon chains occurred [64] (Fig. 2.2). Polyynes spectral features are still visible after six months, demonstrating also in this case their stabilization inside the PVA matrix [64].

This work took a step forward in polyynes-polymer nanocomposites characterization, indeed, differently from the experiments carried on by Okada *et al.*, polyynes have been

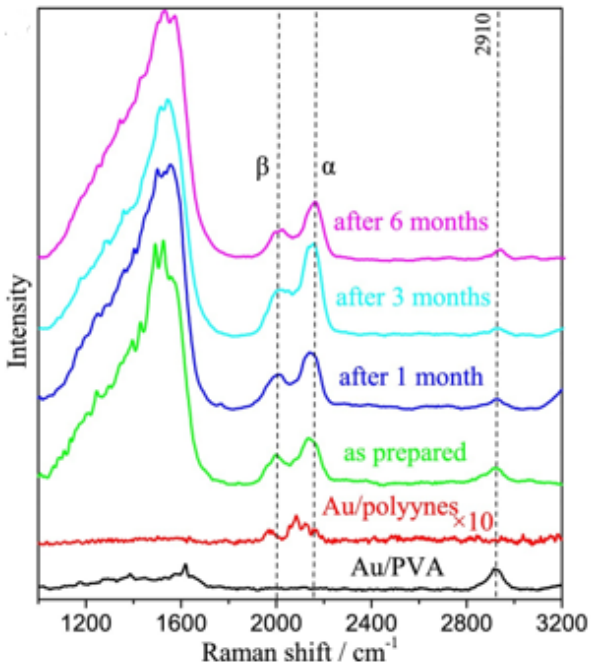

Figure 2.2: SERS spectra of Au/polyynes/PVA film monitored in time [64].

size-selected via HPLC, thus permitting a proper peaks attribution and, consequently, a better understanding of sp-carbon chains stability based on their length. In particular, by monitoring the time evolution of SERS signals of the size-selected polyynes inside the PVA film, it was observed that longer polyynes are less stable than shorter ones [64] (Fig. 2.3). The intensity of the SERS signals attributed to the different polyynes decreases with a different velocity depending on the chain length: after six months, both the C_8H_2 and $C_{10}H_2$ signals can still be clearly seen, while the $C_{12}H_2$ signals have almost vanished.

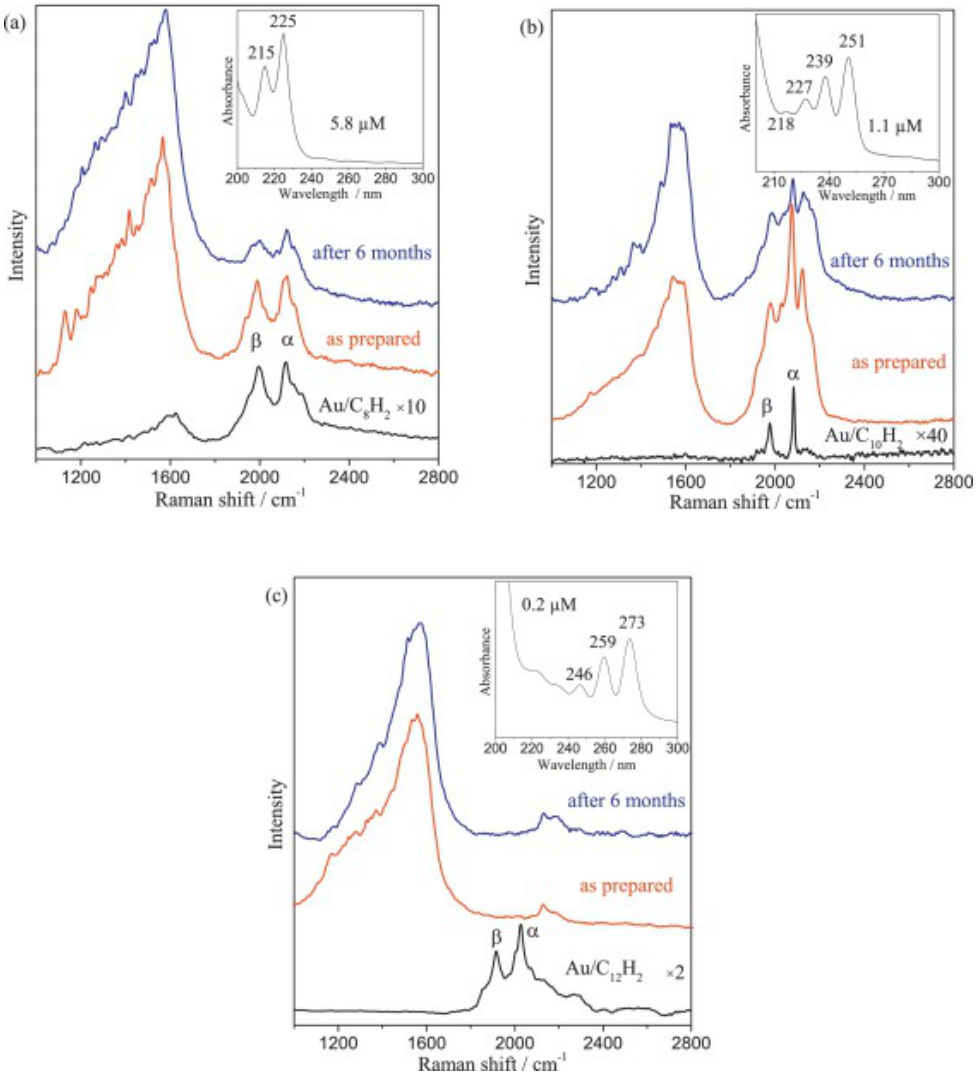

Figure 2.3: SERS spectra of (a) C_8H_2, (b) $C_{10}H_2$ and (c) $C_{12}H_2$ under different conditions: in Au colloids (black line), as prepared Au/C_8H_2 or $C_{10}H_2$/PVA film (red line) and PVA films after 6 months (blue line) [64].

Thermal stability of the analysed size-selected polyynes has been investigated as well: Fig. 2.3 shows also the compared SERS spectrum of polyynes in the Au colloidal solution with the corresponding spectrum in the PVA film, i.e. before and after the heating process

necessary for the PVA granules dissolution [64]. Also in this case, the shortest chain (C_8H_2) shows a better thermal stability with respect to the longer ones. Indeed, passing from $C_{10}H_2$ colloidal solution to the corresponding film, there's the appearance of new spectral features at higher wavenumbers, thought to be due to the partial dissociation of the $C_{10}H_2$ chain into shorter sp-carbon chains which can form other structures by reacting with Au nanoparticles [64]. These hypothesized dissociation phenomena, that in turns are due to the poor thermal stability of longer sp-carbon chains, is also confirmed by Tabata *et al.*, who assumes that bands shifted at higher wavenumbers are characteristic of shorter polyynes [59]. In another work, published by Sata *et al.*, laser ablated size-selected H-polyynes are introduced inside a PVA film by dipping the film itself into a solution containing the sp-carbon chains [90]. Then, polyynes themselves are aligned inside the film through the application of a tensile load and the angular dependence of absorption intensity of these systems is investigated by means of a rotatable linearly polarized UV light source [90].

Finally, the most recent advances in polyynes-polymer nanocomposites synthesis can be ascribed to Peggiani *et al.*, who indeed developed, in 2020, an *in-situ* one-step PLAL method that allows polyynes production directly inside an aqueous solution of PVA. By

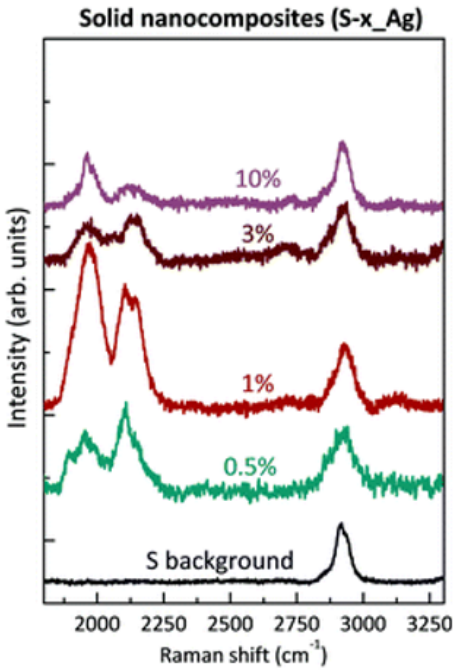

Figure 2.4: SERS spectra of Ag/PVA/polyynes nanocomposites at different weight percentages of PVA in the pristine solutions. In black, the Raman spectrum of an all-PVA film (S background) [50].

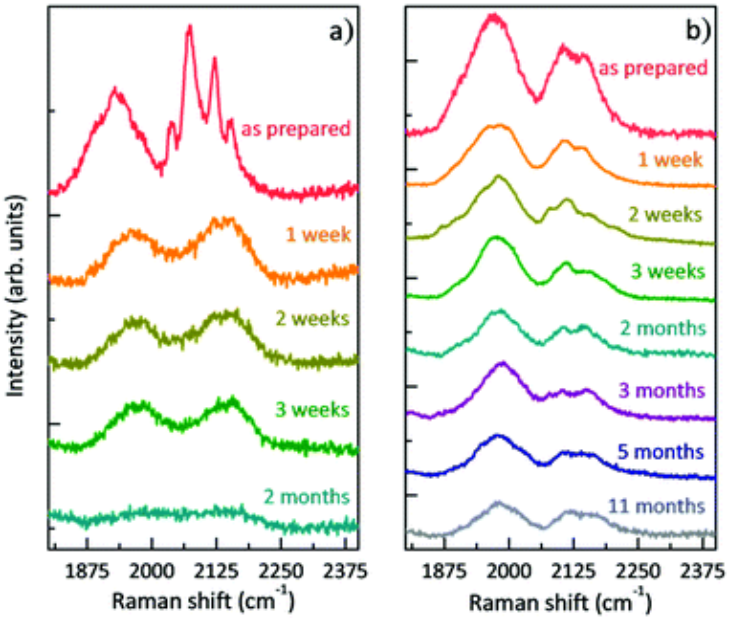

Figure 2.5: SERS spectra of (a) Ag/polyynes/PVA solution and (b) Ag/polyynes/PVA film monitored in time [50].

means of this innovative technique, it is possible to both avoid post-processing procedures, such as the dissolution of polymer granules by heating that could compromise polyynes integrity, and ensure the complete blending between polyynes, polymer, and Ag nanoparticles, lastly added to the PVA/polyynes solution before film casting [49, 50]. Also in this case, the presence of polyynes within the polymeric film can be clearly seen by looking at the compared SERS spectra of a pure PVA film and Ag/PVA/polyynes films [50] (Fig. 2.4). The plot also shows the effect of the change in PVA weight percentage on polyynes production efficiency. As can be seen, the trend reaches a maximum in correspondence with the PVA1% solution, but, when the PVA percentage is furtherly increased, the trend is inverted, and a lower polyynes production efficiency is obtained. A possible explanation can be found by looking at the viscosity of the PVA/water ablation solution. Indeed, if, on one side, a high viscosity contributes to the plasma confinement, and so is expected to promote sp-carbon chains formation, on the other side it hinders the mobility of the already formed chains, forcing them in the plasma region and so determining their eventual thermal degradation [50].

In the same work, by monitoring the evolution in time of the SERS spectrum of the Ag/polyynes/PVA nanocomposite film, normalized with respect to the PVA peak centered at 2910 cm^{-1}, Peggiani noticed that, after a decrease in the intensity of the polyynic signal of about 50% during the first week, it remained substantially unchanged during the following 11 months [50] (Fig. 2.5).

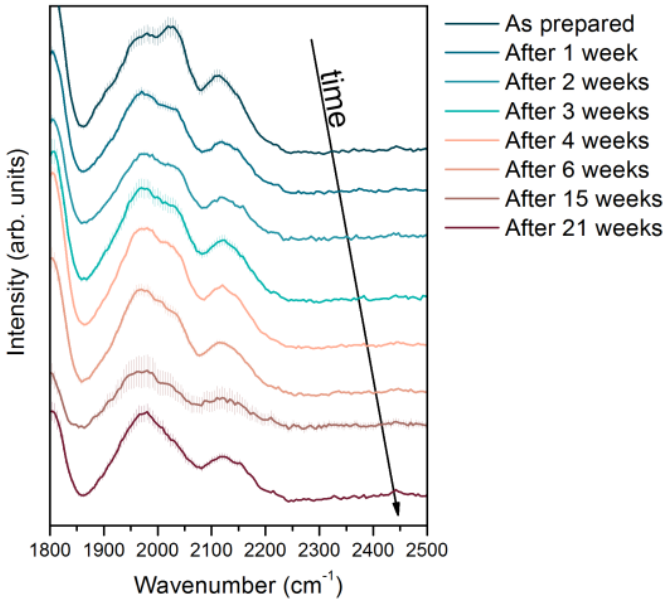

Figure 2.6: Time evolution of SERS spectra for PMMA/polyynes films with Ag NPs as SERS-active substrate [92]

Peggiani and coworkers have also tested for the first time the use of Polymethyl methacrylate (PMMA) as polymeric matrix for the production of polyynes-polymer nanocomposites films [91]. For this purpose, a two-step ablation was carried on: in the first step an Ag colloid was generated by laser ablation of a silver pellet in a PMMA/acetone solution, while in the second step polyynes were produced inside the previous solution by laser ablation of a graphite pellet. Once deposited and let dry, the Ag/polyynes/PMMA nanocomposite films were characterized through SERS spectroscopy, and also in this case the collected spectra show clearly the presence of the sp-carbon chains bands in the region 1800-2200 cm^{-1} [49, 91]. The efficient polyynes stabilization inside these nanocomposites was demonstrated by monitoring their SERS signals in time, which indeed remained visible for at least 5 months [49, 91]. Similar results have been obtained by Sala, who indeed has proven polyynes stability within a PMMA matrix for 21 weeks by adopting Ag nanoparticles as SERS-active substrate (see Fig. 2.6) [92].

Together with the fundamental role played by the nanocomposites polymeric matrix in polyynes stabilization, a special mention must be devoted also to the effect of metal nanoparticles, and the following section will clarify this aspect.

2.2. The role of noble metal nanoparticles in CAWs nanocomposites

PLAL-synthesized polyynes are typically characterized by a very low concentration with respect to the ones that can be produced by means of chemical methods. Hence, as mentioned in Chapter 1, to perform their characterization, SERS technique is usually adopted. By exploiting both electromagnetic and chemical interactions between metal nanoparticles and polyynes, it allows to achieve huge signals enhancement, making possible polyynes detection and identification even if present in very small amounts. It is clear that metal nanoparticles play the major role in SERS enhancement effect for sp-carbon chains. Indeed, the intrinsic low efficiency of Raman scattering, typically around 10^{-29}-10^{-31} $cm^2/molecule$, can be strongly improved if polyynes are close to metal nanoparticles [93]: considering the electromagnetic SERS effect, the field enhancement distribution at the surface of a metal nanoparticle is mainly localized in a small region called "hot spot", structurally identified as a nanogap between adjacent nanoparticles which allow a very efficient amplification of optical signals [94].

However, metal nanoparticles are not only fundamental in polyynes SERS characterization but also in their stabilization. There are many works in literature reporting about the aggregation of metal nanoparticles upon the addition of sp-carbon chains to metal colloidal solutions [63–68]. The occurrence of these aggregation phenomena has been experimentally demonstrated by both UV-Vis measurements [63–68] and TEM images [63, 64, 68].

Okada *et al.*, by comparing the UV-Vis absorption spectrum of an Ag/PVA film with the corresponding one containing also polyynes, noticed a red-shift and a broadening of the nanoparticle surface plasmon resonance band [63]), attributed to their agglomeration. This hypothesis has been furtherly proved by the comparison between TEM images of the Ag/PVA and Ag/polyynes/PVA films (Fig. 2.7) [63]. Also, Lucotti *et al.* observed the same aggregation phenomenon by analysing the UV-vis absorption spectrum of a silver colloid before and after its mixing with a polyynes solution [67].

Similar evidence has been also highlighted by the work of An *et al.* when mixing polyynes solution with Au colloid [64]. As already mentioned in the previous section, this work also investigates polyynes thermal stability through the comparison of the SERS spectra of, respectively, Au/polyynes solution and the Au/polyynes/PVA film. By means of their deconvolution via Lorentzian fit, a shift in the polyynic bands can be observed moving from the solution to the film (Fig. 2.8). According to the studies of Compagnini *et al.* [62],

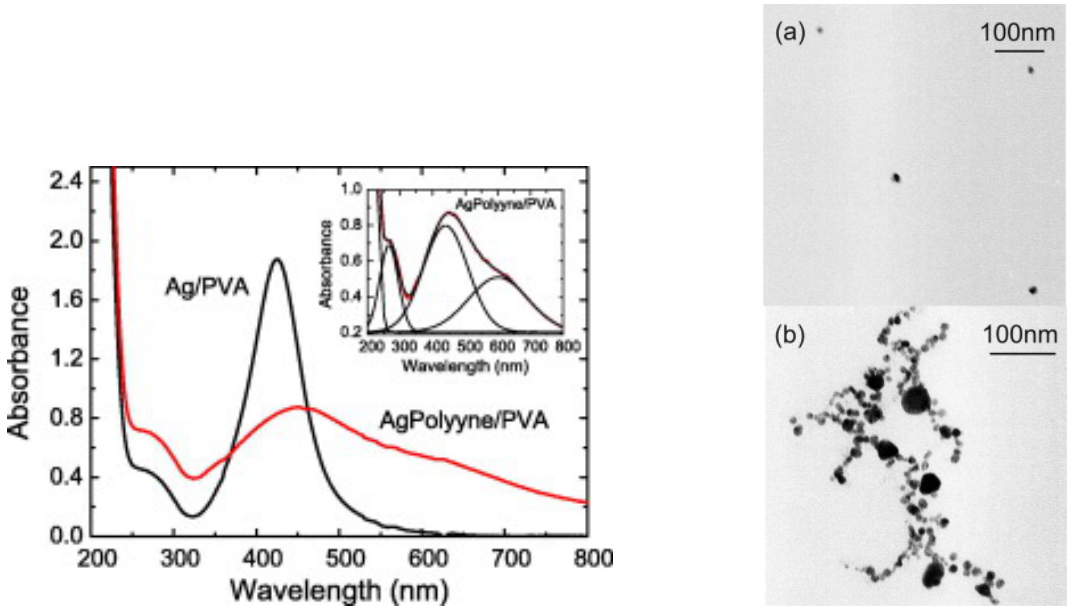

Figure 2.7: (left panel) UV–Vis absorption spectra for Ag/PVA (black line) and AgPolyyne/PVA (red line) films. (right panel) TEM images of Ag/PVA (a) and Ag/Polyynes/PVA (b) films showing nanoparticles aggregates [63].

this can be attributed to the enhanced chemical interaction between metal nanoparticles and polyynes at high temperatures, i.e. the ones reached during PVA granules dissolution.

The aggregation of metal nanoparticles determined by the presence of sp-carbon chains

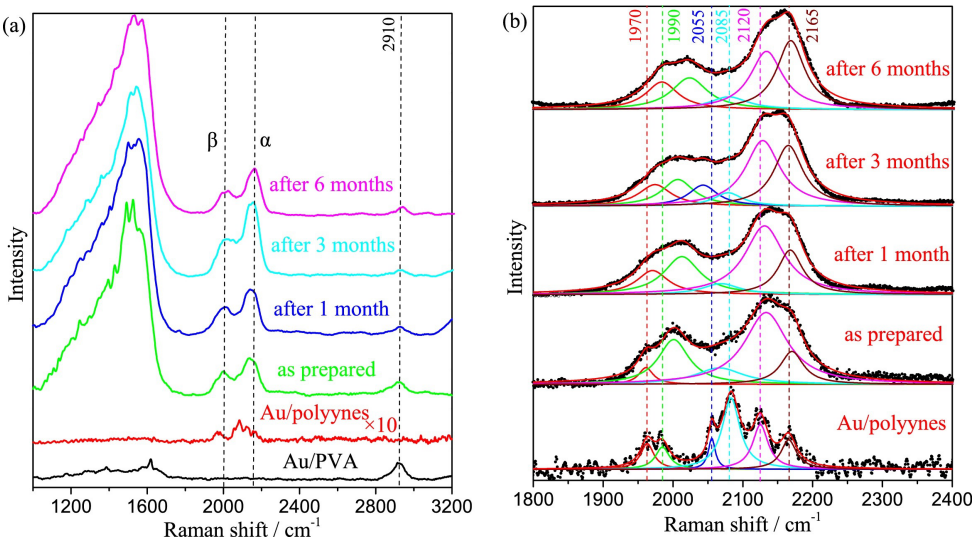

Figure 2.8: (a) SERS spectra of Au/polyynes/PVA film monitored in time and (b) their deconvolution via Lorentzian fit [64].

not only is of crucial importance in the exploitation of SERS enhancement effect, but it also represents a further stabilization strategy for polyynes. This has been demonstrated by Casari *et al.*, who indeed obtained a long-term stabilization (up to 3 months) of polyynes entrapped into a solid assembly of Ag nanoparticles at ambient conditions [69]. In particular, it is thought that, by establishing chemical bonds with silver, the electronic configuration of sp-carbon chains can be stabilized, thus preventing the cross-linking phenomenon and so the sp-to-sp^2 transition [69]. This stabilizing effect takes place also when dealing with Ag/polyynes/polymer nanocomposites. Hence, in this case, the enhancement of polyynes stability is doubled, as it takes advantage of the simultaneous contributions provided by both the polymeric matrix and the nanoparticles.

2.3. Thesis objectives

In this thesis work, the effect of polyynes length and termination on thermal stability of Ag/polyynes/PVA nanocomposite films has been investigated for the first time. The choice of poly(vinyl alcohol) as a matrix is to be ascribed to its low-cost, chemical stability, water solubility, processing ease, film formation properties, compatibility with Ag nanoparticles and good thermal stability above its glass transition temperature. Ag nanoparticles have been introduced due to their fundamental role as both SERS-enhancers and polyynes stabilizers.

Differently from other works, PVA granules have been dissolved directly during the silver colloid synthesis, which has been performed following the Lee-Meisel method [95]. Polyynes, on the other side, have been synthesized by PLAL and then separated via HPLC. In particular, different solvents have been adopted in order to produce the desired polyynes endgroups, namely hydrogen and chlorine atoms. The final nanocomposite solution has been obtained by mixing the polymeric solution, already embedding the Ag nanoparticles, with the size- and termination-selected polyynic solution.

The first part of the work is ascribed to the optimization of the nanocomposite films geometry, chemical composition and SERS measurements parameters. The second part is focused on the development of a methodology aimed at studying Ag/PVA/polyynes thermal behaviour by an *in-situ* SERS mapping process coupled to the use of a Peltier thermoelectric modulus. This, indeed, permitted to study the effect of polyynes length and termination on nanocomposites thermal stability. Also the degradative effect of the laser on the nanocomposite films has been investigated.

3 | Materials and Methods

In this chapter, materials and methods adopted for the synthesis and characterization of Ag/PVA/polyynes nanocomposite films are described. In particular, polyynes mixtures have been produced, characterized and separated by means of, respectively, pulsed laser ablation in liquid, UV-Vis absorption spectroscopy and high performance liquid chromatography. UV-Vis absorption spectroscopy has also been used for characterizing the Ag/PVA solution. Indeed, Ag nanoparticles have been synthesized via Lee-Meisel method [95], here implemented by the simultaneous dissolution of polymer granules within the colloid being formed, resulting in a final PVA solution already embedding the metal nanoparticles, called from now on "Ag/PVA solution".

3.1. Materials

3.1.1. Solvents

In this experimental thesis, both organic and inorganic solvents were employed. The organic ones, namely isopropyl-alcohol (i-PrOH), dichloromethane (DMC), acetonitrile (MeCN) and cyclohexane, all purchased by Sigma Aldrich, were characterized by a purity $\geq$ 99.9%. Milli-Q deionized water, with a conductance of 0.055 μS, was the only non-organic solvent adopted. As mentioned in Chapter 1, in order to maximize the yield and performances of PLAL and HPLC processes, the selection of a proper liquid medium is of crucial importance. This choice implies finding the best compromise between many different solvents properties, namely their density, viscosity, refractive index and polarity.

The chemical structures of the organic solvents adopted in this work are shown in Fig. 3.1.

3.1.2. Targets

The majority of the works reported in literature about polyynes synthesis via pulsed laser ablation in liquid, adopt graphite targets as main source of sp-carbon chains. The choice of this kind of target can be justified by its eco-friendly nature, non-toxicity and high

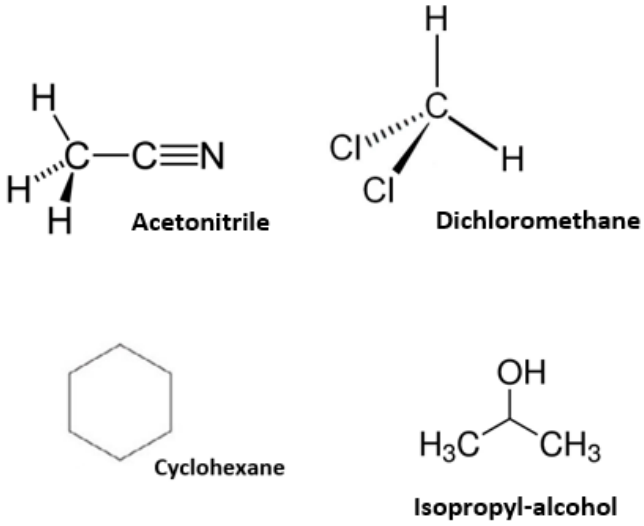

Figure 3.1: Chemical structure of the organic solvents employed in this work.

yield in providing sp-carbon when irradiated by the high-power laser. For these reasons, also in this work graphite planar targets, with a diameter of 15 mm and a thickness of 3 mm, have been used. In particular, their geometry has been selected in order to match the one of the vials adopted for the PLAL process, in such a way to reduce as much as possible the target displacements during the ablation itself.

3.1.3. Polymer

In this work, Polyvinyl alcohol (PVA) has been selected as thermoplastic polymeric matrix for the nanocomposite films synthesis (Fig. 3.2). This choice is justified by its high efficiency in stabilizing polyynes for even very long times at ambient conditions (see Chapter 2), its water solubility, which indeed is of crucial importance to produce colloidal solutions with Ag nanoparticles, its high filmability, non-toxicity and glass transition temperature (about 85°C), adequate for our purposes. The latter, in particular, is a fundamental requirement when performing thermal stability tests on polymeric nanocomposite films, as in fact it permits to reach even high temperatures without detrimental effects on the structural stability of the polymeric matrix. For this reason, this property it is crucial in the present work, where thermal stability of size- and termination-selected polyynes embedded in PVA nanocomposite films is investigated. Specifically, PVA with a molecular

weight of 130000 $g\ mol^{-1}$ and a degree of polymerization of 2700 was employed.

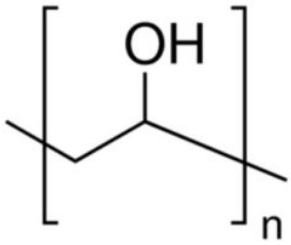

Figure 3.2: Chemical structure of Polyvinyl alcohol (PVA).

Another crucial aspect sustaining the choice of PVA as polymeric matrix concerns nanocomposite films characterization by SERS spectroscopy. Indeed, any of the main Raman spectral feature of PVA, like the intense CH bond stretching between 2800-3000 cm^{-1} (Fig. 3.3), do not overlap with the fingerprint signals of polyynes, lying in the 1800-2200 cm^{-1} region (see Section 1.4.2). This is for sure desired to properly distinguish and monitor the different components of the analysed nanocomposite film, namely the polyynes and the polymeric matrix.

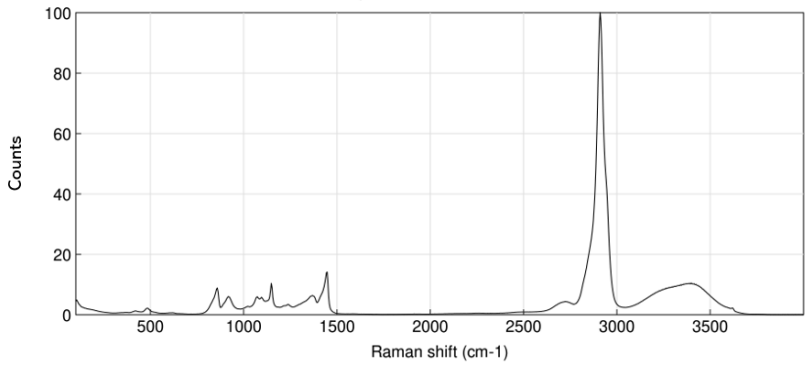

Figure 3.3: PVA Raman spectrum.

3.2. Films synthesis and deposition

3.2.1. Silver colloid synthesis

Ag nanoparticles are a fundamental component of the nanocomposite films studied in this work. Indeed, as already described in Section 2.2, they play a double-key role, acting as both polyynes stabilizers and SERS-enhancers. One of the most widespread experimental procedures for their synthesis is the so called "Lee-Meisel" method [95].

This technique consists, firstly, in the introduction of a silver precursor in an aqueous solution, that results in the release of Ag^+ ions. Subsequently, a reducing agent is added to the solution contributing to the ions reduction into their metallic counterpart, forming the silver nanoparticles, whose precipitation is hindered by a thin capping layer made of apposite surfactant agents [95, 96]. Specifically referring to the present work, silver nitrate ($AgNO_3$) has been employed has silver precursor, while sodium citrate has been used as both the reducing and surfactant agent.

The main advantages of the Lee-Meisel method are its simplicity, the use of a biocompatible reductant and stabilizing agent (sodium citrate), together with the possibility to further functionalize the capping citrate layer itself with other groups [97]. Another advantage of this technique is related to the reduced thickness of the nanoparticles capping layer, that indeed ensures an efficient enhancement of Raman signals [96, 98, 99].

On the other hand, Lee-Meisel method disadvantages are related to the challenging task of controlling Ag nanoparticles nucleation in water, due to the high reactivity of silver precursors in such environment, especially at high temperatures [96, 97]. As a consequence, Ag nanoparticles synthesized via Lee-Meisel method typically exhibit various morphologies and a broad polydispersity [97, 100].

3.2.2. Pulsed Laser Ablation in Liquids (PLAL)

In this experimental work, polyynes have been synthesized via pulsed laser ablation in liquid, whose setup is shown in Fig. 3.4. In particular, the apparatus is equipped with a Quantel Q-switched ns-pulsed Nd:YAG laser with a repetition rate of 10 Hz and a pulse duration of 6 ns. Its path towards the target is clearly visible in Fig. 3.4.

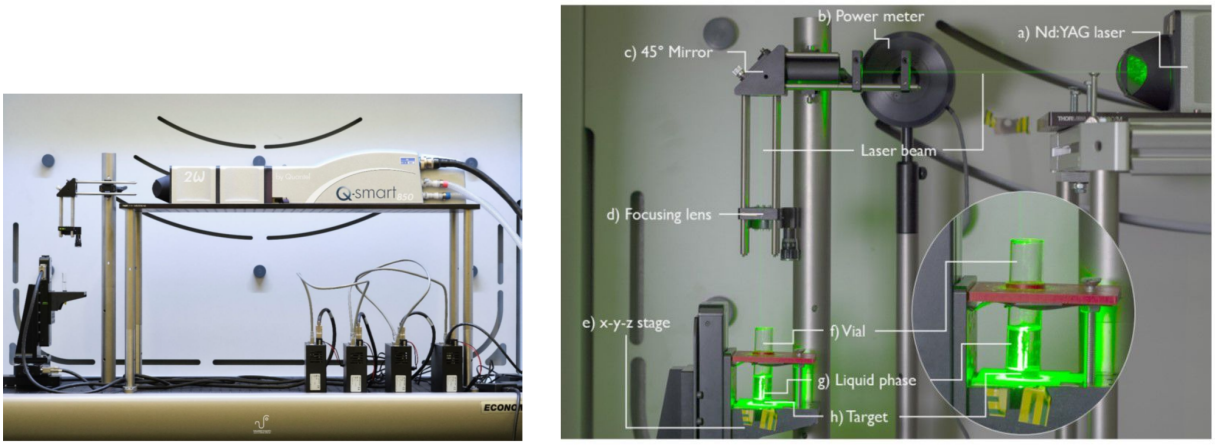

Figure 3.4: On the left, the PLAL setup. On the right, the laser path towards the graphite target [101].

Once generated and crossed the beam attenuator module, the laser impinges on a 45° mirror which deviates it towards the focal lens and to the target, sank into the ablation vial together with a specific solvent.

Isopropyl-alcohol and dichloromethane have been used as PLAL solvents in order to produce, respectively, H-capped and Cl-capped polyynes. In particular, the solvent volume adopted for each ablation was of 5mL, and it was contained into a cylindrical glass vial with a diameter of 16 mm and a height of about 75 mm. All the ablations have been performed at the fundamental harmonics of the laser, i.e. 1064 nm. The energy per pulse delivered by the 1064 nm laser has been fixed at 50 mJ, much smaller than its maximum nominal value (850 mJ), to minimize splashing, target displacements, and solvent explosions or flame ignition. A fluence of 2.71 $\frac{J}{cm^2}$, value optimized in previous works of the research group [51, 91, 102], was set before each ablation. This parameter represents the ratio between the energy per pulse and the areal spot of the laser on the target. Hence, in order to obtain a fluence of 2.71 $\frac{J}{cm^2}$, a spot size of 0.766 mm has been imposed. A custom Python code, controlling both the laser and the sample stage, enables to perform a spiral movimentation of the stage, permitting to homogeneously ablate the graphite target maintaining its planar geometry. Finally, the duration of each ablation was set to 30 minutes.

3.2.3. Purification, phase transfer and concentration

The polyynes mixture obtained after each ablation was processed through purification in cyclohexane, phase transfer into acetonitrile and concentration by rotavapor. Purification was performed to remove impurities and by-products that could react with the sp-chains increasing the probabilities of crosslinking and degradation. It was also performed to avoid the eventual by-products and impurities from contaminating and/or overloading HPLC columns. In particular, cyclohexane was employed due to its compatibility with silica-gel, immiscibility with isopropyl-alcohol and boiling temperature much higher than the one of dichloromethane. Phase transfer of the mixture into acetonitrile was carried out to make it compatible with the HPLC aqueous mobile phase. Finally, the use of rotavapor allowed concentrating the purified solution, which otherwise would be too diluted to produce detectable SERS signals of the polyynic species in the final nanocomposite films.

Purification was carried out through several steps. Firstly, the phase transfer of the produced mixture into cyclohexane was performed, followed by the slow addition of the obtained solution into a silica gel column. Then, other cyclohexane was added for a volume of 2-3 times the silica-gel column length itself. Subsequently, elution and collection of the

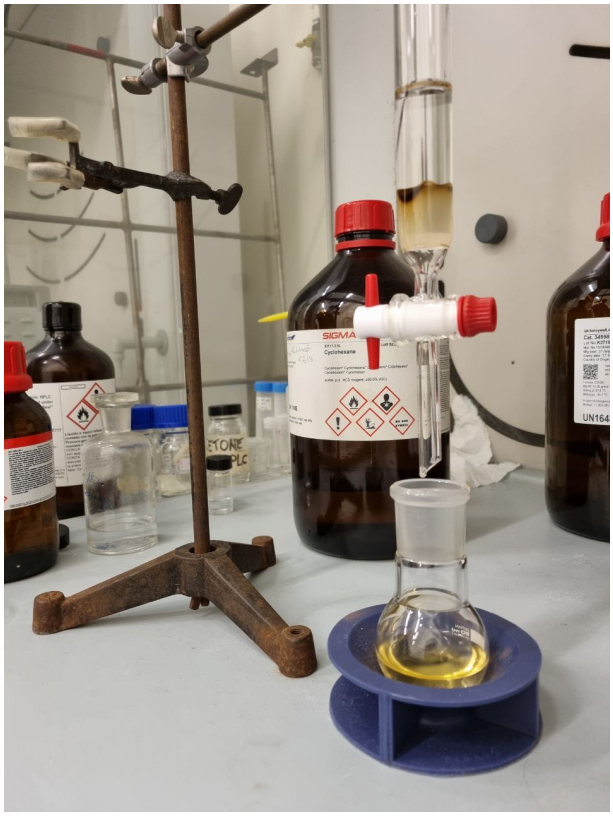

Figure 3.5: Collection of the purified eluate through the silica-gel column.

purified eluted phase were performed (Fig. 3.5), followed by the incorporation of a double volume of acetonitrile to the eluate. Finally, phase transfer and concentration of the purified mixture were obtained by means of the rotavapor.

The gravimetric columns were filled using Silica Gel 60 (0.063-0.200 mm): after having mixed it with cyclohexane into a beaker, the solution was introduced into a borosilicate glass chromatography column and further cyclohexane was added till the silica-gel reached a sufficient compactness.

Due to the different vapor pressure of isopropyl-alcohol and dichloromethane, phase transfer of the original mixture into cyclohexane has been performed differently according to the employed ablation solvent. Indeed, being the former characterized by a much smaller vapor pressure, phase transfer was obtained by repeating 3 times the rotavapor of a solution obtained by the addition of 10 mL of cyclohexane to the 5 mL original mixture setting a bath temperature of 25°C and a rotation higher than 100 rpm. In particular, it was possible to recognize the end of the phase transfer process when the two different liquid phases involved in the process, i.e. isopropyl-alcohol and cyclohexane, were no more distinguishable, meaning that i-PrOH was completely evaporated. On the other side, the phase transfer of the DCM-polyynes original mixture into cyclohexane was simply obtained by adding 5 mL of cyclohexane to the 5 mL mixture and then by performing the rapid evaporation of this solution under a controlled flux of nitrogen till reaching again a total volume of 5 mL.

3.2.4. Film deposition

Two methods have been tested for the nanocomposite films deposition, namely spin coating and drop casting. For what concerns spin coating, a certain amount of the solution to be deposited is casted on top of a substrate that is put under fast rotation, typically above 600 rpm. The combined effect of the centripetal force generated by the rotation of the substrate and the surface tension of the deposited solution, determine the even spread of the liquid on the substrate itself and the fast evaporation of the solvent, generating a very thin and uniform coating on top of it. Drop casting, on the other side, is a very simple process involving the "drop by drop" deposition of the solution onto a substrate. In this case, the dimension of the final film depends on the chemical affinity between the solution and the substrate. Together with the intrinsic simplicity of this process, another advantage of drop casting is that, by properly selecting the substrate in terms of its wettability properties, it is possible to obtain very small films. The main disadvantage of this technique, instead, is to be ascribed to the so called "coffee ring effect": during the

film assembly, solvent evaporation takes place, giving rise to capillary flows within the drop that determine particles accumulation at the film boundaries, visually resulting in the appearance of a coffee-ring.

3.3. Characterization techniques

3.3.1. UV-Vis absorption spectroscopy

A Shimadzu UV-1800 spectrophotometer has been exploited to both perform a preliminary analysis of the purified polyynes mixture and to characterize the Ag/PVA solution. The wavelength range of interest was set between 190 and 600 nm, being indeed the region where it is possible to find both polyynic signals (between 190-400 nm) and Ag nanoparticles plasmonic band (centered at about 430 nm). However, the maximum nominal range covered by the apparatus is from 190 to 1100 nm, by switching between two lamps, a deuterium arc lamp and a tungsten lamp, covering respectively the UV range and the visible range.

The first step needed to perform the UV-Vis absorption characterization of both the polyynic and the Ag/PVA solutions consisted in their dilution with, respectively, acetonitrile and water. This passage was crucial to avoid the detector saturation, and so to allow the correct acquisition of the absorption spectrum. In particular, the polyynes mixture, purified following the method described before, was diluted 37 times with acetonitrile (20 μL:720 μL), while the Ag/PVA solution was diluted 100 times with water.

Then, a quartz cuvette (1 cm optical path length) filled with the diluted solution itself was introduced inside the spectrophotometer together with another cuvette filled with, respectively, acetonitrile or water. This permitted the subtraction of the background absorption provided by the reference solvent (namely acetonitrile and water in the two cases), allowing to obtain directly the absorption spectrum of the analyte.

3.3.2. High Performance Liquid Chromatography (HPLC)

Reverse-Phase High Performance Liquid Chromatography (RP-HPLC) was perfomed through a Shimadzu Prominence UFLC (Fig. 3.6), with the aim to both detect and separate size-selected polyynes from the purified mixture (see Section 3.2.3).

The basic operating principles of HPLC have already been described in Chapter 1. In the present work, the chromatographic column used is the Phenomenex Luna C18 (150 mm $\times$ 4.6 mm, 3 μm particle size), i.e. a column packed with silica particles functionalized by

Figure 3.6: HPLC setup: a) autosampler; b) oven and columns; c) fraction collector; d) quadripartite pump system; e) photodiode array spectrophotometer; f) controller; g) solvent tray [101].

alkyl chains made of 18 carbon atoms. The method selected for all the RP-HPLC runs was characterized by a duration of 45 minutes, and exploited a mobile phase gradient (see Chapter 1). The starting composition of the mobile phase was 35% water and 65% acetonitrile, while the final one was 5% water and 95% acetonitrile. The injection volume was set to 30 μL.

A preliminary run allowed to identify the elution times for all the polyynes of interest, helping their subsequent precise collection in different vials. The concentration of the separated polyynes, calculated looking at their chromatographic peaks extracted from wavelenght-specific chromatograms, was in the order of 10^{-6}M for the most concentrated ones and 10^{-7}M for the less concentrated ones. A chromatogram displayed the absorption of the analytes as a function of the elution time at a fixed wavelength, chosen to match the most intense transition (MIT) of the size- and termination-selected polyyne of interest. In Fig. 3.7 it is reported an example of a chromatogram at 225 nm (i.e. at the MIT of C_8H_2), with also an inset of the chromatografic area of the collected polyyne (C_8H_2), and

its corresponding UV-Vis absorption spectrum.

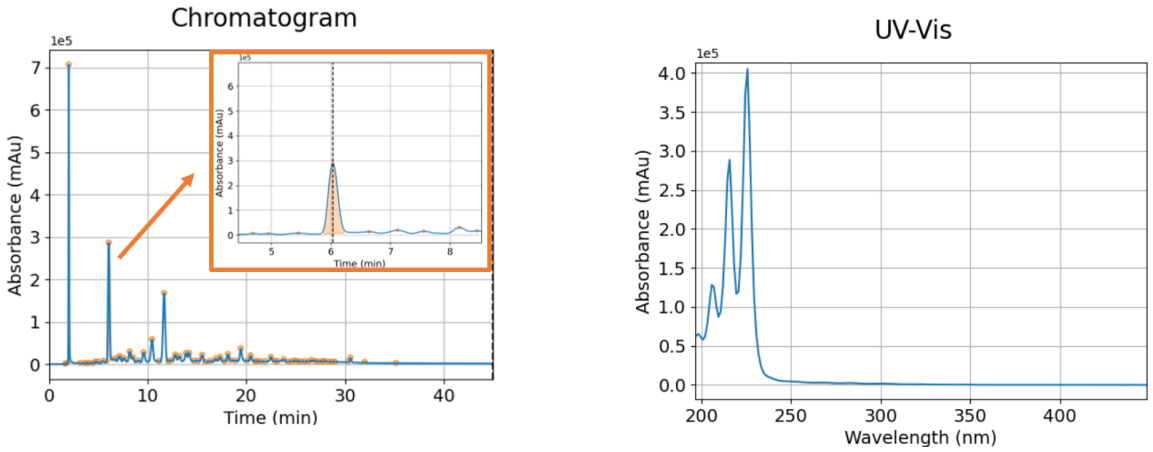

Figure 3.7: (left panel) wavelength-specific chromatogram of C_8H_2. In the inset, its chromatographic area highlighted in orange. (right panel) UV-Vis absorption spectrum corresponding to the maximum of the C_8H_2 chromatographic peak on the left.

3.3.3. Raman and SERS spectroscopy

A Renishaw inVia Raman microscope with a diode-pumped solid-state laser was adopted to perform nanocomposite films characterization and *in-situ* SERS mapping. This apparatus is equipped with two lasers, with a wavelength of 532 nm and 660 nm. The laser beam is driven to the sample by a series of mirrors and filters. A piezo-controlled stage permits the remote movimentation, along the three axes, of the stage carrying the sample, allowing a precise focusing of the laser beam. After the laser-sample interaction, the scattered light is filtered, in such a way to be able to detect, through a CCD camera, just its inelastic component (i.e. the Raman photons, see Section. 1.4.2), and so to collect the Raman spectrum of the sample.

In present work, only the 532 nm laser has been used, and a 20x or 50x microscope objective was employed. Spectral acquisitions were performed in static mode, i.e. by recording only a fixed frequency range defined by the interplay between the dispersing grating and the CCD dimension. However, the adopted equipment would have also permitted to operate in extended mode, i.e. by scanning all the possible scattered photons on a wider spectral range. Hence, if, on one side, static mode leads to a faster characterization of the sample but on a limited range of wavelengths, on the other side extended mode requires a longer time but permits the sample characterization over a wider range of wavelengths.

A very useful feature provided by the instrument, and extensively exploited in this work, is the possibility to perform maps of the analysed samples. This advanced tool allowed the obtainment of a reliable statistical description of the nanocomposite films under investigation, as will be described in Chapter 5.

4 | Results - Nanocomposite films composition and characterization

In this experimental work, the effect of polyynes length and terminations on the thermal stability of Ag/PVA/polyynes nanocomposite films has been investigated, and the obtained results are reported in two distinguished chapters, Chapter 4 and Chapter 5.

Chapter 4 is focused on nanocomposites synthesis, with a deeper insight on the optimization of both their composition and SERS measurements parameters. These results have been exploited to develop a custom *in situ* SERS mapping procedure to perform thermal stability tests on the synthesized nanocomposite films, as explained in Chapter 5.

4.1. Polymer implementation in the Lee-Meisel method

In Section 3.2.1, synthesis of silver colloids via Lee-Meisel method was described. In present work, this technique has been implemented by the direct dissolution of PVA granules during the Ag nanoparticles formation. In particular, a beaker containing 19.2 g of the aqueous solution of the silver precursor, i.e. $AgNO_3$, having a molar concentration of $10^{-3}M$, was heated up and put under magnetic stirring. Once its boiling point was reached, 0.4 mL of sodium citrate were added to trigger the silver ions reduction into silver nanoparticles. During this process, 800 mg of PVA granules were slowly added to the silver colloid being formed and, thanks to the heat provided by the hotplate stirrer, they were dissolved into it. By means of this procedure, it was possible to obtain the final Ag/PVA/polyynes nanocomposites by simply mixing the Ag/PVA solution itself with the polyyne solution of interest, without risk of affecting polyynes stability. In the works of Okada *et al.* and An *et al.* (see Section 2.1), where the final nanocomposite film was obtained by firstly mixing the polyynes solution with the Ag nanoparticles colloid and then by dissolving the polymer granules into the mixed solution by heating [63, 64], polyynes could undergo thermal degradation. With this method, instead, PVA thermal

dissolution was performed during the Ag nanoparticles formation. Hence, there was no risk for polyynes degradation during the preparation of the polymer-colloidal solution.

The optimal composition of the Ag/PVA solution was obtained by adding 4% of the total solution weight of PVA. Indeed, it permitted a good trade-off between solution viscosity, and so magnetic stirring ease, filmability, and PVA detection via SERS spectroscopy. Once synthesized, the Ag/PVA solution, called from now on "NPPVA4%" solution, was characterized by UV-Vis absorption spectroscopy (see Section 3.3.1). This allowed to both monitor the position of the nanoparticles plasmonic band, typically located at about 430 nm, and to obtain a qualitative indication of their concentration in the solution, typically in the order of 10^{-3}M (Fig. 4.1).

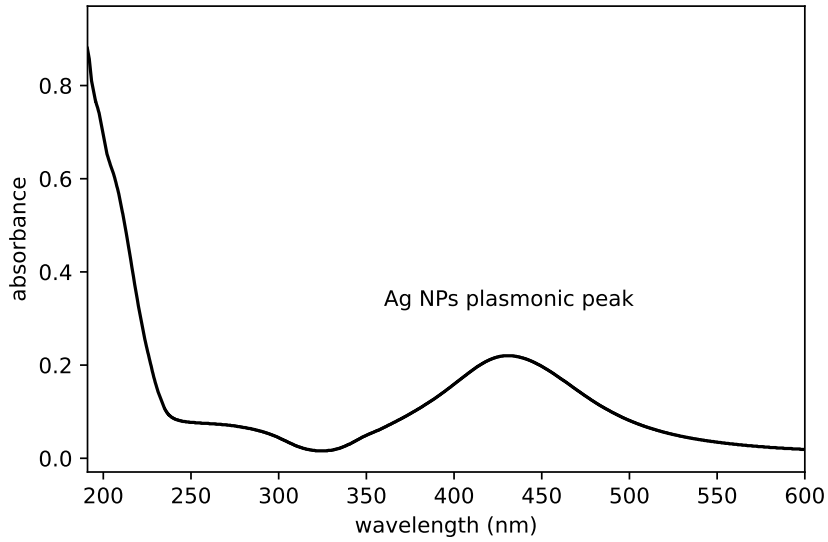

Figure 4.1: UV-Vis absorption spectrum of the solution obtained by diluting in a volume ratio of 1:100 the NPPVA4% solution with water. It is highlighted the Ag nanoparticles plasmonic peak.

Fig. 4.2 shows the SERS spectrum of the film obtained upon solvent evaporation of the NPPVA4% solution. The analysis was performed by using the green laser, in static acquisition mode, with a laser power set to 0.7 mW, an acquisition time of 10s (10 accumulation, each with a duration of 1 s) and a 20x microscope objective. As expected, it is possible to observe the main Raman spectral feature of PVA, located at about 2930 cm^{-1}. The peak that appears at about 2100 cm^{-1} could be due to the presence of the Ag nanoparticles.

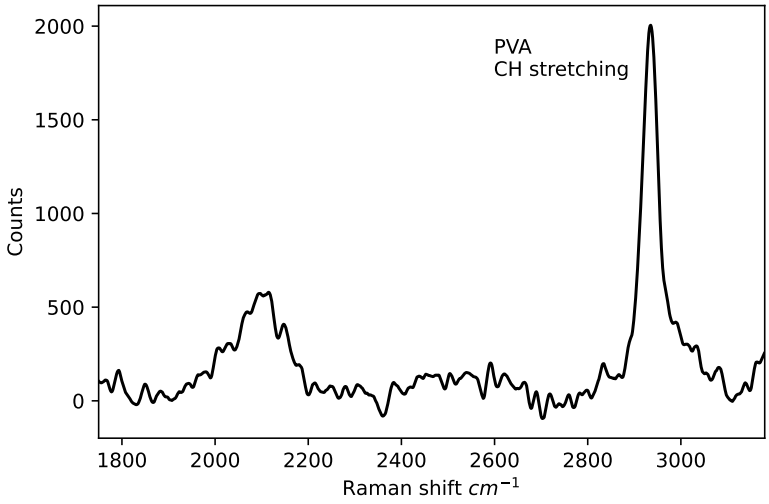

Figure 4.2: Raman spectrum of the NPPVA4% solution.

4.2. Polyynes stability after mixture purification

Purification of the polyynes mixtures (see Section 3.2.3) allowed to perform several collections runs by HPLC without the need for repeating the PLAL synthesis process every time. Indeed, I observed a highly efficient stabilizing effect of the purification processes on PLAL-synthesized polyynes mixtures. Specifically, this was obtained by monitoring the UV-Vis absorption spectrum of purified mixtures in time (see Fig. 4.3 and Fig. 4.4).

In particular, the stability of H-capped polyynes in their purified mixture from ablations

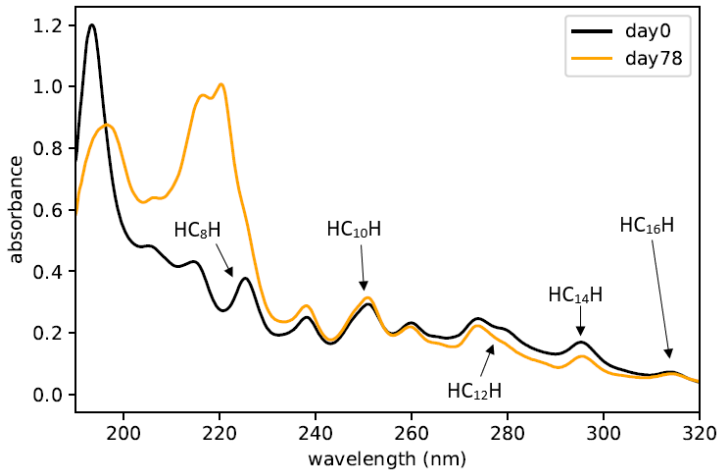

Figure 4.3: UV-Vis absorption spectrum of the purified H-capped polyynes mixture monitored in time. In black, the as purified mixture. In orange the purified mixture after 78 days.

in isopropyl-alcohol (see Section 3.2.2) was monitored up to 78 days (Fig. 4.3). The unexpected peak that appears at about 220 nm after 78 days can be attributed to a by-product generated from the partial degradation of the mixture, which covers the 225 nm peak of the HC_8H.

In Fig. 4.4 it is reported the same plot, this time referred to Cl-capped polyynes. In this case, the monitoring of the UV-Vis absorption spectrum has been performed up to 50 days from the mixture purification.

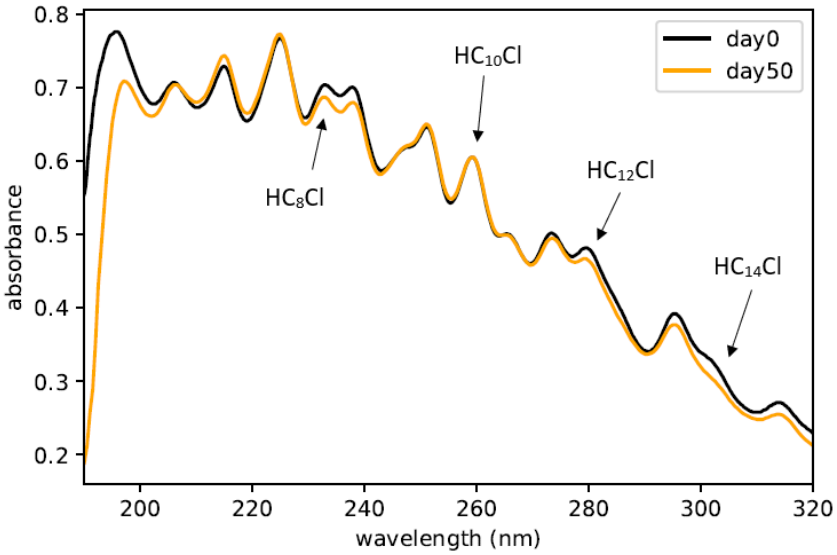

Figure 4.4: UV-Vis absorption spectrum of the purified HC_nCl polyynes mixture monitored in time. In black, the as purified mixture. In orange the purified mixture after 50 days.

Both mixtures, upon purification, show a great stability in time. Indeed, in both cases, the ratio between the polyynes absorption peaks intensity after 50 days (extrapolated, in the case of H-capped polyynes, from the data at 78 days) and just after the purification, is almost unchanged.

4.3. Deposition method and substrate selection for Ag/PVA/polyyne nanocomposites

In order to select the most appropriate deposition method for the nanocomposite films to be analysed, both spin coating and drop casting were performed. The solution employed for these tests was obtained by mixing, in a volume ratio of 1:2, the polyynes mixture with the NPPVA4% solution.

Despite, from a theoretical point of view, spin coating is the most performing technique, since it permits the production of very thin films at a high rate, drop casting was chosen as the deposition method. This choice is to be ascribed to the final goal of this work, i.e. the SERS mapping of the synthesized nanocomposite films. Indeed, to perform this kind of analysis with an effective statistical meaning, it was necessary to deposit very small films, all characterized by the same geometry and by a sufficient thickness, needed to probe PVA Raman peaks in short acquisition times with a reasonable signal-to-noise ratio. This was achieved by drop casting, which, in fact, contrary to spin coating, allowed to produce films with very small dimensions and a highly reproducible geometry. In particular, each film has been obtained by depositing a single drop of the solution by means of a micropipette, corresponding to a volume of about 10 μL.

The other fundamental step of this preliminary part of the work consisted in finding the optimal film deposition substrate. With this purpose, the same solution described in the previous paragraph was drop casted on several materials and, once obtained the corresponding film after solvent evaporation, its SERS characterization was carried out. Specifically, spectral acquisitions were performed with a microscopy objective of 20x, in static mode, on a frequency range centered at 2500 cm^{-1}, and by acquiring 10 accumulations of 1 s each with a laser power of 0.7 mW. The analysed frequency range has been selected to cover both the polyynic and the CH-stretching of PVA regions. The collected spectra allowed me to find out the most appropriate deposition substrate for the nanocomposite films and confirmed the capability of the PVA matrix to embed the polyynes.

By comparing the SERS spectra of a pure NPPVA4%wt. film (Fig. 4.2) and an Ag/PVA/polyynes film obtained by the reported procedure on different substrates (Fig. 4.5, left), it was possible to observe the appearance of the typical SERS spectral features of polyynes in the region 1850-2220 cm^{-1}, confirming their effective embedding inside the polymer. The tested deposition substrates were a cut of aluminium coil, a piece of an aluminium disk, a block of steel and a block of teflon.

An interesting result came out when performing a preliminary test on polypropylene. Because the resulting film did not show any SERS signal in the polyynic region, an attempt was made to observe whether polyynes had been "absorbed" by the polymeric substrate itself. The measurement, carried out by depositing a drop of Ag nanoparticles colloid onto the PP substrate after the extraction of the deposited film, confirmed this hypothesis. Indeed, the SERS analysis of the PP substrate demonstrated the presence of the typical polyynic spectral features in the region 1800-2200 cm^{-1}(Fig. 4.6). For this reason, polypropylene was excluded from the substrates list.

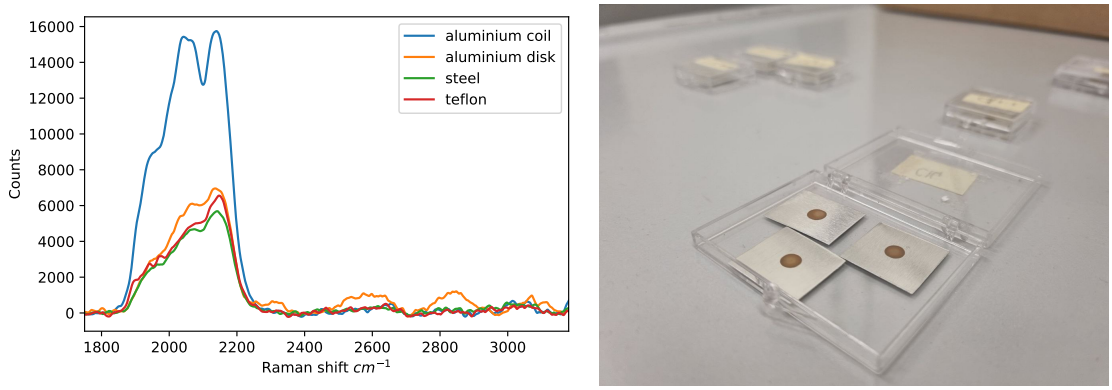

Figure 4.5: (left panel) SERS spectra of the nanocomposite film deposited on different substrates. (right panel) Example of Ag/PVA/polyynes nanocomposite films drop-casted on aluminium.

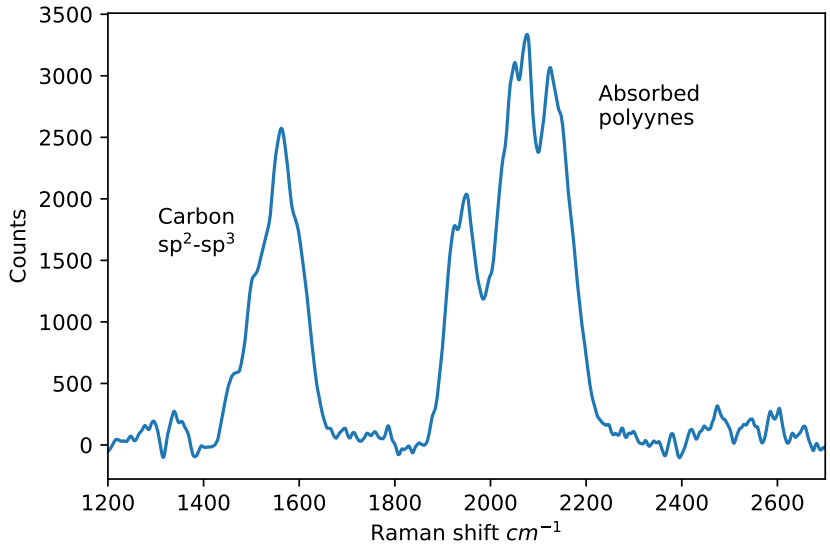

Figure 4.6: SERS spectrum of the PP substrate after the extraction of the deposited nanocomposite film.

Among the other tested substrates, aluminium came out on top as the only material capable of both ensuring the planarity of the deposited film and facilitating the laser focusing during SERS analysis. In Fig. 4.5 the higher performances of the aluminium substrate with respect to all the other tested materials can be clearly seen (Fig. 4.5, left), especially by looking at the polyynic SERS signals in the 1850-2220 cm^{-1} region. By following the drop casting method explained before, films having a diameter of about 3 mm and a thickness of about 1 micrometer were obtained (Fig. 4.5, right).

In particular, the deposition substrates were obtained as cuts of an aluminium coil, subsequently cleaned by the use of pure acetone and then uniformly pressed in order to make them as planar as possible.

The selection of aluminium as deposition substrate determined another crucial advantage. Indeed, due to its high thermal conductivity, it was also directly employed in nanocomposite films thermal stability experiments. This implied the possibility to avoid that the mechanical stress resulting from the film detachment and subsequent re-deposition onto another material affected polyynes stability.

4.4. Ag/PVA/polyynes nanocomposites: composition and SERS parameters optimization

This section is devoted to describe the optimization of both Ag/PVA/polyynes films composition and SERS measurement parameters. To achieve this, an iterative approach was followed. First, I found the best mixing ratio between the ablated polyynes mixture and the Ag/PVA solutions. Then, I optimized the SERS measurement parameters to maximize Raman signals without damaging the films by laser heating. With these results, I refined the films composition employing size- and termination-selected polyynes, hypothesizing a different interaction between hydrogen and chlorine terminations with Ag nanoparticles, and discussing about how this factor influences the films composition optimization.

The optimized proportion between polyynes mixture and NPPVA4% solution that allowed to detect the SERS features of both polyynes and PVA was achieved by depositing, on several aluminium substrates, different solutions obtained by mixing the ablated polyynes mixture with the NPPVA4% solution in a volume ratio going from 1:2 to 1:10. After solvent evaporation, the obtained films were analysed through SERS spectroscopy, with the same parameters used in Section. 4.3, and their spectra are shown in Fig. 4.7.

With the mentioned purpose, the nanocomposite film obtained by mixing the two solutions in a volume ratio 1:10, turned out to be the best. Indeed, this composition allows for the obtainment of a clear and intense SERS spectrum of the nanocomposite film. Also the film obtained upon mixing the two solutions in a volume ratio 1:2 allowed to obtain a clear polyynic SERS signal. Contrarily, the other films, characterized by an intermediate composition, showed a less defined and less intense SERS spectrum.

A series of films characterized by this composition, called from now on "1:10 films", have been employed in the subsequent optimization process of the SERS measurement parameters. Up to now, SERS analysis was performed with the main goal of observing

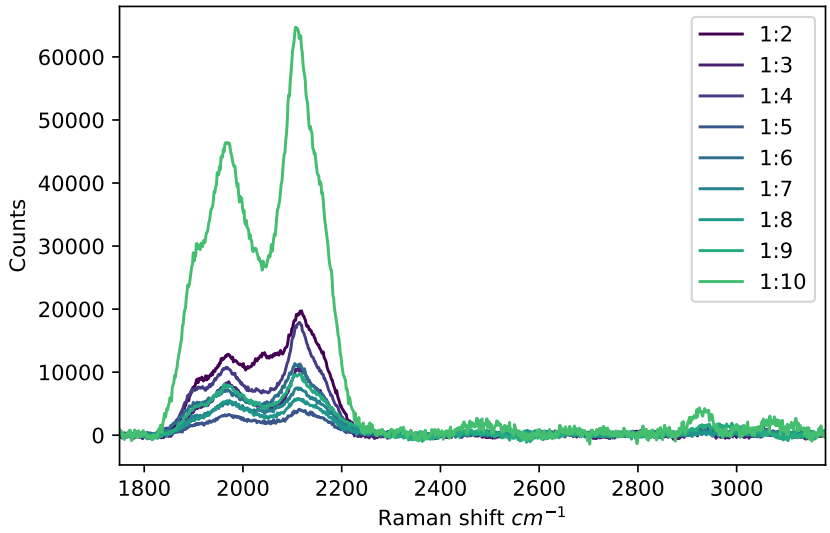

Figure 4.7: SERS spectra of nanocomposite films obtained by mixing the polyynes mixture with the NPPVA4% solution in a volume ratio going from 1:2 to 1:10.

whether or not polyynes had been embedded effectively in the polymeric matrix. However, the choice of the most appropriate SERS parameters was a key step to optimize the nanocomposites characterization without damaging them through laser heating.

4.4.1. Measurements parameters optimization for SERS analysis

The second step of this optimization process was to find the set of instrumental parameters that allowed me to clearly see both the polyynic and polymeric SERS signals, without compromising the stability of the nanocomposite films due to undesirable laser heating effects.

This required to find the best compromise between the laser power delivered to the sample and the duration of each acquisition. In particular, a higher laser power corresponds to a higher peaks intensity, but it can compromise the integrity of the films. On the other hand, a longer acquisition time allows to obtain a good signal to noise ratio, but implies time-consuming measurements, still risking to damage the film.

A series of 1:10 films, each drop-casted onto an aluminium substrate, was measured with static mode SERS analysis, performed with the 532 nm Raman laser, a 50x microscope objective, and a grating of 1800 lines/mm, covering a frequency range from 1750 to 3180 cm^{-1} (see Section 4.3). The effect of the change in the laser power and in the SERS measurement duration was investigated by operating several analysis with a laser power

of, respectively, 0.875 mW and 1.3825 mW and total acquisition times of 10s, 20s and 40s. These tests allowed to find the desired trade-off in a value of 0.875 mW as laser power and of 10s as total acquisition time, consisting of 40 accumulations with a duration of 0.25s each (Fig. 4.8). Indeed, despite the higher SERS signals achieved with a higher laser power and a longer acquisition time, these parameters made the films burn.

From now on, all the SERS spectra will be performed by exploiting the optimized parameters described above, both the single-acquisition measurements and the samples maps.

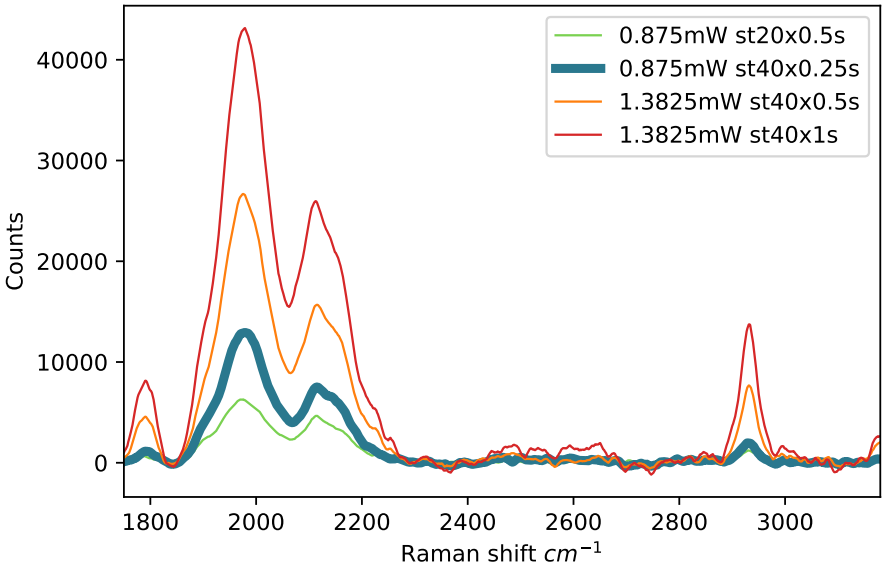

Figure 4.8: SERS spectra of a series of 1:10 films at varying SERS measurement parameters. The bold blue line corresponds to the SERS spectrum with the set of optimized parameters.

4.4.2. Composition optimization of nanocomposite films embedding size- and termination-selected polyynes

The final part of this optimization process regarded the composition of the nanocomposite films embedding size- and termination-selected polyynes. In particular, the optimal composition resulted to be different depending on polyynes terminations, namely hydrogen or chlorine.

In Section. 4.4 it was demonstrated that the nanocomposites obtained by mixing the polyynes mixture with the NPPVA4% solution in a volume ratio of 1:10 were the ones providing the best SERS signals of both polyynes and PVA. Actually, also the films obtained by mixing the two solutions in a volume ratio of 1:2 were able to clearly highlight

the polyynes SERS signals (see Fig. 4.7).

For this reason, more accurate measurements have been performed on both 1:2 and 1:10 films, using, this time, size- and termination-selected polyynes solutions instead of the polyynes mixture, and exploiting the SERS parameters previously optimized (see Section 4.4.1). In particular, the size- and termination-selected polyynes employed for these films were HC_nH, with $n = 6, 8, 10, 12, 14$ and HC_nCl, with $n = 6, 8, 10, 12$. The obtained results are shown in Fig. 4.9 and Fig. 4.10.

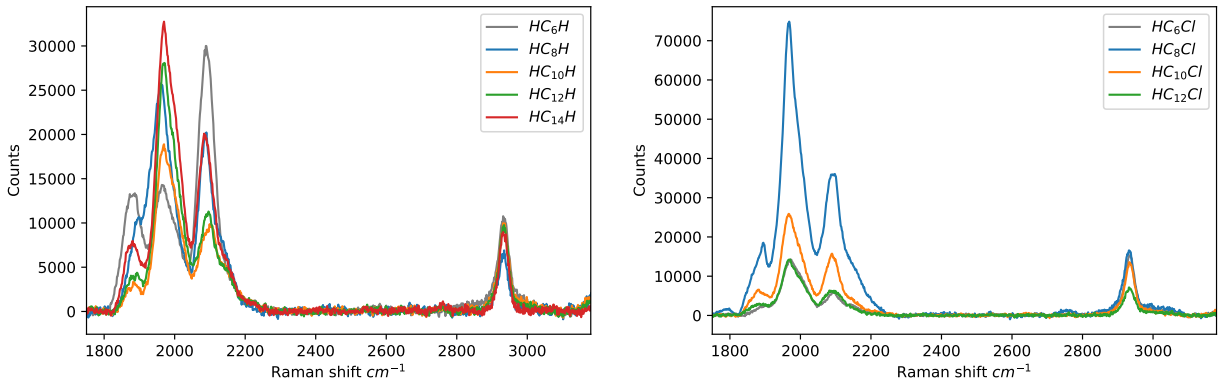

Figure 4.9: SERS spectra of 1:2 films embedding size- and termination-selected polyynes performed with the optimized SERS parameters

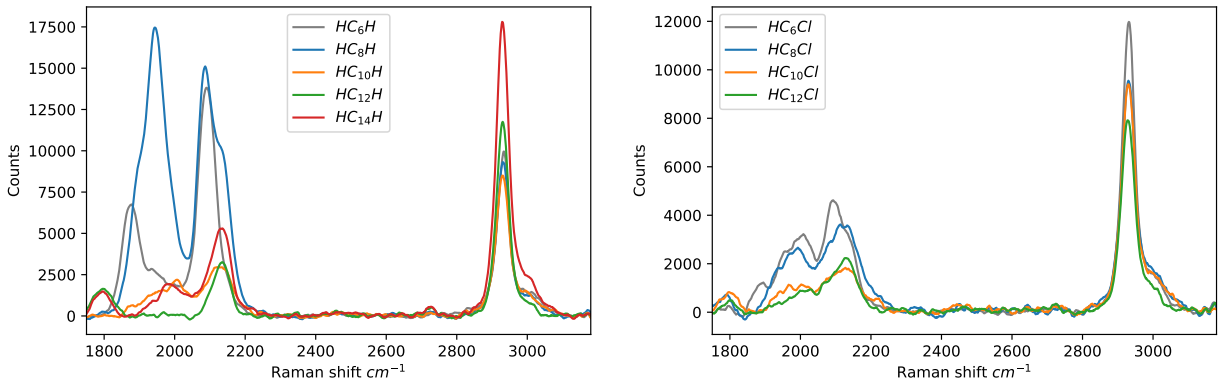

Figure 4.10: SERS spectra of 1:10 films embedding size- and termination-selected polyynes performed with the optimized SERS parameters

Since the aim of this thesis work is to understand the effect of polyynes length and terminations on nanocomposites thermal stability, their signal intensity and differentiation

are of fundamental importance. It is well known that each polyyne is characterized by well-defined SERS bands [50, 59, 103]. By comparing the SERS spectra of the 1:10 films with the ones of the 1:2 films reported above, it is possible to observe a different behaviour between the most concentrated species (HC_8H) and all the other, less concentrated, ones. If, on one side, the intensity of the SERS signal attributed to the HC_8H is optimized in both films, on the other side, for all the other polyynes, an increase in the peaks intensity and a simultaneous decrease in the polyynes signals differentiation is observed passing from the 1:10 to the 1:2 films.

The higher peaks intensity observed passing from the 1:10 to the 1:2 films can be justified by the larger amount of polyynes dispersed in the film, relatively to the one of the Ag nanoparticles, that is found in the second case. On the other hand, the decrease in the polyynic signals differentiation observed for the less concentrated species is for sure undesired when dealing with size- and termination-selected polyynes, especially considering the aim of this work.

I interpreted this peculiar behaviour on the basis of polyynes interaction, both among themselves and with the Ag nanoparticles. By looking at Fig. 4.10 and Fig. 4.11, I established a relationship between the Ag nanoparticles content and the signal differentiation among the different polyynes. Indeed, it seems that, by reducing the Ag nanoparticles concentration (i.e. passing from the 1:10 films to the 1:2 films), the signals attributed to each specific polyyne undergo a "homogenisation" process. Being the 1:10 films characterized by a much smaller content of polyynes, with respect to the one of Ag nanoparticles, than the 1:2 films, a higher probability of interaction between polyynes and nanoparticles, rather then among polyynes themselves, is expected in the 1:10 films. This can lead to both polyynes stabilization and efficient SERS enhancement by means of the Ag nanoparticles aggregates, in turn generated as result of the polyynes introduction in the system, as reported in previous chapters. On the other side, in the 1:2 films, polyynes are present in a much larger proportion with respect to Ag nanoparticles. This can determine a more probable interaction between the sp-chains themselves rather than with the nanoparticles, resulting into crosslinking reactions that, consequently, lead to polyynes partial degradation. The products that are thought to be generated upon this degradative phenomenon are sp-sp^2 carbon complexes that, by interacting with the Ag nanoparticles, would generate, independently from the polyyne originally introduced in the system, the same SERS features. This determines the indistinguishability among the different size- and termination-selected polyynes embedded in the nanocomposites, resulting in the mentioned signals homogenization.

Hence, to obtain a satisfying trade-off between the intensity and the differentiation of the

polyynes SERS signals in the different nanocomposite films, a custom synthesis method was developed. By exploiting the idea of a constant molar ratio (R) between polyynes and Ag nanoparticles, it was possible to synthesize nanocomposite films which both maximised the polyynic SERS signals and allowed for their differentiation (based on their length and terminations), even in case of low concentrated species.

The ratio was calculated by considering, as reference system, the film obtained by mixing the HC_8H and the NPPVA4% solutions in a volume ratio of 1:10, which indeed provided the best SERS spectrum considering both polyynes intensity and stabilization, intended in terms of signals differentiation (see Fig. 4.10 and Fig. 4.11). In particular, the molarity of the HC_8H solution was obtained by multiplying the chromatographic area of the HC_8H extracted from its wavelength-specific chromatogram (see Section. 3.3.2) by a constant factor ($1.349 * 10^{-12}\ mol/L$) derived from a calibration curve previously determined by the research group. The concentration of the Ag nanoparticles in the NPPVA4% solution was in the order of 10^{-3} M, as mentioned in Section. 4.1. The calculated ratio, R=($7.13 * 10^{-4}$), has been maintained constant in all films. By keeping fixed the volumetric content of the polyynes solution inside each film to 30μL, the only variable parameter in the preparation of the nanocomposite films was the volume of NPPVA4% solution to be added to maintain R constant at varying concentrations of the polyyne solution of interest. Indeed, the polyynes obtained by PLAL synthesis and separated through HPLC analysis are characterized by different concentrations depending on their sizes and terminations. In particular, longer polyynes are produced in a smaller amount by the PLAL process. Consequently, also the diluted solution collected after the HPLC process is less concentrated for increasing chains length.

In the cases where the collected polyynes solution were small concentrated, below 10^{-6}M, the NPPVA4% volume to be added to the polyynic solution to maintain R constant (about 20 μL) would be smaller than the volume of the polyynic solution itself (set to 30 μL). This would result in PVA precipitation and the formation of an amorphous PVA aggregate upon the mixing of the two solutions. Indeed, acetonitrile is a non-solvent for PVA, and the polyynic solution collected from the HPLC consists of 95% acetonitrile (see Section 3.3.2). This would determine the impossibility to obtain a nanocomposite film. Hence, in these cases, occurring specifically for $HC_{16}H$ and $HC_{14}Cl$ polyynes, it was employed the minimum NPPVA4% volume which ensured to avoid the described issue, i.e. 45μL.

The proposed method was proved to be highly effective for all the analysed H-capped polyynes, as can be seen in Fig. 4.11. In Table 4.1, the calculated NPPVA4% volumes adopted for the synthesis of the films analysed in Fig. 4.11 are reported.

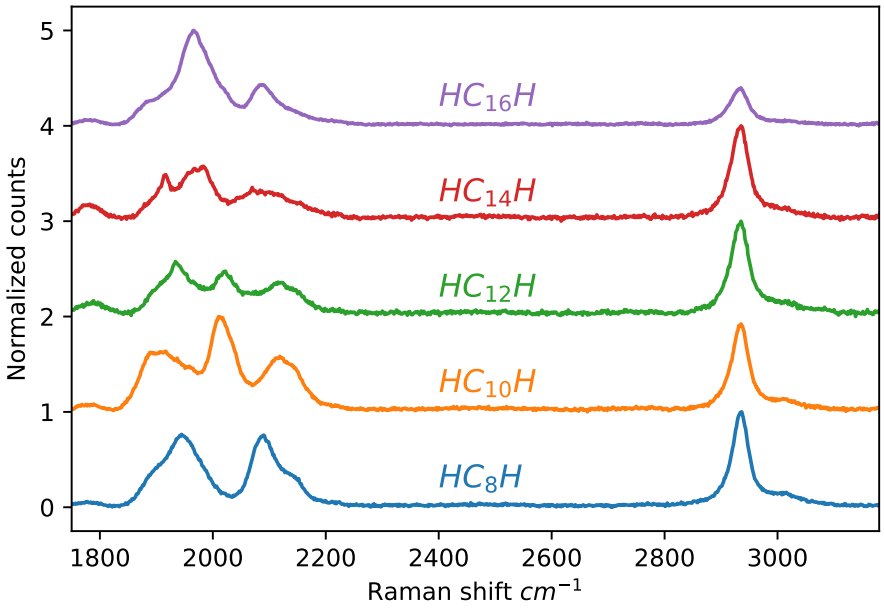

Figure 4.11: Normalized SERS spectra of nanocomposite films embedding H-capped polyynes of different lengths.

polyyne	calculated NPPVA volume (μL)
HC_8H	300
$HC_{10}H$	246
$HC_{12}H$	184
$HC_{14}H$	178
$HC_{16}H$	113

Table 4.1: Calculated volumes of NPPVA4% solution adopted for the synthesis of nanocomposite films embedding H-capped polyynes of different lengths.

When considering, instead, HC_nCl polyynes, the method seemed to remain valid for the less concentrated species, while it completely failed when dealing with the most concentrated one, i.e. HC_8Cl. Specifically, the nanocomposite film embedding the less concentrated polyyne, i.e. $HC_{14}Cl$, showed the best SERS signals, while the film embedding the HC_8Cl, in which the volumetric content of NPPVA4% was much larger, exhibited an almost flat spectrum in the polyynic region, as can be seen in Fig. 4.12 (left). To improve the quality of the SERS signal of the HC_8Cl polyyne, several tests have been performed, varying the NPPVA4% volume inside the nanocomposite film. In particular, the HC_8Cl

spectral features became clearly visible only by reducing the nanoparticles solution volume from the value predicted by the method calculations, namely 160 μL, down to 45 μL, obtaining a final volume ratio of 1:1.5 between the polyyne and the NPPVA4% solutions (see Fig. 4.12 (right)).

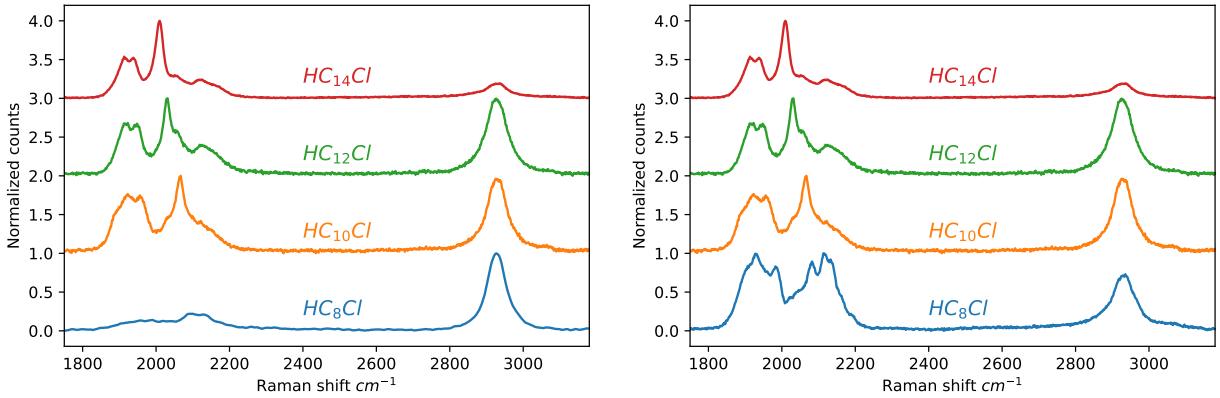

Figure 4.12: Normalized SERS spectra of nanocomposite films embedding HC_nCl polyynes of different lengths, without (left) and with (right) optimized HC_8Cl-based film composition.

In Table 4.2 and Table 4.3, the NPPVA4% volumes adopted for the synthesis of the films analysed in Fig. 4.12 are reported.

polyyne solution	**calculated NPPVA volume (μL)**
HC_8Cl	160
$HC_{10}Cl$	131
$HC_{12}Cl$	66
$HC_{14}Cl$	45

Table 4.2: Calculated volumes of NPPVA4% solution adopted for the synthesis of nanocomposite films embedding HC_nCl polyynes of different lengths.

polyyne solution	**calculated NPPVA volume (μL)**
HC_8Cl	45
$HC_{10}Cl$	131
$HC_{12}Cl$	66
$HC_{14}Cl$	45

Table 4.3: Calculated volumes of NPPVA4% solution adopted for the synthesis of nanocomposite films embedding $HC_{10}Cl$, $HC_{12}Cl$, $HC_{14}Cl$ polyynes, and optimized volume of NPPVA4% solution adopted for the synthesis of the HC_8Cl based film.

I hypothesized to justify this different behaviour between HC_nH and HC_nCl polyynes by assuming a different interaction between hydrogen and chlorine terminations with Ag nanoparticles. Indeed, by approximating the Ag nanoparticles as electrons sources, and considering the much higher electronegativity of chlorine with respect to hydrogen, it is possible to suppose a much stronger interaction among silver and chlorine with respect to the corresponding one with hydrogen. It follows that, to obtain the same degree of SERS enhancement, a smaller content of nanoparticles is required for HC_nCl compared to HC_nH polyynes. Moreover, the stronger interaction between chlorine and Ag nanoparticles hinders crosslinking between these chains, such that no sign of "homogenization", i.e. formation of sp-sp^2 compounds, is observed. This would justify the obtainment of a clear and intense SERS spectrum for the HC_8H and the HC_8Cl by employing, respectively, a volume ratio of 1:10 and 1:1.5 between the different polyyne solution and the NPPVA4% solution.

5 | Results – Thermal stability of PVA-nanocomposite films

In this chapter, the thermal stability of the nanocomposite films described in Chapter 4 is investigated. Specifically, the effect of both length and terminations of the polyynes embedded inside the PVA polymeric matrix on the nanocomposites thermal stability is examined. This was achieved through the development of an *in situ* methodology aimed at performing SERS maps of the analysed nanocomposite films when thermally excited by a Peltier thermoelectric modulus. The composition of the tested films was selected according to the results obtained in Section 4.4.2. Also the SERS measurements parameters set to perform the maps were the ones optimized in Section 4.4.1. Together with the investigation on the nanocomposite films thermal behaviour, also the degradative effect of the laser employed during the maps has been analysed. By decoupling these two effects, it was possible to properly study films degradation determined by the solely increase in temperature.

5.1. A methodology to monitor nanocomposites thermal behaviour through *in situ* SERS mapping

5.1.1. Experimental setup

The experimental setup, designed and assembled by myself, to study the thermal stability of the synthesized nanocomposite films is shown in Fig. 5.1. The two most important components of the setup shown in Fig. 5.1 are the SERS probe, necessary to perform the *in situ* SERS maps of the samples, and the Peltier thermoelectric modulus, needed to thermally excite the films under investigation.

A Peltier module is constituted by several thermocouples, connected electrically in series (by copper tabs) and thermally in parallel, enclosed by two alumina ceramic plates. Its schematic representation is reported in Fig. 5.2.

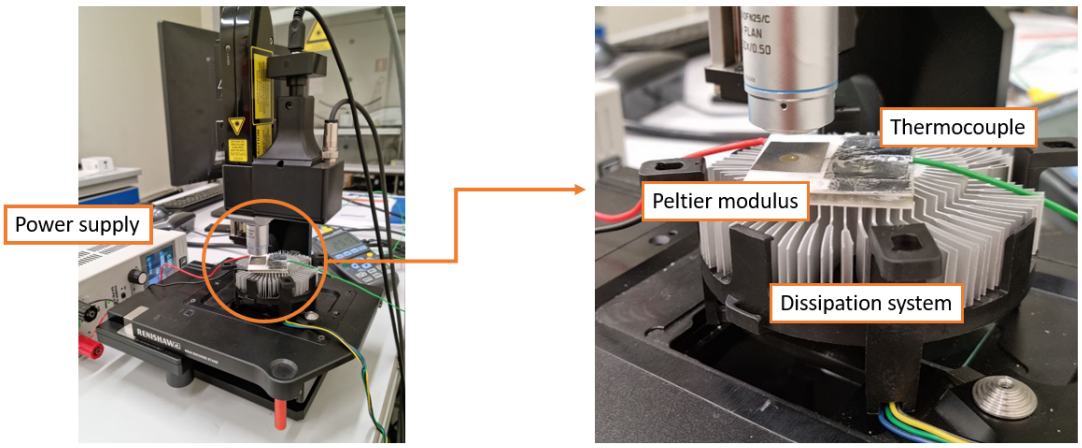

Figure 5.1: Experimental setup for nanocomposites thermal treatment during in situ SERS measurements.

Each thermocouple consists of an n-type and a p-type semiconductors, and when a DC current crosses the device, a temperature difference is generated among its sides. As a result, one face is cooled and the opposite, called "hot side", is heated.

An example of commercially available Peltier modulus, also adopted for this work, is shown in Fig. 5.3.

A custom system, coupled with the Raman microscope already described in Chapter 3, was assembled with the aim to thermally excite the films under investigation. A Peltier thermoelectric modulus was connected to a power supply system and was placed onto a

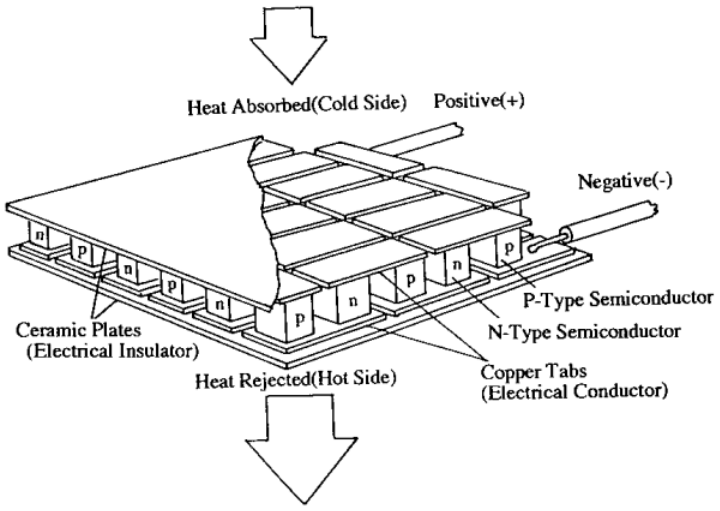

Figure 5.2: Schematic representation of Peltier thermoelectric modulus [104].

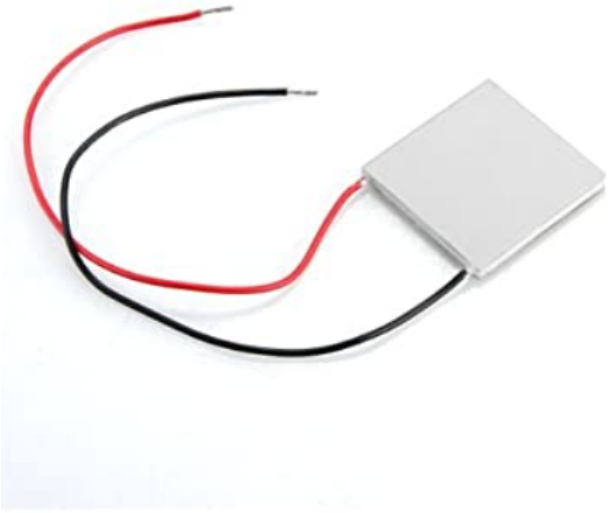

Figure 5.3: Typical commercially available Peltier thermoelectric modulus.

heat dissipation system. The current-voltage (I-V) couple necessary to reach the desired temperature was provided by a power supply generator to the Peltier modulus. On the other side, the dissipation system, fixed to the Raman stage, allowed to safely maintain the reached temperature during the whole thermal treatment, also favouring the rapid cooling of the Peltier modulus once turned off the power supply system. A thermocouple, fixed to the hot side of the thermoelectric modulus by means of aluminium tape, allowed to monitor its temperature during the whole thermal treatment.

5.1.2. Nanocomposite films mapping procedure

The software responsible for the control of the Raman instrument (WiRE, Renishaw) allows for the acquisition of several spectra along an area of the analysed sample that can be not limited to a single frame but which can be extended over a much larger area. This is at the basis of the mapping process, through which, indeed, it is possible to recover a statistical description of the investigated sample. As reported in Chapter 4, the dimension of the synthesized nanocomposite films has been optimized in order to be the smallest possible, in such a way to be able to perform maps of their whole surface area in a reasonable time providing their most reliable statistical description.

The mapping procedure adopted during this work consisted, firstly, in the montage of the image of the film area to be mapped. This step was carried out by acquiring a 7 x 9 frames image of the area to be analysed (Fig. 5.4). In particular, it was possible to manually

Figure 5.4: Montage of the sample area to be mapped (7 x 9 frames).

set the focus for each frame, and this was fundamental for the mapping process. Indeed, once set during this preliminary phase, it was memorized by the instrument, allowing to acquire each spectrum being always in focus.

Once completed the image montage, the area to be mapped was selected onto the image itself by highlighting the region of interest with a rectangle. Then, a step of 100 μm in both the horizontal and vertical directions was set to fill the selected region with a grid (Fig. 5.6). Each intersection along the grid corresponded to a point of the SERS map, and so to a collected SERS spectrum, whose measurement parameters were the ones optimized

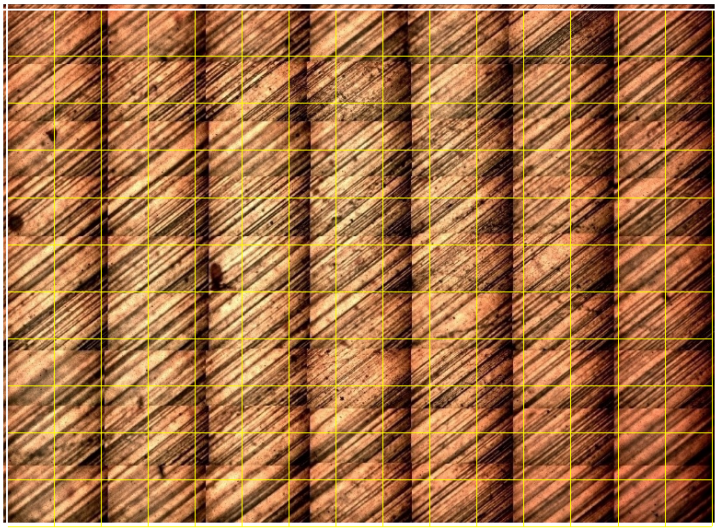

Figure 5.5: Area to be mapped filled by the grid obtained by setting a 100 μm step along both x and y axes.

in Section 4.4.1. Having set the step along x and y to 100 μm, each map of each analysed film consisted of 192 spectra, resulting in an overall mapping time of approximately 45 minutes per map.

The type of path followed by the laser during the mapping process, called "snake coverage", permitted to follow the grid smoothly, without abrupt changes in the stage position. In this way, it was possible to minimize the sample displacements determined by the movimentation of the stage itself and maximise the reproducibility of the measurements.

The great advantages of performing SERS maps on the analysed films were the possibility to carry out long SERS measurements without burning the samples, and to obtain a reliable statistical description of the samples themselves, being indeed inhomogeneous.

5.1.3. Thermal treatment of the nanocomposite films

All the analysed films have been subjected to thermal treatment, carried out through the Peltier modulus. Two SERS maps, a preliminary map at room temperature and, just after, an *in situ* map during the sample heating, have been acquired for all the nanocomposite films. In this sense, the spectra obtained from each point of the preliminary map represent the pristine SERS signal of the film. On the other hand, the spectra coming from same points measured during the *in situ* SERS map after a certain time since the start of the thermal treatment quantify the degradation of the embedded polyynes.

Basically, each film, stick to its aluminium substrate, was placed on top of the hot side of the Peltier modulus. Before turning on the power supply, and so the Peltier modulus itself, the preliminary map of the sample was performed. To ensure the same operating conditions during the two maps, and avoid undesired displacements of the sample, the dissipation system (made of a heat sink and a fan) was turned on also during the preliminary map. Once terminated the preliminary map, the power supply was turned on, and a specific I-V couple, i.e. a specific temperature, was set in order to perform the *in situ* SERS map of the sample.

The adopted Peltier modulus had a maximum operating temperature of about 115°C. Hence, the thermal treatment of the nanocomposites samples, whose behaviour was monitored by the described SERS mapping process, was performed at 40°C, 60°C, 80°C and 100°C. In Table 5.1, the corresponding I-V couples are reported. It is actually also reported the I-V couple corresponding to 110°C, employed to test the thermal stability of the PVA polymeric matrix only (see Section 5.2).

Together with the power supply, also the software responsible for the monitoring of the

Temperature (°C)	Current (A)	Voltage (V)
40	2.10	3.20
60	2.10	5.10
80	2.10	6.80
100	2.10	8.30
110	2.10	8.90

Table 5.1: I-V couples applied for the functioning of the Peltier thermoelectric modulus.

temperature of the film, performed through the thermocouple fixed to the Peltier modulus, was turned on, and the *in situ* SERS map started. After an initial transient that rapidly brought the temperature of the hot site of the Peltier modulus from the room one to the one selected for the analysis (usually lasting for about 1 minute), its temperature was maintained constant during the whole thermal treatment (i.e. during the whole *in situ* SERS map), and so for a duration of 45 minutes.

Maps analysis procedure

Once performed the preliminary and the *in situ* SERS maps, according to the procedure described above, the collected spectra were analysed through a custom Python code. Fig. 5.6 shows a spectrum collected during the preliminary map of the nanocomposite film embedding HC_8H chains. As the parameter of merit, the integrated area corresponding to the frequency range of the SERS band of the embedded polyyne, i.e. 1850-2220 cm^{-1},

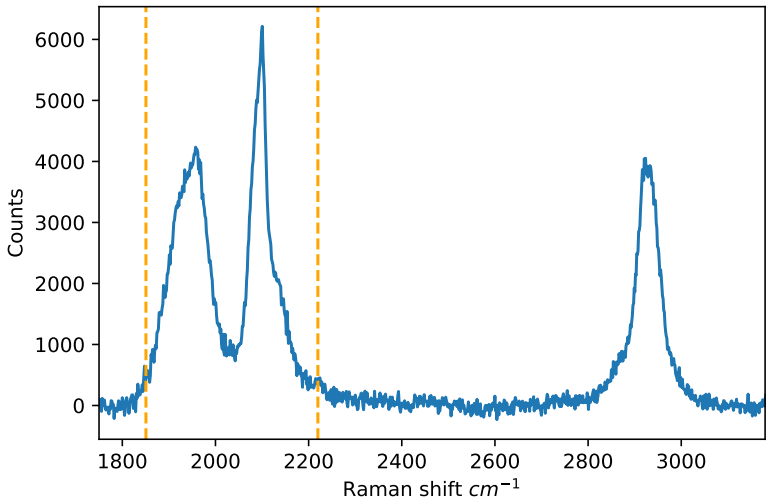

Figure 5.6: A SERS spectrum collected during the HC_8H-film preliminary map. The two dashed lines highlight the frequency region corresponding to the polyynic SERS band.

highlighted in Fig. 5.6, was computed for each spectrum and then plotted as a function of the mapping time. In this way, it was possible to observe the SERS signal from each sampled point of the film before the thermal treatment and how responded to it.

This data analysis was applied to both the SERS maps (i.e. before and during the thermal treatment), obtaining a first impression about the thermal stability of the nanocomposite films. In Fig. 5.7 it is reported an example of the comparison between the polyynic SERS areas measured, respectively, during the "preMAP", i.e. the preliminary map (a_0), and the "*in situ* MAP", i.e. the map performed during the thermal treatment (a_1). Through this preliminary analysis, it was possible to observe the eventual differences in the behaviour of the nanocomposite film when the map was performed at room temperature and when, instead, it was performed during the heating process. To perform a more accurate analysis of the collected data, the ratio a_1/a_0 between the two polyynic SERS areas, measured before and during the thermal treatment, was plotted as a function of the mapping time. Another great advantage of performing this two-steps mapping process on the nanocomposites films was that, being each SERS spectrum collected on the same point of the sample during the preliminary map and the *in situ* map, the issue related to the inhomogeneity of the film was eliminated. On one side, if the plot reporting the absolute value of the polyyne integrated area as a function of the mapping time gave only qualitative information which can be influenced by the sample inhomogeneity, on the other side, the plot reporting the a_1/a_0 ratio overcame this issue. Once obtained the plots reporting the a_1/a_0 ratio as a function of the mapping time, I modelled the decay

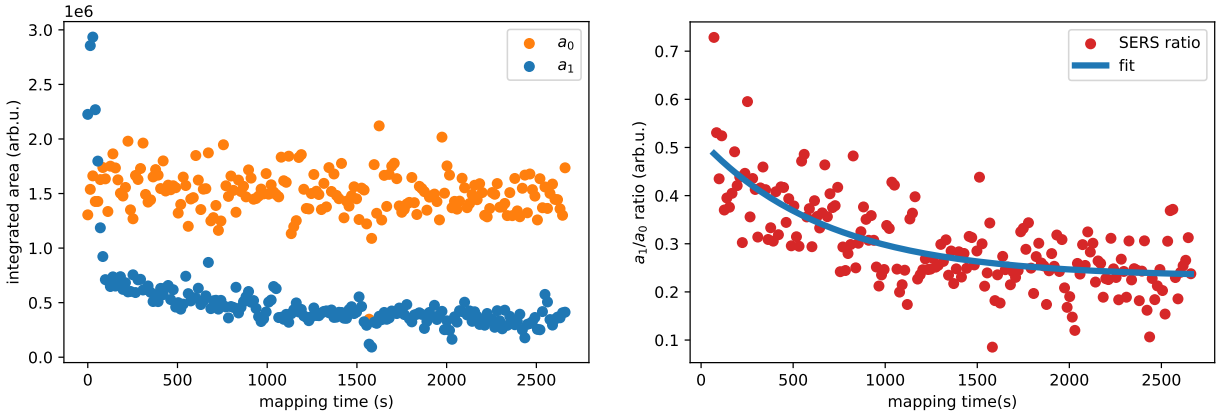

Figure 5.7: (left panel) An example of the $HC_{14}H$ integrated area as a function of the mapping time. In orange, the plot corresponds to the preliminary map (a_0). In blue, the plot corresponds to the *in situ* SERS map at 100°C (a_1). (right panel) $HC_{14}H$ a_1/a_0 ratio plotted as a function of the mapping time after thermal treatment at 100°C.

of the a_1/a_0 ratio with an exponential decay function, namely $ratio = a \cdot exp(-k \cdot t) + b$, being k the decay constant, and t the mapping time (Fig. 5.7).

5.2. Thermal stability of the PVA polymeric matrix

With the aim to investigate the thermal behaviour of the synthesized nanocomposite films, the thermal stability of the PVA polymeric matrix was assessed first. Specifically, a PVA 4% wt. aqueous solution was prepared and drop casted onto four aluminium substrates, obtaining the corresponding films. Then, by heating them through the Peltier modulus, their thermal stability was evaluated. Being the PVA glass transition temperature of about 85°C, the PVA4% films were tested both at temperatures approaching its glass transition point, i.e. 80°C and 90°C, and at temperatures above it, i.e. 100°C and

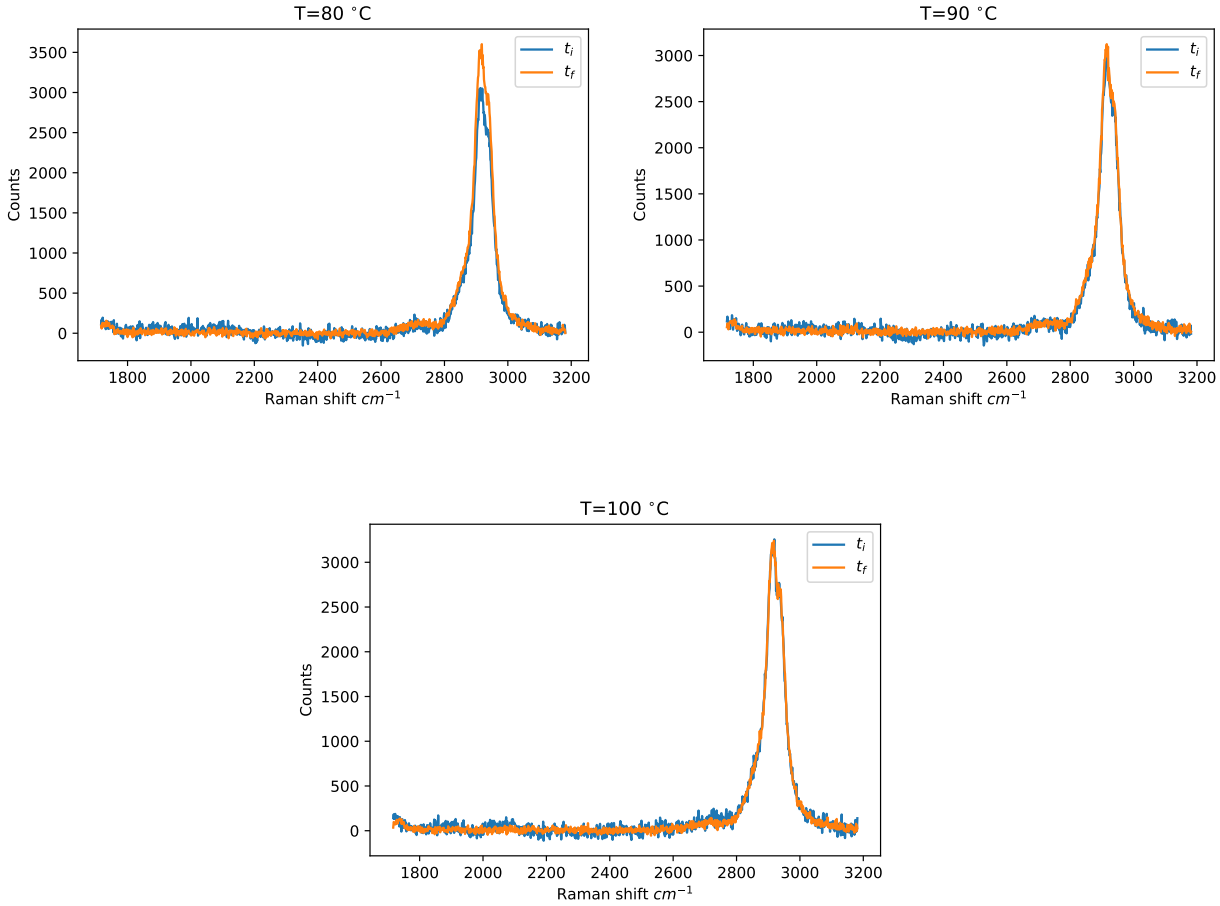

Figure 5.8: Raman spectra of the pure PVA film subjected to thermal treatment at 80°C, 90°C and 100°C. The compared spectra at the beginning (blue line) and at the end (orange line) of the heating process are shown.

110°C. The experiment was carried out safely, indeed, as mentioned in Section 5.1.2, the maximum operating point of the employed Peltier modulus was about 115°C.

The PVA4% film thermal treatment, having a duration similar to the one of the thermal treatment performed on the nanocomposite films (see Section 5.1.2), was monitored by means of a series of subsequent SERS acquisitions, and permitted to separately determine the effect of the thermal treatment on the nanocomposites' polymeric matrix. The employed SERS parameters were the ones optimized in Section 4.4.1, also adopted for the preliminary and *in situ* SERS maps. In this case the measurement was performed onto a single point of the PVA4% film. Indeed, being the sample homogeneous and not affected by any laser heating side-effect, a statistical description of the sample was not necessary.

The Raman spectra of the PVA4% films tested at 80°C, 90°C, 100°C and 110°C are shown, respectively, in Fig. 5.8 and Fig. 5.9 , each comparing the spectrum collected at the beginning and at the end of the thermal treatment.

The shape and intensity of the main PVA Raman band (located at about 2930 cm^{-1}) remain unchanged upon the thermal treatment at 80°C, 90°C and 100°C, as can be seen in Fig. 5.8. Hence, the stability of the polymeric matrix of the synthesized nanocomposite films is not affected by the heating process up to a temperature of 100°C, larger than its glass transition temperature. On the contrary, the 110°C thermal treatment makes no more possible to find the PVA Raman spectral feature located at about 2930 cm^{-1} (Fig. 5.9). Indeed, when the treatment temperature is raised up to 110°C, the PVA4% film undergoes a degradation process also visible at naked eye by its yellowing.

Given these results, to avoid the degradation of their polymeric matrix, the maximum temperature for the thermal treatments of the nanocomposite films was set to 100°C.

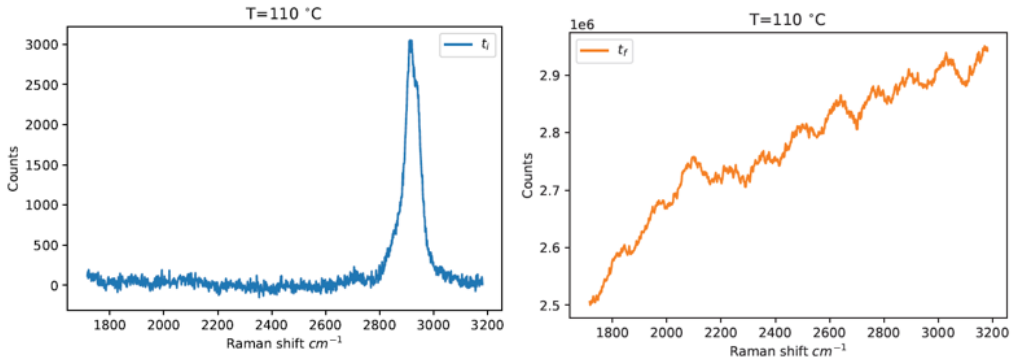

Figure 5.9: Raman spectra of the pure PVA film subjected to thermal treatment at 110°C. The compared spectra at the beginning (left panel) and at the end (right panel) of the heating process are shown.

5.3. Decoupling of thermal and laser effects on polyynes degradation

In this section, it is reported the data analysis accomplished to obtain information about the nanocomposites thermal stability and their eventual degradation due to laser interaction.

As mentioned in Section 5.1.2, each point along the mapping grid of the analysed sample was irradiated by the laser two times, the first during the preliminary map and the second during the *in situ* SERS map. Hence, the SERS spectra collected during the sample heating may embody both the thermal and the eventual laser degradative effects. Consequently, to properly investigate the stability of the polyynes embedded in the synthesized nanocomposite films after thermal treatment, the degradation effect determined by the laser, if present, should be decoupled.

Analysis of the laser effect

I developed a procedure to determine the effect of the laser on the H-polyynes based nanocomposite films stability. As mentioned before, each film was subjected to two subsequent maps, hence, each point of the mapped area was irradiated by the laser two times, spaced out by an interval of 45 minutes, i.e. the time needed to end a single map. By means of the interaction with the laser, the film was heated up, especially close to the Ag nanoparticles due to the plasmonic effect, and this could lead to polyynes degradation. Assuming a rapid heat dissipation through the metallic nanoparticles themselves [105], the thermal recovery from the laser heating between the first and the second measure was experimentally simulated on films as follows.

For each hydrogen-capped polyyne, two nanocomposite films were deposited, and two random points of each were subjected to SERS characterization. In particular, each point was analysed using the optimized parameters discussed in Section 4.4.1, the same of the SERS maps. To obtain a reliable statistics, six acquisitions have been performed on each of the four points. One minute interval was set between each acquisition, to experimentally simulate the film recovery from the laser heating between the two maps. Then, the integrated SERS area of the embedded polyyne was computed for each of them and plotted as a function of the number of acquisitions.

Each point of the plot corresponds to a laser-sample interaction having a duration equal to a single spectrum of the SERS maps. Hence, the first point will correspond to the integrated polyynic SERS area of the preliminary map, while the second point will corre-

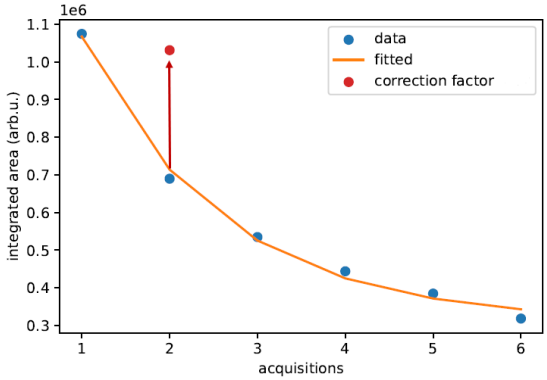

Figure 5.10: Equalization of the $HC_{14}H$ integrated area of the $n = 2$ acquisition to that of the $n = 1$ acquisition.

spond to the second measurement on the same point, i.e. to the integrated polyynic SERS area during the *in situ* SERS map. The decrease of the integrated SERS area observed in all nanocomposite films, despite the specific polyyne embedded, confirmed the supposed degradation of polyynes due to laser heating. I decided, thus, to correct the laser effect only for the *in situ* SERS map, being it the only map that could embody both the thermal and the laser effects, and so the only where it could be useful to perform their decoupling.

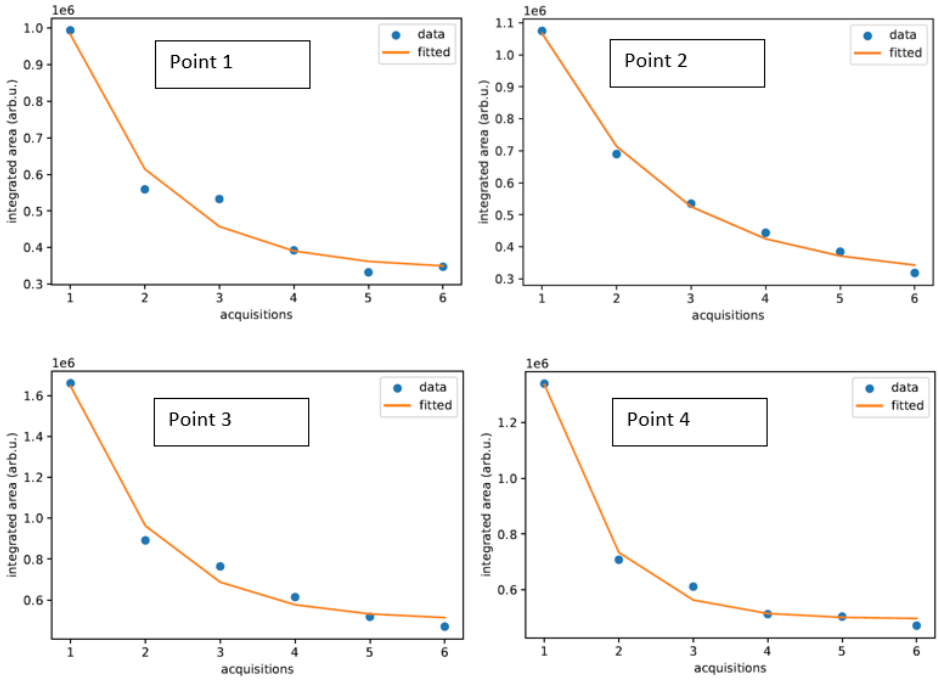

Figure 5.11: Integrated area of the polyynic SERS band of $HC_{14}H$ after each acquisition (blue circles) and fitted exponential decay (orange line).

polyyne	analysed point	f +/- err	mean f +/- mean err
HC_8H	1	1.34 +/- 0.09	1.3 +/- 0.2
	2	1.4 +/- 0.3	
	3	1.1 +/- 0.7	
	4	1.23 +/- 0.22	
$HC_{10}H$	1	2 +/- 2.7	1.6 +/- 0.7
	2	1.618 +/- 0.231	
	3	1.425 +/- 0.211	
	4	1.52 +/- 0.24	
$HC_{12}H$	1	1.4 +/- 0.9	1.65 +/- 1.46
	2	1.72 +/- 1.44	
	3	2 +/- 5	
	4	1.5 +/- 0.7	
$HC_{14}H$	1	1.6 +/- 0.98	1.7 +/- 0.4
	2	1.5 +/- 0.3	
	3	1.7 +/- 0.8	
	4	1.8 +/- 0.8	
$HC_{16}H$	1	1.7 +/- 0.3	1.73 +/- 0.23
	2	1.75 +/- 0.16	
	3	1.8 +/- 0.5	
	4	1.66 +/- 0.66	

Table 5.2: For each hydrogenated polyyne-based nanocomposite, the four values of the correction factor obtained from each of the analysed point and the corresponding mean value are shown.

In practice, the area of the $n = 2$ acquisition should be equalized to that of the $n = 1$ acquisition (Fig. 5.10). With this aim, a fit of the experimental data points was performed by means of an exponential decay, namely $area = a \cdot exp(-n/f) + b$, being "area" the integrated SERS area of the embedded polyyne, f the "correction factor" between each acquisition, and n the number of acquisitions (Fig. 5.11).

Once performed the fit of each point dataset (i.e. six acquisitions per point), the adimensional "correction factor" f was extracted for each polyyne, by averaging those calculated from the other points (i.e. four per nanocomposite film), and reported in Table 5.2.

The highest value obtained for the correction factor is, as expected, the one of $HC_{16}H$. Indeed, being the longer considered hydrogenated polyyne, it is expected to be the one with the lowest stability, and so with the larger correction due to the decoupling of the laser effect.

Decoupling of laser and thermal effects

To separate the degradation due to the laser from the thermal one, the integrated area a_1 of the embedded polyyne was multiplied by the corresponding mean correction factor. As expected, being the value of the mean correction factor always > 1, the resulting a_1/a_0 ratio was increased with respect to the original one. Fig. 5.12 shows the corrected in situ SERS integrated areas and a comparison between the uncorrected and corrected a_1/a_0 ratios in the case of data shown in Fig. 5.7.

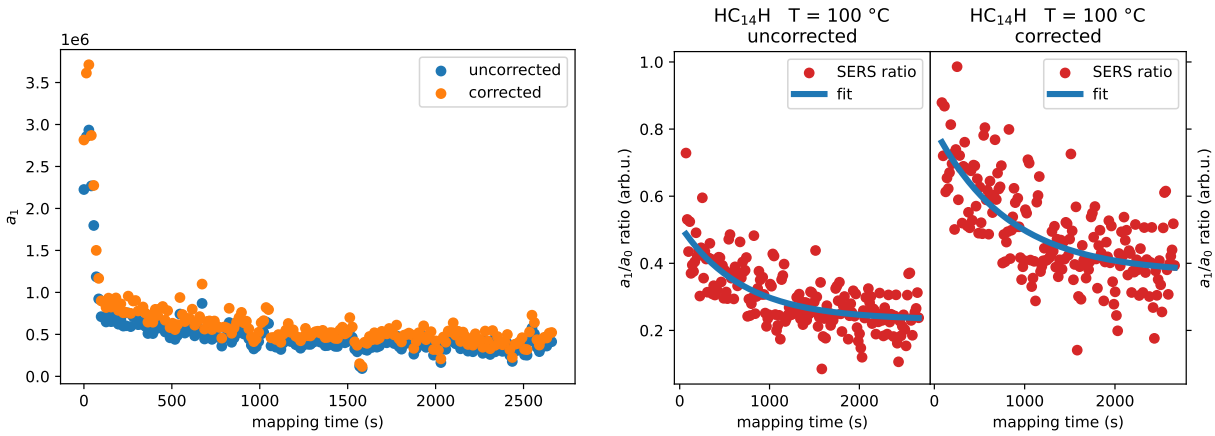

Figure 5.12: (left panel) comparison between the $HC_{14}H$ SERS integrated area during the thermal treatment at 100°C with (orange dots) and without (blue dots) laser correction. (right panel) $HC_{14}H$ a_1/a_0 ratio plotted as a function of the mapping time without (left) and with (right) laser correction.

The thermal stability of the different polyynes embedded in the nanocomposite films was, thus, evaluated by looking at the evolution of the a_1/a_0 SERS ratio during the thermal treatments at different temperatures. Each plot was fitted with the exponential decay function defined in Section 5.1.2. In particular, for those ratios showing a clear decay exponential trend, the decay constant k was extracted, and the corresponding time constant calculated. This analysis, carried out in the next section, was performed with laser-corrected ratios for hydrogen-capped polyynes, while for chlorine-capped polyynes, for which no laser heating effect was available, pristine data (without laser correction) were used.

In principle, the value of the a_1/a_0 ratio is expected to be always < 1, as a consequence of polyynes degradation during the thermal treatment. Actually, due to the films inhomogeneity, it is possible to find some of the a_1/a_0 ratio values above 1. In these cases, due to possible sample displacements, the specific point of the film irradiated by the laser was different in the preliminary map and in the *in situ* SERS map. Hence, to avoid invalidating the exponential decay model, only the a_1/a_0 ratio values < 1 were considered.

5.4. Thermal stability of size-selected HC_nH and HC_nCl polyynes embedded in PVA nanocomposite films

5.4.1. Thermal stability of H-capped polyynes based nanocomposites

All tested films have been subjected to a thermal treatment at 60°C, 80°C and 100°C. Following the procedure explained in Section 5.1.3, the corresponding results, relative to the HC_nH-based nanocomposite films, are here reported, going from $n = 8$ in Fig. 5.13 to $n = 16$ in Fig. 5.17. In every figure, each panel displays the uncorrected a_1/a_0 ratio on the left and the laser-corrected ratio on the right. The HC_8H film was the only one to be tested also at 40°C since it was taken as an internal benchmark. Indeed, being the resulting plot characterized by a mean value of the a_1/a_0 ratio approaching 1 and almost constant in time, this temperature was excluded from the analysis procedure for all subsequent films.

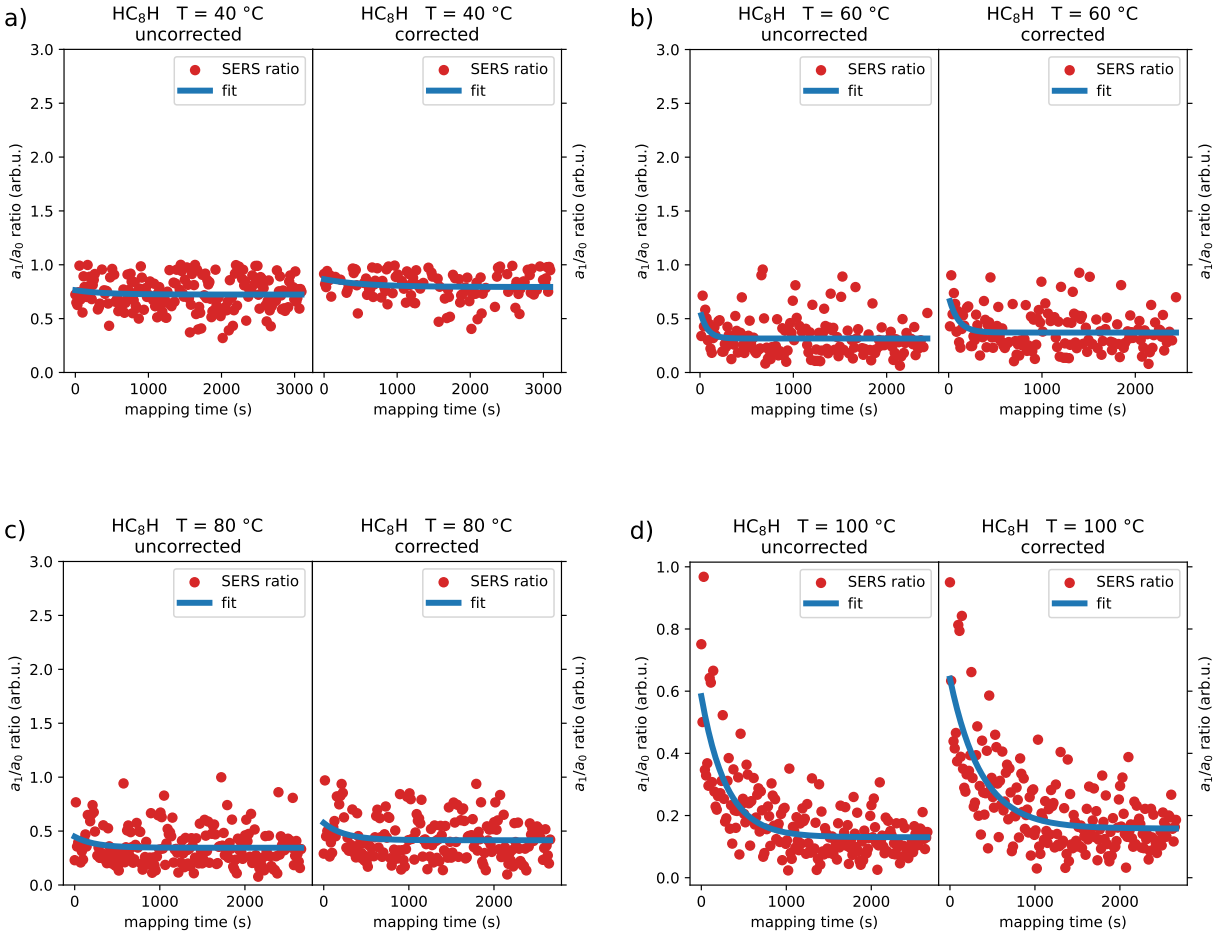

Figure 5.13: HC_8H a_1/a_0 ratio plotted as function of the mapping time. Plots obtained by performing the *in situ* SERS map at 40°C (a), 60°C (b), 80°C (c), 100°C (d) are shown. Each panel displays the uncorrected a_1/a_0 ratio on the left and the corrected ratio on the right.

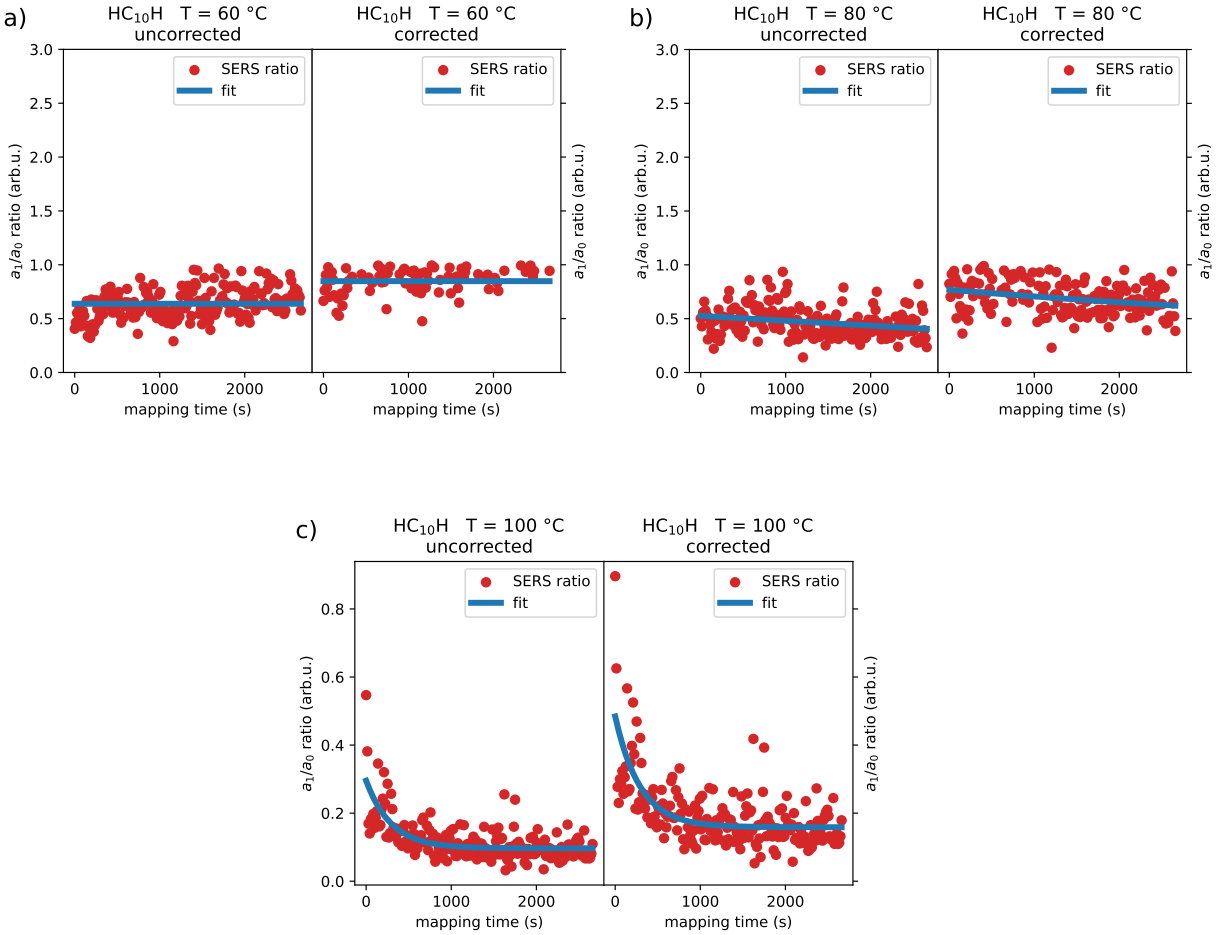

Figure 5.14: $HC_{10}H$ a_1/a_0 ratio plotted as function of the mapping time. Plots obtained by performing the *in situ* SERS map at 60°C (a), 80°C (b), 100°C (c) are shown. Each panel displays the uncorrected a_1/a_0 ratio on the left and the corrected ratio on the right.

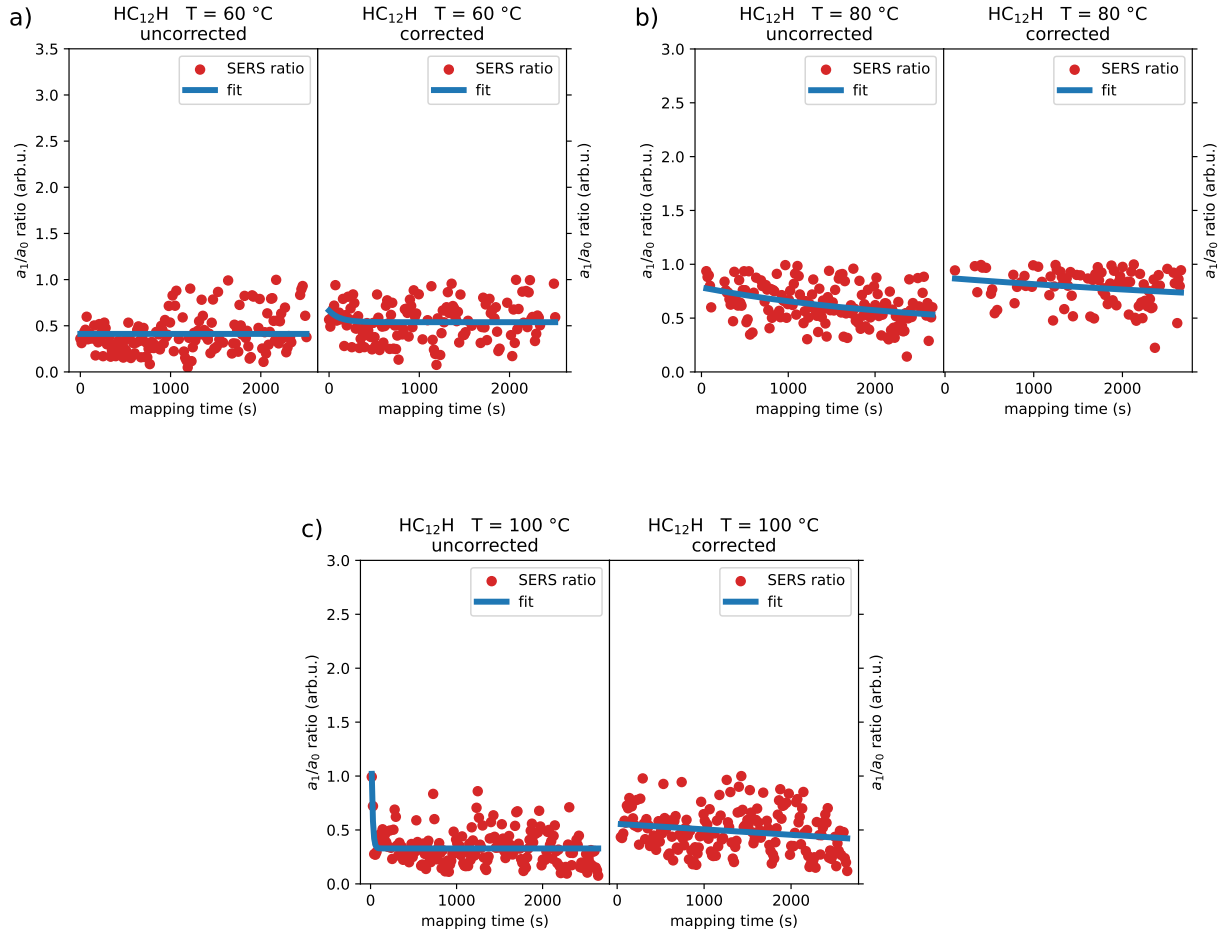

Figure 5.15: $HC_{12}H$ a_1/a_0 ratio plotted as function of the mapping time. Plots obtained by performing the *in situ* SERS map at 60°C (a), 80°C (b), 100°C (c) are shown. Each panel displays the uncorrected a_1/a_0 ratio on the left and the corrected ratio on the right.

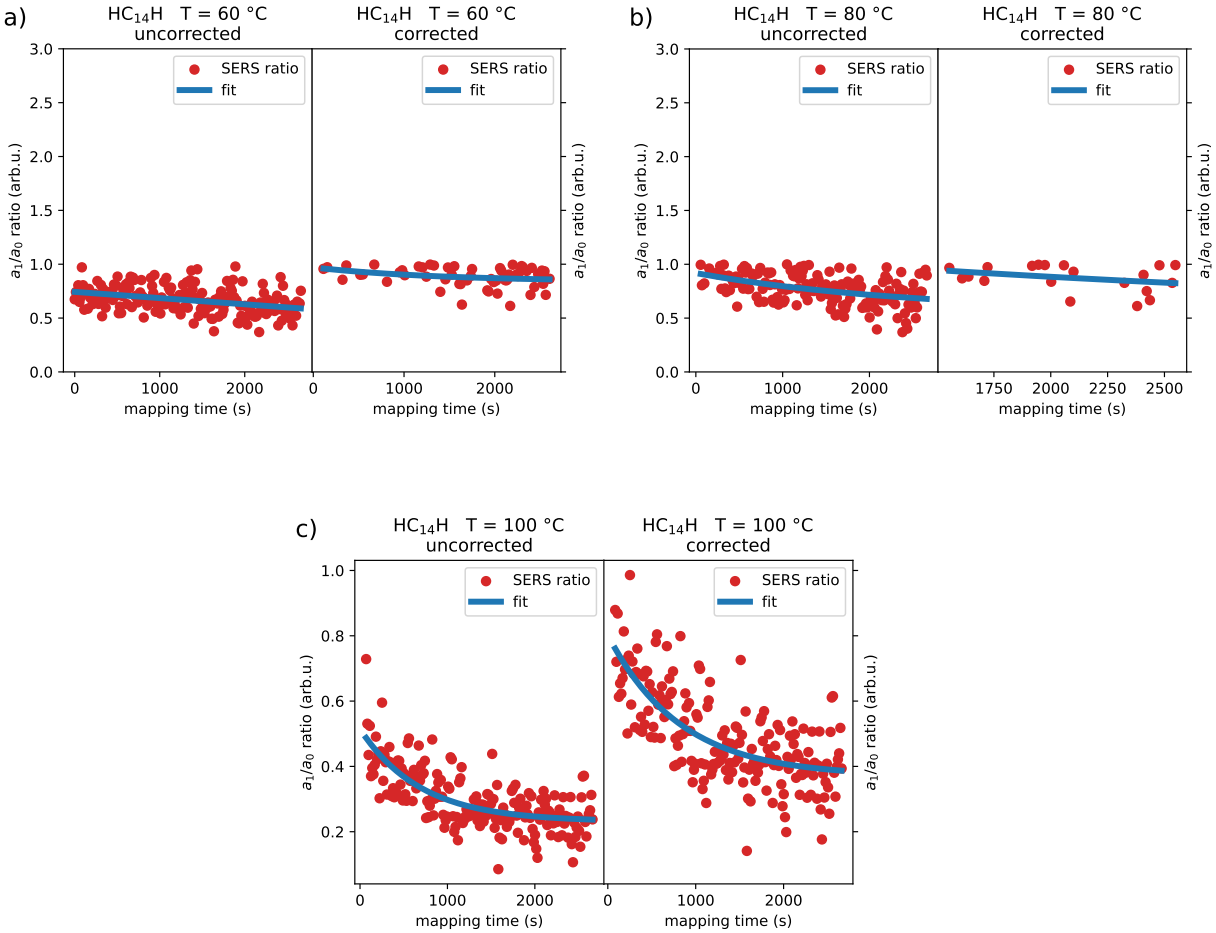

Figure 5.16: $HC_{14}H$ a_1/a_0 ratio plotted as function of the mapping time. Plots obtained by performing the *in situ* SERS map at 60°C (a), 80°C (b), 100°C (c) are shown. Each panel displays the uncorrected a_1/a_0 ratio on the left and the corrected ratio on the right.

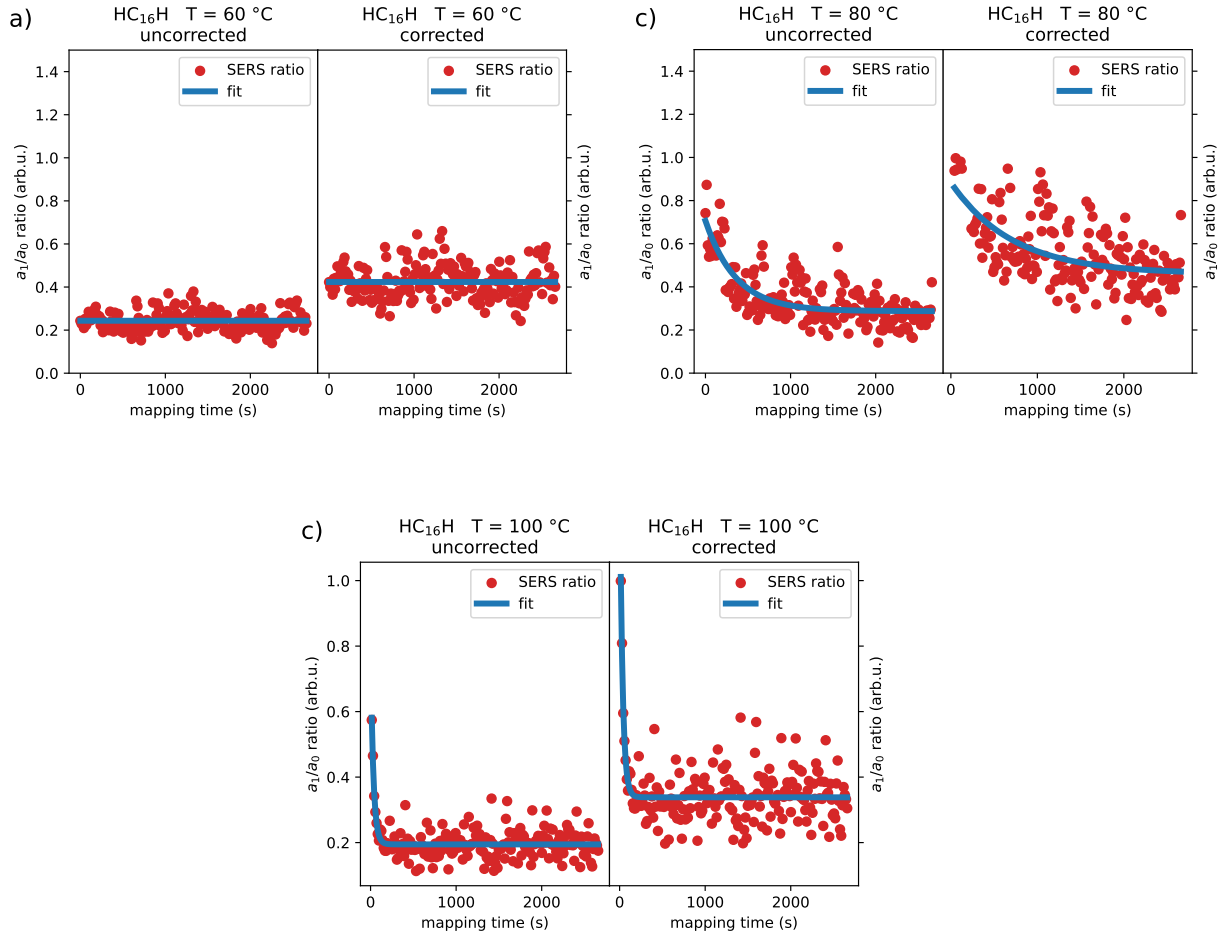

Figure 5.17: $HC_{16}H$ a_1/a_0 ratio plotted as function of the mapping time. Plots obtained by performing the *in situ* SERS map at 60°C (a), 80°C (b), 100°C (c) are shown. Each panel displays the uncorrected a_1/a_0 ratio on the left and the corrected ratio on the right.

For the a_1/a_0 ratios showing a clear exponential decay trend, the exponential decay function described in Section 5.1.2 was employed as fitting model. In this way, it was possible to give a quantitative evaluation of the stability of the different polyynes at a certain temperature. Table 5.3 shows, for each polyyne-based nanocomposite, the comparison between the time constants obtained from the fit of the plot describing the overall degradation effects of the *in situ* SERS map with the time constants obtained from the corresponding laser-corrected plot. In particular, the time constants have been calculated as the inverse of the decay constants extracted from each fit.

In principle, by increasing the thermal treatment temperature the degradation becomes faster. Indeed, a higher temperature corresponds to a higher molecular mobility, increas-

polyyne	map T (°C)	(uncorrected) time constant +/- err (s)	(corrected) time constant +/- err (s)
HC_8H	100	293 +/- 40	369 +/- 55
$HC_{10}H$	100	293 +/- 47	293 +/- 47
$HC_{14}H$	100	690 +/- 132	823 +/- 183
$HC_{16}H$	80	361 +/- 50	714 +/- 189

Table 5.3: For each hydrogenated polyyne-based nanocomposite, the compared value of the decay constant with and without the laser correction is shown.

ing the probability of crosslinking and degradation into sp^2 carbon. All the analysed films show an almost constant (or slightly variable) value of the a_1/a_0 ratio in time when the temperature is 40°C (only for HC_8H) or 60°C, while it decrease more rapidly for increasing temperatures and for longer chains. A common exponential decay trend can be observed in most films when heated up to 100°C (80°C in case of $HC_{16}H$). In particular, the decrease in the a_1/a_0 ratio is very pronounced during the very first stages of the test and then becomes much slower till the end of the map process. The initial fast a_1/a_0 ratio decrease could be the result of polyynes degradation due to the fast temperature increase, especially of chains at the surface, exposed to oxidising agents. On the other side, the following, much slower, reduction of the a_1/a_0 ratio could be due to the formation of sp-sp^2 carbon complexes that could improve polyynes stabilization in time. A note should be reserved to the plot reporting the $HC_{14}H$ ratio after the thermal treatment at 80°C. In this case, the value of the a_1/a_0 ratio is > 1 in most of the mapped points, indicating a high film inhomogeneity. For coherence with the other data, and to avoid invalidating the employed fitting model, only the a_1/a_0 ratio values below 1 have been considered, but, since they are very limited, this plot does not provide a reliable statistical description of the sample.

Looking at the exponential decay fit of the a_1/a_0 ratios corresponding to the nanocomposites thermal treatment at 80°C (only for $HC_{16}H$) and 100°C (for HC_8H,$HC_{10}H$ and $HC_{14}H$), it is possible to make some considerations. First of all, as expected, the time constants calculated with the laser-corrected data are larger than the corresponding ones calculated with the pristine data (i.e. those embodying both the thermal and laser effects), indicating that a role is effectively played by the laser in the polyynes degradation process. Secondly, it is possible to observe a peculiar behaviour when comparing the shorter chains (namely HC_8H and $HC_{10}H$) and the longer ones (i.e. $HC_{14}H$ and $HC_{16}H$). Indeed, the time constants found for the $HC_{14}H$ and $HC_{16}H$ are longer than the one obtained for

the $HC_{10}H$ and HC_8H, characterized by almost the same degradation velocity. This result can be explained by means of what reported in Section 4.4.2 about polyynes interaction with the Ag nanoparticles and among themselves. Indeed, the nanocomposite films embedding the more concentrated species, i.e. HC_8H and $HC_{10}H$ polyynes, are characterized by a content of Ag nanoparticles much smaller than the one used to synthesize the films embedding the less concentrated species, i.e. $HC_{14}H$ and $HC_{16}H$. Thus, the thermal treatment heating effect, localized especially near the metal nanoparticles, is much larger in the HC_8H and $HC_{10}H$ nanocomposites, explaining their smaller time constant. Moreover, a high thermal treatment temperature determines a higher polyynes mobility, leading, in case of more concentrated species (i.e. HC_8H and $HC_{10}H$), to a larger crosslinking probability, and so to a faster degradation.

5.4.2. Thermal stability of HC_nCl polyynes based nanocomposites

Following the procedure explained in Section 5.1.3, the results relative to the HC_nCl polyynes based nanocomposites are reported, going from $n = 8$ in Fig. 5.18 to $n = 14$ in Fig. 5.21.

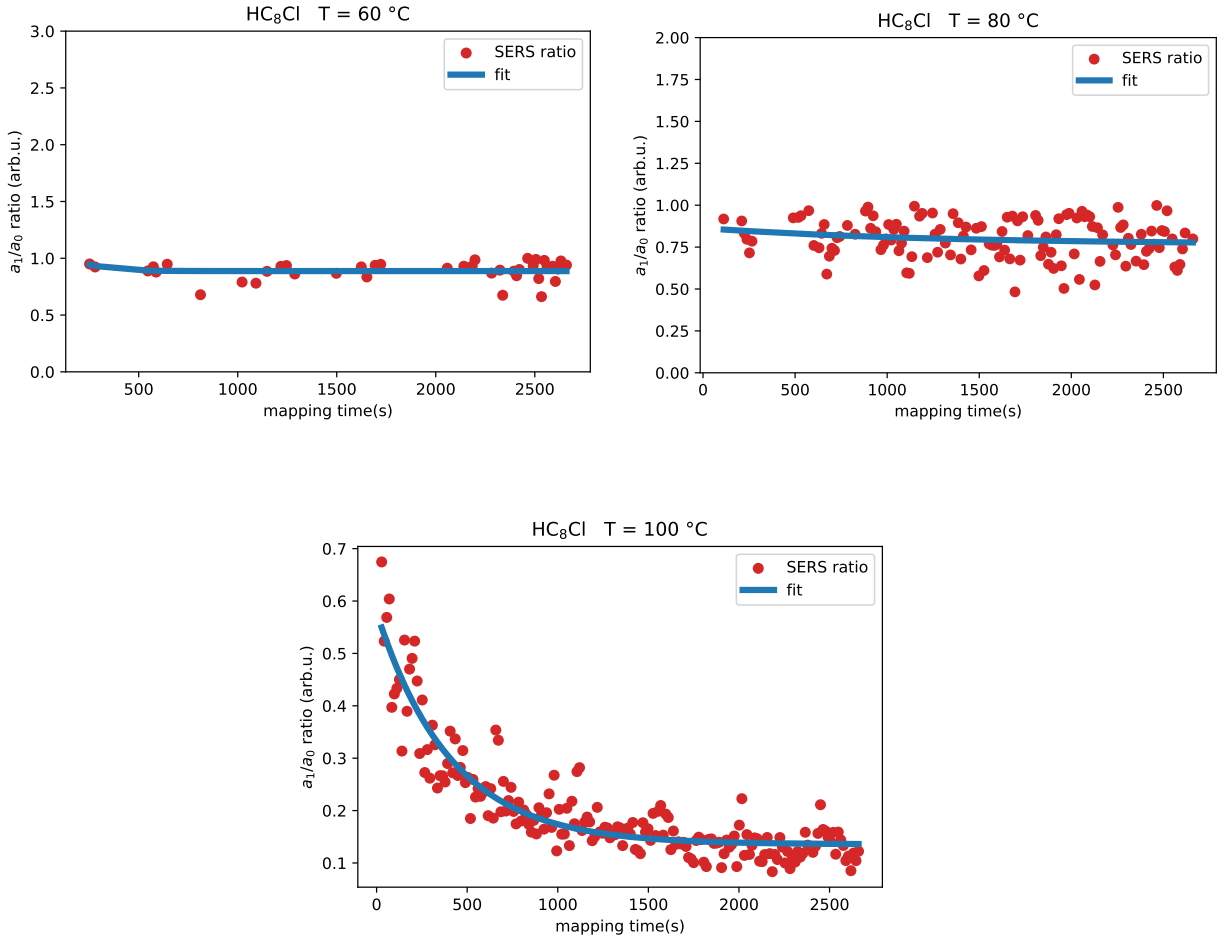

Figure 5.18: HC_8Cl a_1/a_0 ratio plotted as function of the mapping time. Plots obtained by performing the *in situ* SERS map at 60°C (a), 80°C (b), 100°C (c) are shown.

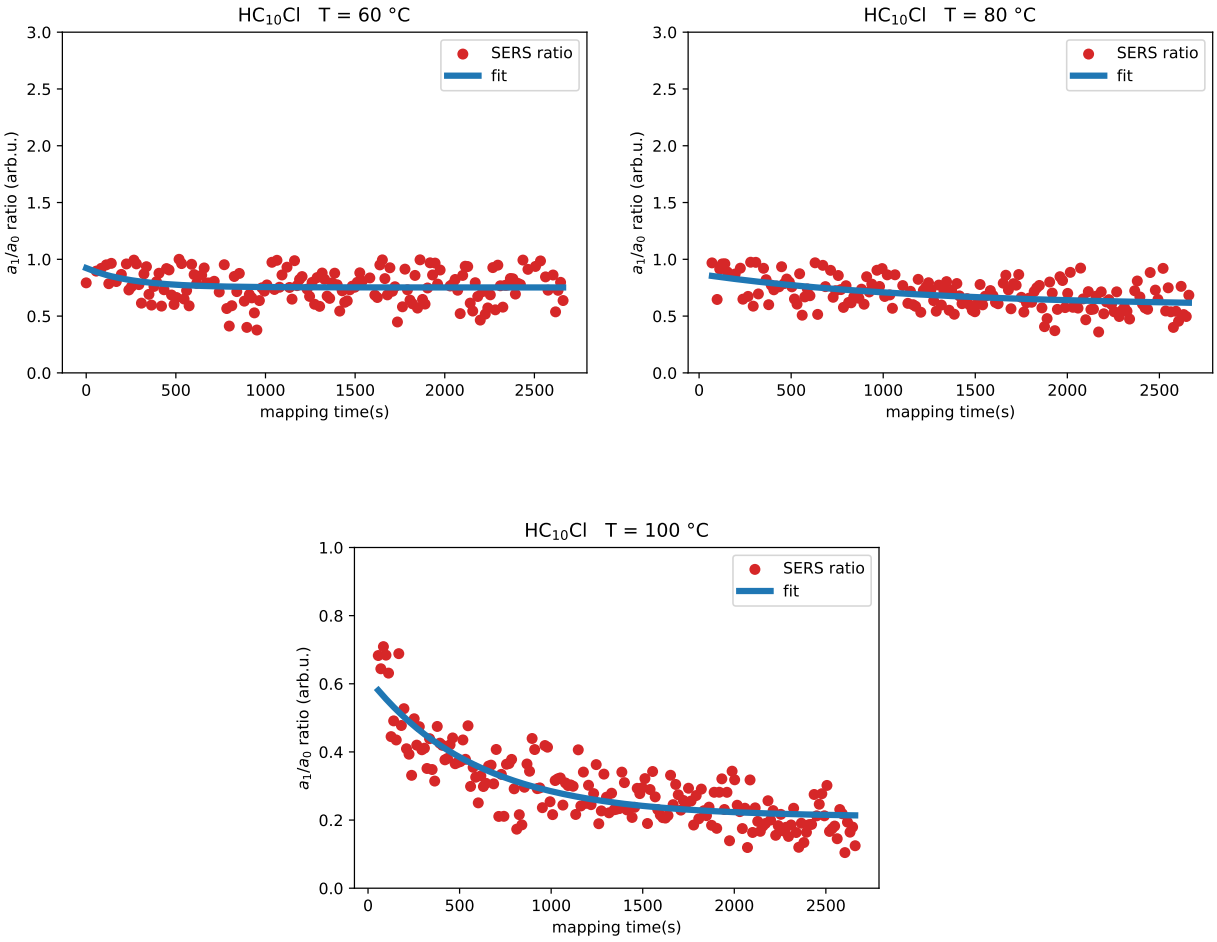

Figure 5.19: $HC_{10}Cl$ a_1/a_0 ratio plotted as function of the mapping time. Plots obtained by performing the *in situ* SERS map at 60°C (a), 80°C (b), 100°C (c) are shown.

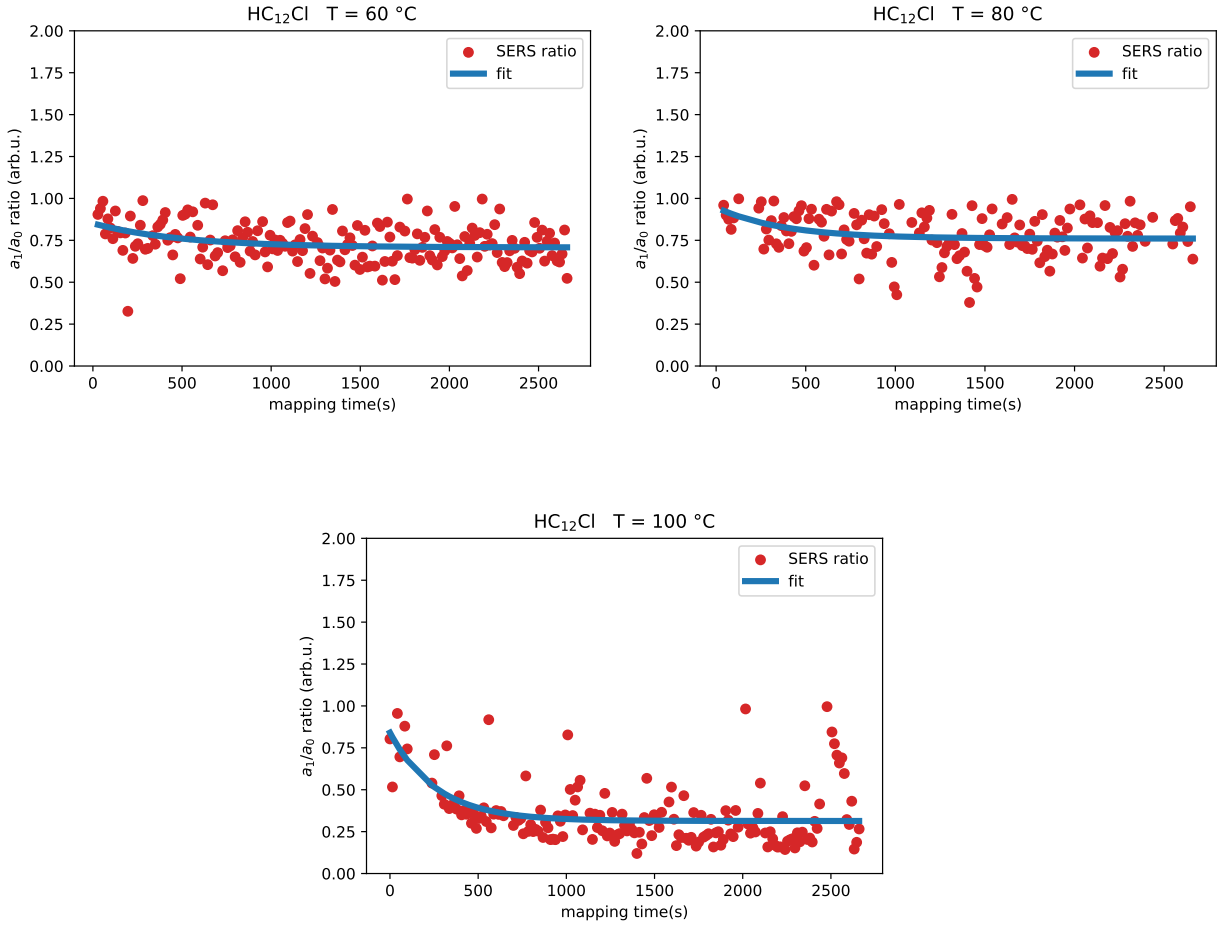

Figure 5.20: $HC_{12}Cl$ a_1/a_0 ratio plotted as function of the mapping time. Plots obtained by performing the *in situ* SERS map at 60°C (a), 80°C (b), 100°C (c) are shown.

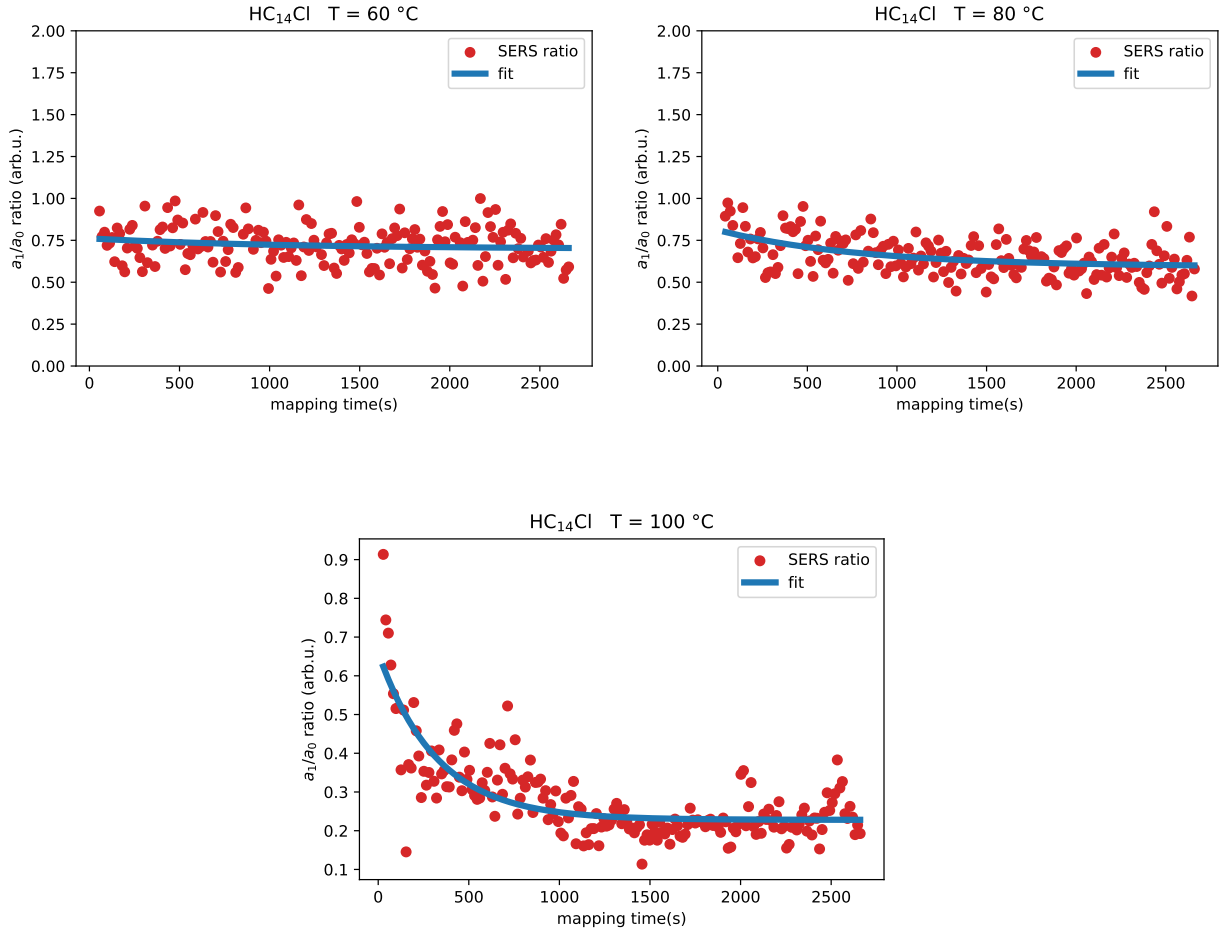

Figure 5.21: $HC_{14}Cl$ a_1/a_0 ratio plotted as function of the mapping time. Plots obtained by performing the *in situ* SERS map at 60°C (a), 80°C (b), 100°C (c) are shown.

Also in this case, for the a_1/a_0 ratios showing a clear exponential decay trend, the exponential decay function described in Section 5.1.2 was employed as fitting model. In this way, it was possible to give a quantitative evaluation of the stability of the different polyynes at a certain temperature. Table 5.4 shows, for each polyyne-based nanocomposite, the time constant obtained from the fit of the corresponding a_1/a_0 ratio plotted as a function of the mapping time. In particular, the time constants have been calculated as the inverse of the decay constants extracted from each fit.

As seen for the hydrogenated polyynes based nanocomposites, the general trend that can be outlined for all chains is that, by increasing the thermal treatment temperature, the polyynes stability decreases and their degradation becomes faster. However, differently from the hydrogenated ones, HC_nCl polyynes stability remains almost unchanged up to a

polyyne	map T(°C)	time constant (s) +/- err
HC_8Cl	100	409 +/- 28
$HC_{10}Cl$	100	592 +/- 71
$HC_{14}Cl$	100	263 +/- 64
$HC_{16}Cl$	80	324 +/- 39

Table 5.4: For each hydrogenated polyyne-based nanocomposite, the compared value of the decay constant with and without the laser correction is shown.

temperature of 80°C, and only at 100°C undergoes a more evident degradation. This can be observed by looking at the plots reporting the a_1/a_0 ratio as function of the mapping time for the 100°C thermal treatment case, characterized by a clear exponential decay trend. A note should be reserved to the plot reporting the HC_8Cl ratio after the thermal treatment at 60°C. In this case, the value of the a_1/a_0 ratio is > 1 in most of the mapped points, indicating a high film inhomogeneity. For coherence with the other data, and to avoid invalidating the employed fitting model, only the a_1/a_0 ratio values below 1 have been considered, but, since they are very limited, this plot does not provide a reliable statistical description of the sample.

Looking at the time constants extracted from the fit of the a_1/a_0 ratios corresponding to the nanocomposite films thermal treatment at 100°C, it is possible to make some considerations. As expected, the shorter chains, i.e. $HC_{10}Cl$ and HC_8Cl, are characterized by larger time constants with respect to the longer chains, i.e. $HC_{12}Cl$ and $HC_{14}Cl$, resulting in a higher stability of the former with respect to the latter.

5.4.3. Termination effect on thermal stability of polyynes nanocomposites

A first comparison between the behaviour of the nanocomposite films embedding, respectively, HC_nH and HC_nCl polyynes after thermal treatment, can be done by comparing the time constants reported in Table 5.3 and Table 5.4. For more coherence, the uncorrected time constants of H-capped polyynes must be considered to be compared with those of HC_nCl polyynes, for which, indeed, no data regarding the laser heating effect were available.

It can be seen that, overall, the time constant values obtained for the nanocomposite films embedding the HC_nCl polyynes are larger than the ones obtained in the HC_nH polyynes

case.

Moreover, by a direct comparison of the results obtained in Section 5.4.1 and Section 5.4.2, a common feature can be observed. Indeed, looking at each tested temperature, the nanocomposite films embedding the HC_nCl polyynes result to be more resistant compared to the ones embedding the HC_nH chains. I formulated different explanations that can justify the improved stability of HC_nCl polyynes, all related to the interaction between the embedded polyynes and the Ag nanoparticles and among polyynes themselves.

The first is related to the stronger interaction observed between the chlorine termination and the Ag nanoparticles (see Section 4.4.2). As a consequence, it is reasonable to assume that the stabilizing effect provided to the polyynes by the Ag nanoparticles agglomerates is larger than in the case of the hydrogenated chains, hence, also the thermal degradation is less effective.

Another explanation is referred to the amount of Ag nanoparticles inside the nanocomposite films. As described in Section 4.4.2, the volumetric content of NPPVA4% solution employed for the synthesis of the H-capped polyynes based films is much larger than the corresponding one used for the production of the HC_nCl polyynes based films. As a consequence, the effect of the pronounced heating localized especially in the region next to the metallic nanoparticles is, overall, smaller in those films embedding the HC_nCl sp-carbon chains. For this reason, their stability results to be larger.

Finally, as also reported in literature, the presence of bulky endgroups, characterized by a large steric hindrance, limits the interaction among the polyynic chains themselves. Specifically, this has been proved to be valid when dealing with polyynes solutions. However, when considering a large increase in the film temperature, that is the case of the performed maps, especially the ones performed during thermal treatments at 100°C, a corresponding increase in molecular mobility is obtained. Hence, crosslinking could be favoured. Thanks to the higher steric hindrance of the chlorine atoms with respect to the hydrogen ones, this degradative process is less probable in case of HC_nCl polyynes based films. Following this argument, it was detected in literature that Ag atoms can substitute halogen atoms, in particular chlorine, during on-surface synthesis experiments by heating up to 350 K [106, 107]. Since the strong field enhancement given by Ag nanoparticles is relaxed thermally, a local increase in temperature can lead to Ag-terminated polyynes, increasing much more their stability due to this new bulkier endgroup.

6 | Conclusions and future perspectives

The main purpose of this experimental thesis was to investigate the thermal stability of size- and termination-selected polyynes embedded in PVA nanocomposite films. To reach this goal, a preliminary research was performed to optimize both the films composition and the SERS measurements parameters. Regarding films composition optimization, different new strategies and findings can be outlined. The first is the prolonged stability of polyynes within their ablated mixtures upon purification. Indeed, both the mixtures obtained by performing the PLAL process into isopropyl-alcohol and dichloromethane showed an almost unchanged UV-Vis absorption spectrum after 50 days from the purification, and the first one even after 78 days. The second is that, differently from other works, nanocomposites were obtained by mixing HPLC-collected polyynes with a colloidal solution of Ag nanoparticles in which PVA was dissolved previously, i.e. during nanoparticles formation. This method allowed to avoid the risk of polyynes degradation upon heating needed for the PVA granules dissolution. Third, by comparing the SERS spectra of the nanocomposites obtained by mixing polyynes and Ag/PVA solutions in different volume ratios, I established a correlation between the relative amount of polyynes and nanoparticles and the maximisation of polyynes SERS signal and stability inside the film. In particular, the homogenisation of the polyynic SERS signals observed passing from 1:10 to 1:2 volume ratio was interpreted as the consequence of the more favoured chain-chain crosslinking occurring in presence of a higher polyynes concentration. Due to this degradative phenomenon, sp-sp^2 complexes would be generated, and their interaction with the Ag nanoparticles aggregates would result in the production of equalized SERS signals independently from the polyyne originally embedded into the nanocomposite. Being the polyynes SERS signals distinguishability fundamental in this work, a films composition optimization method was developed. Specifically, all nanocomposites were obtained by setting a constant molar ratio (R) between polyynes and nanoparticles, calculated from the optimized HC_8H-based film, taken as reference, i.e. R = 7.13 * 10^{-4}. With this method, I was able to obtain nanocomposites SERS spectra with maximised

SERS bands intensity and distinguishable signals of the specific embedded polyyne. To explain the different behaviour observed when dealing with the composition optimization of the nanocomposites embedding the most concentrated HC_nH and HC_nCl polyyes, I hypothesized a different interaction strength between the chlorine and the hydrogen terminations with the Ag nanoparticles, based on electronegativity considerations. Indeed, considering the Ag nanoparticles as a source of electrons, it seemed reasonable to assume a stronger interaction between them and chlorine, due to its much higher electronegativity compared to the one of hydrogen. As a consequence, a much smaller amount of Ag nanoparticles is required in case of HC_nCl-based nanocomposites, compared to HC_nH-based ones, to obtain the same SERS enhancement. This was proved by comparing the optimized NPPVA4% volumetric content employed for the obtainment of, respectively, the HC_8H-based film, i.e. 300 μL, and the HC_8Cl-based film, i.e. 45 μL. Together with the film composition, also the SERS measurement parameters have been optimized. In particular, I found a compromise between the laser power delivered to the sample and the duration of the spectral acquisitions that allowed me to perform SERS analysis with the highest signal-to-noise ratio without the risk of burning the films.

Exploiting the results obtained in the preliminary part of this work, I developed a new methodology to perform the thermal treatment of the nanocomposite films and to monitor polyynes thermal stability by means of a Peltier thermoelectric modulus coupled with an *in situ* SERS mapping procedure. The main advantages of this methodology were the possibility to perform long SERS measurements on the nanocomposite films without damaging them, and to eliminate the issue resulting from films inhomogeneity, allowing for a statistical description of the samples SERS signal and thermal stability. I also decoupled the eventual H-polyynes degradation, promoted by the laser irradiation only, from the thermal one.

By means of the developed methodology, I first investigated the nanocomposites PVA polymeric matrix thermal stability. In particular, the deposited PVA4% films were able to sustain the applied thermal treatment up to 100°C, much above PVA glass transition temperature, of about 85°C. Regarding polyynes thermal stability, different findings can be outlined. Independently from their terminations, the investigated chains showed a similar a_1/a_0 ratio trend as a function of the thermal treatment temperature. In particular, a slow ratio reduction was observed at 60°C, followed by a faster degradation at 80°C and finally by an evident exponential decay trend at 100°C, already visible at 80°C for $HC_{16}H$. The thermal degradation process affecting the polyynes embedded in the nanocomposite films, when subjected to high temperatures, is thought to occur in two phases. During the first, the a_1/a_0 ratio decreases rapidly due to the fast polyynes degradation resulting from the

high increase in temperature, which is rapidly brought from room one to the one selected for the thermal treatment; then, its reduction becomes very slow, approaching an almost constant value during the whole remaining thermal treatment time. This large slowdown in polyynes degradation was justified by assuming chains stabilizing effect determined by the eventual formation of more stable sp-sp^2 complexes, already described above.

On the other side, considering the different chain terminations, it was possible to observe a much higher thermal resistance of the Cl-capped polyynes with respect to the hydrogenated ones. Indeed, contrarily to HC_nH-based films, where an already marked degradation was visible at 80°C, HC_nCl-based films showed, independently from their length, very high stability up to 80°C, almost unchanged with respect to the one found at 60°C. The higher thermal resistance of Cl-capped polyynes with respect to H-capped ones was justified by the stronger interaction established between Ag nanoparticles and chlorine atoms, by the smaller heating effect provided to the samples due to the smaller amount of Ag nanoparticles present in HC_nCl polyynes based nanocomposites, and by the stabilizing effect provided by chlorine terminations with respect to hydrogen ones, being the first characterized by a much larger steric hindrance.

This thesis work took a step forward in the investigation of polyynes stability in polymeric nanocomposites. Indeed, a valid methodology was developed to study the effect of polyynes length and terminations on their behaviour during thermal treatments of PVA nanocomposite films embedding them.

As future perspectives, I would suggest to further investigate the sp^2 spectral region, located below 1600 cm^{-1}, to observe whether or not the assumed formation of sp-sp^2 carbon complexes occurs, and deepen their eventual role in polyynes stabilization during thermal treatment. Moreover, it would be interesting to extend the research to other chains terminations and different polymeric matrices.

In this framework, few preliminary experiments using polyethylene oxide (PEO) as the polymeric matrix of the nanocomposite films were done. The great advantage of this polymer concerns its capability to be easily dissolved into both water and acetonitrile, i.e. the solvent solution of polyynes separated with HPLC. Thanks to the high degree of PEO solubility into acetonitrile, it was possible to obtain Ag/PEO/polyynes nanocomposites by employing larger amounts of polyynic solution compared to the volumetric content of Ag/PEO solution without the occurrence of polymer aggregation, observed instead in the case of PVA. In this way, I would expect to be able to obtain more intense SERS bands in correspondence of the polyynic region. However, these performed preliminary tests were excluded from this analysis for the following reasons. Due to the extremely small

glass transition temperature of PEO (of approximately -50°C), the Ag/PEO/polyynes films could not sustain thermal treatments even at 40°C, and were highly damaged by the interaction with the laser even at room temperature. Another great advantage of PEO is that, thanks to its transparency in the polyynic UV-Vis absorption region (190-400 nm), it was possible to detect the presence of polyynes inside PEO/polyynes films by means of UV-Vis absorption spectroscopy, without the need for SERS enhancement, and so Ag nanoparticles inside the film. For these reasons, it would be interesting to find a way to improve PEO thermal stability, for example by mixing it with a more thermal-resistant polymer, in order to observe the polyynes thermal stability inside another polymeric matrix.

Another crucial aspect that should be improved is related to the poor concentration of polyynes synthesized by PLAL. By increasing polyynes concentration, indeed, it would be possible to characterize them and their thermal stability without the need for Ag nanoparticles. Besides the possibility to observe their properties without the interaction of Ag nanoparticles, this would lead to a great improvement of polyynes stability, which indeed would not be affected by the extensive heating localized in the nanoparticles aggregates.

Bibliography

[1] Th Henning and F Salama. Carbon in the universe. *science*, 282(5397):2204–2210, 1998.

[2] Carlo S Casari. Carbon atomic wires: From stars to nanotechnology. *Istituto Lombardo-Accademia di Scienze e Lettere-Rendiconti di Scienze*, 2012.

[3] M. Weller, T. Overton, F. Armstrong, and J. Rourke. *Inorganic Chemistry*. Oxford University Press, 2018.

[4] P.W. Atkins, J. De Paula, and J. Keeler. *Atkins' Physical Chemistry*. Oxford University Press, 2018.

[5] Yu P. Kudryavtsev. *The Discovery of Carbyne*, pages 1–6. Springer Netherlands, Dordrecht, 1999.

[6] Carlo S Casari, Matteo Tommasini, Rik R Tykwinski, and Alberto Milani. Carbon-atom wires: 1-d systems with tunable properties. *Nanoscale*, 8(8):4414–4435, 2016.

[7] Salisu Nasir, Mohd Zobir Hussein, Zulkarnain Zainal, and Nor Azah Yusof. Carbon-based nanomaterials/allotropes: A glimpse of their synthesis, properties and some applications. *Materials*, 11(2), 2018.

[8] Andreas Hirsch. The era of carbon allotropes. *Nature materials*, 9(11):868–871, 2010.

[9] C Glaser. Beiträge zur kenntniss des acetenylbenzols. *Berichte der deutschen chemischen Gesellschaft*, 2(1):422–424, 1869.

[10] Adolf Baeyer. Ueber polyacetylenverbindungen. *Berichte der deutschen chemischen Gesellschaft*, 18(2):2269–2281, 1885.

[11] Marjorie Anchel. Identification of an antibiotic polyacetylene from clitocybe diatreta as a suberamic acid ene-diyne. *Journal of the American Chemical Society*, 75(18):4621–4622, 1953.

[12] John D Bu'Lock. Acetylenic compounds as natural products. *Quarterly Reviews, Chemical Society*, 10(4):371–394, 1956.

[13] Gen Nakaminami. The structures of natural acetylenic compounds and their biogenesis. *Journal of Synthetic Organic Chemistry, Japan*, 21(10):751–765, 1963.

[14] Adrian Webster. Carbyne as a possible constituent of the interstellar dust. *Monthly Notices of the Royal Astronomical Society*, 192(1):7P–9P, 1980.

[15] A Greenville Whittaker, Ethel J Watts, Roy S Lewis, and Edward Anders. Carbynes: carriers of primordial noble gases in meteorites. *Science*, 209(4464):1512–1514, 1980.

[16] Ryoichi Hayatsu, Robert G Scott, Martin H Studier, Roy S Lewis, and Edward Anders. Carbynes in meteorites: detection, low-temperature origin, and implications for interstellar molecules. *Science*, 209(4464):1515–1518, 1980.

[17] Aleksei Mikhailovich Sladkov and Yu P Kudryavtsev. Polyynes. *Russian Chemical Reviews*, 32(5):229, 1963.

[18] Carlo S Casari and Alberto Milani. Carbyne: from the elusive allotrope to stable carbon atom wires. *Mrs Communications*, 8(2):207–219, 2018.

[19] Rik R Tykwinski, Wesley Chalifoux, Sara Eisler, Andrea Lucotti, Matteo Tommasini, Daniele Fazzi, Mirella Del Zoppo, and Giuseppe Zerbi. Toward carbyne: Synthesis and stability of really long polyynes. *Pure and Applied Chemistry*, 82(4):891–904, 2010.

[20] Shujiang Yang and Miklos Kertesz. Linear c n clusters: are they acetylenic or cumulenic? *The Journal of Physical Chemistry A*, 112(1):146–151, 2008.

[21] Sara Eisler, Aaron D Slepkov, Erin Elliott, Thanh Luu, Robert McDonald, Frank A Hegmann, and Rik R Tykwinski. Polyynes as a model for carbyne: synthesis, physical properties, and nonlinear optical response. *Journal of the American Chemical Society*, 127(8):2666–2676, 2005.

[22] Thomas Gibtner, Frank Hampel, Jean-Paul Gisselbrecht, and Andreas Hirsch. End-cap stabilized oligoynes: Model compounds for the linear sp carbon allotrope carbyne. *Chemistry â€“ A European Journal*, 8(2):408–432, 2002.

[23] Alberto Milani, Matteo Tommasini, Mirella Del Zoppo, Chiara Castiglioni, and Giuseppe Zerbi. Carbon nanowires: Phonon and π-electron confinement. *Physical Review B*, 74(15):153418, 2006.

[24] Alberto Milani, Matteo Tommasini, Daniele Fazzi, Chiara Castiglioni, Mirella Del

Zoppo, and Giuseppe Zerbi. First-principles calculation of the peierls distortion in an infinite linear carbon chain: the contribution of raman spectroscopy. *Journal of Raman Spectroscopy: An International Journal for Original Work in all Aspects of Raman Spectroscopy, Including Higher Order Processes, and also Brillouin and Rayleigh Scattering*, 39(2):164–168, 2008.

[25] Franco Cataldo. *Polyynes: synthesis, properties, and applications*. CRC Press, 2005.

[26] Yueze Gao, Yuxuan Hou, Fernando Gordillo Gamez, Mike J Ferguson, Juan Casado, and Rik R Tykwinski. The loss of endgroup effects in long pyridyl-endcapped oligoynes on the way to carbyne. *Nature Chemistry*, 12(12):1143–1149, 2020.

[27] Wesley A Chalifoux, Robert McDonald, Michael J Ferguson, and Rik R Tykwinski. tert-butyl-end-capped polyynes: Crystallographic evidence of reduced bond-length alternation. *Angewandte Chemie International Edition*, 48(42):7915–7919, 2009.

[28] Johanna A Januszewski and Rik R Tykwinski. Synthesis and properties of long [n] cumulenes (n 5). *Chemical Society Reviews*, 43(9):3184–3203, 2014.

[29] Alessandro La Torre, Andrés Botello-Mendez, Walid Baaziz, J-C Charlier, and Florian Banhart. Strain-induced metal–semiconductor transition observed in atomic carbon chains. *Nature communications*, 6(1):1–7, 2015.

[30] Alberto Milani, Matteo Tommasini, Valentino Barbieri, Andrea Lucotti, Valeria Russo, Franco Cataldo, and Carlo S Casari. Semiconductor-to-metal transition in carbon-atom wires driven by sp2 conjugated end groups. *The Journal of Physical Chemistry C*, 121(19):10562–10570, 2017.

[31] Francesco Innocenti, Alberto Milani, and Chiara Castiglioni. Can raman spectroscopy detect cumulenic structures of linear carbon chains? *Journal of Raman Spectroscopy: An International Journal for Original Work in all Aspects of Raman Spectroscopy, Including Higher Order Processes, and also Brillouin and Rayleigh Scattering*, 41(2):226–236, 2010.

[32] Matteo Tommasini, Alberto Milani, Daniele Fazzi, Andrea Lucotti, Chiara Castiglioni, Johanna A Januszewski, Dominik Wendinger, and Rik R Tykwinski. π-conjugation and end group effects in long cumulenes: Raman spectroscopy and dft calculations. *The Journal of Physical Chemistry C*, 118(45):26415–26425, 2014.

[33] Mingjie Liu, Vasilii I Artyukhov, Hoonkyung Lee, Fangbo Xu, and Boris I Yakobson. Carbyne from first principles: chain of c atoms, a nanorod or a nanorope. *ACS nano*, 7(11):10075–10082, 2013.

[34] Pavel B Sorokin, Hoonkyung Lee, Lyubov Yu Antipina, Abhishek K Singh, and Boris I Yakobson. Calcium-decorated carbyne networks as hydrogen storage media. *Nano letters*, 11(7):2660–2665, 2011.

[35] Ovidiu Cretu, Andres R Botello-Mendez, Izabela Janowska, Cuong Pham-Huu, Jean-Christophe Charlier, and Florian Banhart. Electrical transport measured in atomic carbon chains. *Nano letters*, 13(8):3487–3493, 2013.

[36] Martin R Bryce. A review of functional linear carbon chains (oligoynes, polyynes, cumulenes) and their applications as molecular wires in molecular electronics and optoelectronics. *Journal of Materials Chemistry C*, 2021.

[37] Fanghao Hu, Chen Zeng, Rong Long, Yupeng Miao, Lu Wei, Qizhi Xu, and Wei Min. Supermultiplexed optical imaging and barcoding with engineered polyynes. *Nature methods*, 15(3):194–200, 2018.

[38] Wai-Yeung Wong, Xingzhu Wang, Hai-Liang Zhang, Kai-Yin Cheung, Man-Kin Fung, Aleksandra B Djurišić, and Wai-Kin Chan. Synthesis, characterization and photovoltaic properties of a low-bandgap platinum (ii) polyyne functionalized with a 3, 4-ethylenedioxythiophene-benzothiadiazole hybrid spacer. *Journal of Organometallic Chemistry*, 693(24):3603–3612, 2008.

[39] Alberto D Scaccabarozzi, Alberto Milani, Sonia Peggiani, Stefano Pecorario, Bozheng Sun, Rik R Tykwinski, Mario Caironi, and Carlo S Casari. A field-effect transistor based on cumulenic sp-carbon atomic wires. *The journal of physical chemistry letters*, 11(5):1970–1974, 2020.

[40] Stefano Pecorario, Alberto D Scaccabarozzi, Daniele Fazzi, Edgar Gutiérrez-Fernández, Vito Vurro, Lorenzo Maserati, Mengting Jiang, Tommaso Losi, Bozheng Sun, Rik R Tykwinski, et al. Stable and solution-processable cumulenic sp-carbon wires: A new paradigm for organic electronics. *Advanced Materials*, 34(15):2110468, 2022.

[41] Yu P Kudryavtsev. Oxidative dehydropolycondensation—a new method to synthesize polymers with triple bonds, 1969.

[42] Martyn Jevric and Mogens Brøndsted Nielsen. Synthetic strategies for oligoynes. *Asian Journal of Organic Chemistry*, 4(4):286–295, 2015.

[43] Bartłomiej Pigulski, Nurbey Gulia, and Sławomir Szafert. Reactivity of polyynes: complex molecules from simple carbon rods. *European Journal of Organic Chemistry*, 2019(7):1420–1445, 2019.

[44] Wesley A Chalifoux and Rik R Tykwinski. Synthesis of extended polyynes: Toward carbyne. *Comptes Rendus Chimie*, 12(3-4):341–358, 2009.

[45] Franco Cataldo. Simple generation and detection of polyynes in an arc discharge between graphite electrodes submerged in various solvents. *Carbon (New York, NY)*, 41(13):2671–2674, 2003.

[46] Paolo Milani and Salvatore Iannotta. *Cluster beam synthesis of nanostructured materials*. Springer Science & Business Media, 2012.

[47] Masaharu Tsuji, Takeshi Tsuji, Shingo Kuboyama, Seong-Ho Yoon, Yozo Korai, Teppei Tsujimoto, Kanji Kubo, Akira Mori, and Isao Mochida. Formation of hydrogen-capped polyynes by laser ablation of graphite particles suspended in solution. *Chemical physics letters*, 355(1-2):101–108, 2002.

[48] M Bogana, L Ravagnan, Carlo Spartaco Casari, A Zivelonghi, Andrea Baserga, A Li Bassi, Carlo Enrico Bottani, S Vinati, E Salis, P Piseri, et al. Leaving the fullerene road: presence and stability of sp chains in sp2 carbon clusters and cluster-assembled solids. *New Journal of Physics*, 7(1):81, 2005.

[49] Pietro Marabotti, Sonia Peggiani, Alessandro Vidale, and Carlo Spartaco Casari. Pulsed laser ablation in liquid of sp-carbon chains: status and recent advances. *arXiv preprint arXiv:2206.01238*, 2022.

[50] Sonia Peggiani, Anna Facibeni, Alberto Milani, Chiara Castiglioni, Valeria Russo, Andrea Li Bassi, and Carlo S Casari. In situ synthesis of polyynes in a polymer matrix via pulsed laser ablation in a liquid. *Materials Advances*, 1(8):2729–2736, 2020.

[51] Sonia Peggiani, Pietro Marabotti, Riccardo Alberto Lotti, Anna Facibeni, Patrick Serafini, Alberto Milani, Valeria Russo, Andrea Li Bassi, and Carlo Spartaco Casari. Solvent-dependent termination, size and stability in polyynes synthesized via laser ablation in liquids. *Physical Chemistry Chemical Physics*, 22(45):26312–26321, 2020.

[52] Vincenzo Amendola and Moreno Meneghetti. What controls the composition and the structure of nanomaterials generated by laser ablation in liquid solution? *Physical Chemistry Chemical Physics*, 15(9):3027–3046, 2013.

[53] A Kanitz, MR Kalus, EL Gurevich, A Ostendorf, S Barcikowski, and David Amans. Review on experimental and theoretical investigations of the early stage, femtoseconds to microseconds processes during laser ablation in liquid-phase for the synthesis

of colloidal nanoparticles. *Plasma Sources Science and Technology*, 28(10):103001, 2019.

[54] Tomonari Wakabayashi, Mao Saikawa, Yoriko Wada, and Toshie Minematsu. Isotope scrambling in the formation of cyanopolyynes by laser ablation of carbon particles in liquid acetonitrile. *Carbon*, 50(1):47–56, 2012.

[55] Ali Ramadhan, Michal Wesolowski, Tomonari Wakabayashi, Haruo Shiromaru, Tatsuya Fujino, Takeshi Kodama, Walter Duley, and Joseph Sanderson. Synthesis of hydrogen-and methyl-capped long-chain polyynes by intense ultrashort laser pulse irradiation of toluene. *Carbon*, 118:680–685, 2017.

[56] Ryutaro Matsutani, Kohei Inoue, Noriyuki Wada, and Kazuo Kojima. Wavelength dependence of polyyne preparation by liquid-phase laser ablation using pellet targets. *Chemical communications*, 47(20):5840–5842, 2011.

[57] Masaharu Tsuji, Shingo Kuboyama, Takeshi Tsuji, and Taro Hamagami. Formation of c2nh2 polyynes by laser ablation of graphite, coal or c60 particles suspended in selected solvents. In *Polyynes*, pages 147–174. CRC Press, 2005.

[58] Young Eun Park, Seung Keun Shin, and Seung Min Park. The physical effects on the formation of polyynes by laser ablation. *Chemical Physics Letters*, 568:112–116, 2013.

[59] Hiroshi Tabata, Minoru Fujii, Shinji Hayashi, Tatsuya Doi, and Tomonari Wakabayashi. Raman and surface-enhanced raman scattering of a series of size-separated polyynes. *Carbon*, 44(15):3168–3176, 2006.

[60] Alberto Milani, Matteo Tommasini, Valeria Russo, Andrea Li Bassi, Andrea Lucotti, Franco Cataldo, and Carlo S Casari. Raman spectroscopy as a tool to investigate the structure and electronic properties of carbon-atom wires. *Beilstein journal of nanotechnology*, 6(1):480–491, 2015.

[61] Andrea Lucotti, MATTEO Tommasini, Mirella Del Zoppo, Chiara Castiglioni, Giuseppe Zerbi, Franco Cataldo, Carlo Spartaco Casari, A Li Bassi, Valeria Russo, M Bogana, et al. Raman and sers investigation of isolated sp carbon chains. *Chemical physics letters*, 417(1-3):78–82, 2006.

[62] Giuseppe Compagnini, Giacomo Patane, Luisa D'Urso, Orazio Puglisi, Rosario Sergio Cataliotti, and Bruno Pignataro. On the interaction of carbon nanowires with noble metals through a study of their surface-enhanced raman spectra. *The Journal of Physical Chemistry C*, 112(51):20301–20306, 2008.

[63] Shu Okada, Minoru Fujii, and Shinji Hayashi. Immobilization of polyynes adsorbed on ag nanoparticle aggregates into poly (vinyl alcohol) films. *Carbon*, 49(14):4704–4709, 2011.

[64] Kang An, Guotong Wei, Gongmin Qi, Leimei Sheng, Liming Yu, Wei Ren, and Xinluo Zhao. Stability improvement of c8h2 and c10h2 embedded in poly (vinyl alcohol) films with adsorption on gold nanoparticles. *Chemical Physics Letters*, 637:71–76, 2015.

[65] Luisa D'Urso, Giuseppe Grasso, Elena Messina, Corrado Bongiorno, Viviana Scuderi, Silvia Scalese, Orazio Puglisi, Giuseppe Spoto, and Giuseppe Compagnini. Role of linear carbon chains in the aggregation of copper, silver, and gold nanoparticles. *The Journal of Physical Chemistry C*, 114(2):907–915, 2010.

[66] Kuk-Ki Kim, Seung-Keun Shin, and Seung-Min Park. Aggregation of polyynes on metal nanoparticles. *Bulletin of the Korean Chemical Society*, 33(2):625–628, 2012.

[67] Andrea Lucotti, Carlo Spartaco Casari, M Tommasini, A Li Bassi, Daniele Fazzi, Valeria Russo, M Del Zoppo, Chiara Castiglioni, F Cataldo, Carlo Enrico Bottani, et al. sp carbon chain interaction with silver nanoparticles probed by surface enhanced raman scattering. *Chemical Physics Letters*, 478(1-3):45–50, 2009.

[68] Kenji Hanamura, Minoru Fujii, Tomonari Wakabayashi, and Shinji Hayashi. Surface-enhanced raman scattering of size-selected polyynes (c8h2) adsorbed on silver colloidal nanoparticles. *Chemical Physics Letters*, 503(1-3):118–123, 2011.

[69] Carlo Spartaco Casari, Valeria Russo, Andrea Li Bassi, Carlo Enrico Bottani, F Cataldo, Andrea Lucotti, M Tommasini, M Del Zoppo, Chiara Castiglioni, and Giuseppe Zerbi. Stabilization of linear carbon structures in a solid ag nanoparticle assembly. *Applied physics letters*, 90(1):013111, 2007.

[70] Alessandro Zalla. Quantum chemical simulations of the interaction of polyynes with silver nanoparticles. 2021.

[71] Franco Cataldo. Spectroscopical characterization of carbonaceous matter prepared through the glaser coupling reaction route. *Carbon*, 37(1):161–163, 1999.

[72] Veronika R Meyer. *Practical high-performance liquid chromatography*. John Wiley & Sons, 2013.

[73] Franco Cataldo, Luca Ravagnan, Eugenio Cinquanta, Ivano Eligio Castelli, Nicola Manini, Giovanni Onida, and Paolo Milani. Synthesis, characterization, and model-

ing of naphthyl-terminated sp carbon chains: dinaphthylpolyynes. *The Journal of Physical Chemistry B*, 114(46):14834–14841, 2010.

[74] Sonia Peggiani, Andrea Senis, Anna Facibeni, Alberto Milani, Patrick Serafini, Gianmarco Cerrato, Andrea Lucotti, Matteo Tommasini, Daniele Fazzi, Chiara Castiglioni, et al. Size-selected polyynes synthesised by submerged arc discharge in water. *Chemical Physics Letters*, 740:137054, 2020.

[75] Franco Cataldo, Ornella Ursini, Alberto Milani, and Carlo S Casari. One-pot synthesis and characterization of polyynes end-capped by biphenyl groups (α, ω-biphenylpolyynes). *Carbon*, 126:232–240, 2018.

[76] Franco Cataldo. Synthesis of polyynes in a submerged electric arc in organic solvents. *Carbon*, 42(1):129–142, 2004.

[77] Sonia Peggiani, Anna Facibeni, Pietro Marabotti, Alessandro Vidale, Stefano Scotti, and Carlo S Casari. A single liquid chromatography procedure to concentrate, separate and collect size-selected polyynes produced by pulsed laser ablation in water. *arXiv preprint arXiv:2206.10325*, 2022.

[78] Franco Cataldo. Stability of polyynes in air and their degradation by ozonolysis. *polymer degradation and stability*, 91(2):317–323, 2006.

[79] NR Agarwal, Andrea Lucotti, Daniele Fazzi, MATTEO Tommasini, Chiara Castiglioni, WA Chalifoux, and RR Tykwinski. Structure and chain polarization of long polyynes investigated with infrared and raman spectroscopy. *Journal of Raman Spectroscopy*, 44(10):1398–1410, 2013.

[80] Thomas Gibtner, Frank Hampel, Jean-Paul Gisselbrecht, and Andreas Hirsch. End-cap stabilized oligoynes: model compounds for the linear sp carbon allotrope carbyne. *Chemistry–A European Journal*, 8(2):408–432, 2002.

[81] Wesley A Chalifoux and Rik R Tykwinski. Synthesis of polyynes to model the sp-carbon allotrope carbyne. *Nature chemistry*, 2(11):967, 2010.

[82] Lei Shi, Philip Rohringer, Kazu Suenaga, Yoshiko Niimi, Jani Kotakoski, Jannik C Meyer, Herwig Peterlik, Marius Wanko, Seymur Cahangirov, Angel Rubio, et al. Confined linear carbon chains as a route to bulk carbyne. *Nature materials*, 15(6):634–639, 2016.

[83] Thomas S Neugebauer, Michael Franz, Stephanie Frankenberger, Rik R Tykwinski, and Thomas Drewello. Laser desorption vs. electrospray of polyyne-threaded ro-

taxanes: preventing covalent cross-linking and promoting noncovalent aggregation. *The Journal of Chemical Physics*, 148(6):064308, 2018.

[84] Ryutaro Matsutani, Fumiyoshi Ozaki, Riyo Yamamoto, Tomoe Sanada, Yutaka Okada, and Kazuo Kojima. Preparation of polyynes up to c22h2 by liquid-phase laser ablation and their immobilization into sio2 gel. *Carbon*, 47(7):1659–1663, 2009.

[85] Sibananda Sana and Chandan Adhikary. Synthesis and entrapment of polyynes inside nano-pores of anodized alumina membrane: A linear allotrope of carbon. *International Journal for Science and Advance Research in Technology (IJSART)*, 3(9):400–406, 2009.

[86] Carlo Spartaco Casari, A Li Bassi, L Ravagnan, F Siviero, C Lenardi, P Piseri, G Bongiorno, Carlo Enrico Bottani, and P Milani. Chemical and thermal stability of carbyne-like structures in cluster-assembled carbon films. *Physical review B*, 69(7):075422, 2004.

[87] Karen I Winey and Richard A Vaia. Polymer nanocomposites. *MRS bulletin*, 32(4):314–322, 2007.

[88] Diego Molina. Polymer nanocomposites based on carbon nanotubes. 2012.

[89] Orna Breuer and Uttandaraman Sundararaj. Big returns from small fibers: a review of polymer/carbon nanotube composites. *Polymer composites*, 25(6):630–645, 2004.

[90] R Sata, H Suzuki, N Ueno, Y Morisawa, M Hatanaka, and T Wakabayashia. Uv-polarizing linear polyyne molecules aligned in pva. *Chinese Journal of Chemical Physics*, 32(2):175–181, 2019.

[91] Sonia Peggiani. Fabrication and characterization of carbon-atom wires and wire-based nanocomposites. 2021.

[92] Stefano Sala. Linear sp carbon chains-polymer nanocomposites by pulsed laser ablation in liquid. 2020.

[93] Vincenzo Amendola, Roberto Pilot, Marco Frasconi, Onofrio M Maragò, and Maria Antonia Iatì. Surface plasmon resonance in gold nanoparticles: a review. *Journal of Physics: Condensed Matter*, 29(20):203002, 2017.

[94] Roberto Pilot, Raffaella Signorini, Christian Durante, Laura Orian, Manjari Bhamidipati, and Laura Fabris. A review on surface-enhanced raman scattering. *Biosensors*, 9(2):57, 2019.

[95] PC Lee and D Meisel. Adsorption and surface-enhanced raman of dyes on silver and gold sols. *The Journal of Physical Chemistry*, 86(17):3391–3395, 1982.

[96] Yu Wan, Zhirui Guo, Xiaoli Jiang, Kun Fang, Xiang Lu, Yu Zhang, and Ning Gu. Quasi-spherical silver nanoparticles: Aqueous synthesis and size control by the seed-mediated lee–meisel method. *Journal of colloid and interface science*, 394:263–268, 2013.

[97] Bin Dong, Ning Xue, Guohao Mu, Mengjun Wang, Zonghua Xiao, Lin Dai, Zhixiang Wang, Dechun Huang, Hongliang Qian, and Wei Chen. Synthesis of monodisperse spherical agnps by ultrasound-intensified lee-meisel method, and quick evaluation via machine learning. *Ultrasonics Sonochemistry*, 73:105485, 2021.

[98] Xiaohu Xia, Miaoxin Yang, Yucai Wang, Yiqun Zheng, Qingge Li, Jingyi Chen, and Younan Xia. Quantifying the coverage density of poly (ethylene glycol) chains on the surface of gold nanostructures. *ACS nano*, 6(1):512–522, 2012.

[99] William E Doering, Marcelo E Piotti, Michael J Natan, and R Griffith Freeman. Sers as a foundation for nanoscale, optically detected biological labels. *Advanced Materials*, 19(20):3100–3108, 2007.

[100] Zeena S Pillai and Prashant V Kamat. What factors control the size and shape of silver nanoparticles in the citrate ion reduction method? *The Journal of Physical Chemistry B*, 108(3):945–951, 2004.

[101] Martino Cambiaggio. Investigation on the effect of benzoyl peroxide on the synthesis of polyynes via pulsed laser ablation in liquid. 2022.

[102] Riccardo Alberto Lotti. Sp-carbon chains by pulsed laser ablation in liquid: synthesis and stability. 2019.

[103] Pietro Marabotti, Sonia Peggiani, Anna Facibeni, Patrick Serafini, Alberto Milani, Valeria Russo, A Li Bassi, and Carlo Spartaco Casari. In situ surface-enhanced raman spectroscopy to investigate polyyne formation during pulsed laser ablation in liquid. *Carbon*, 189:219–229, 2022.

[104] Kin-ichi Uemura. Commercial peltier modules. In *CRC handbook of thermoelectrics*, pages 621–632. CRC Press, 2018.

[105] D Keith Roper, Keith R Berry, Jeremy R Dunklin, Caitlyn Chambers, Vinith Bejugam, Gregory T Forcherio, and Megan Lanier. Effects of geometry and composition of soft polymer films embedded with nanoparticles on rates for optothermal heat dissipation. *Nanoscale*, 10(24):11531–11543, 2018.

[106] Jing Liu, Qiwei Chen, Lianghong Xiao, Jian Shang, Xiong Zhou, Yajie Zhang, Yongfeng Wang, Xiang Shao, Jianlong Li, Wei Chen, et al. Lattice-directed formation of covalent and organometallic molecular wires by terminal alkynes on ag surfaces. *ACS nano*, 9(6):6305–6314, 2015.

[107] Jing Liu, Qi-Wei Chen, and Kai Wu. On-surface construction of low-dimensional nanostructures with terminal alkynes: Linking strategies and controlling methodologies. *Chinese Chemical Letters*, 28(8):1631–1639, 2017.

List of Figures

List of Tables

Ringraziamenti

Ci tengo a ringraziare il mio relatore, professor Carlo Casari, per avermi dato la possibilità di svolgere l'attività di tesi presso il NanoLab, per i suoi preziosi consigli, e per il suo contributo alla stesura di questo lavoro. Ringrazio Pietro, per avermi insegnato ad adottare uno sguardo critico verso i risultati ottenuti e per avermi seguita con pazienza e dedizione durante l'intero percorso. Ringrazio Sonia, Ale ed Anna per i loro consigli e per l'interesse sempre mostrato verso il mio lavoro. In particolare, ringrazio Sonia che, nonostante la sua interminabile lista di impegni quotidiani, ha sempre trovato tempo per discutere con me i risultati ottenuti e mi ha spronata nei momenti più stressanti. Grazie all'esperienza delle persone che ho avuto intorno, ho potuto imparare moltissimo, ed il costante confronto di idee con il gruppo EspLORE mi ha arricchita molto.

Ringrazio la mia famiglia. I miei genitori, Adon e Cartocen, in primis, che mi hanno permesso di coltivare le mie passioni, credendo in me e spronandomi a dare il massimo in ogni situazione. Ringrazio mia sorella Greta, il mio punto di riferimento, che con i suoi consigli e la sua esperienza mi ha permesso di crescere, insieme a lei, come persona. Ringrazio infine i miei nonni, Marisa ed Edmondo, che hanno sempre festeggiato le mie vittorie con entusiasmo, ed in particolare mio nonno, che mi ha sempre ricordato che "2 più 2 fa 4". Vi voglio molto bene.

Ringrazio Chiara, la mia migliore amica, una delle persone più forti che abbia mai conosciuto, che è sempre stata al mio fianco, con cui ho condiviso le gioie più grandi e superato i momenti più bui.

Ringrazio Diego, il mio più grande amico, una persona speciale che avrà sempre un grande posto nel mio cuore. Mi hai insegnato tanto, anche, e soprattutto, a conoscere meglio me stessa, facendomi scoprire il bello di migliorarsi giorno dopo giorno. Ti voglio bene.

Ringrazio Giulia, la mia compagna di merende (e di aperitivi), con cui ho condiviso tutte le gioie e le disperazioni degli esami, e senza la quale non avrei avuto la stessa spinta propulsiva per affrontare questi due ultimi anni.

Ringrazio Arman, che con il suo carattere solare ed il suo approccio alla vita mi ha

insegnato a non prendermi troppo sul serio e a relativizzare i problemi.

Ringrazio Matteo, per aver sempre creduto in me molto più di quanto lo facessi io, e per tutti i bei momenti passati insieme.

Infine, ringrazio tutti i componenti della mia squadra, vi voglio un sacco bene.